ASYMPTOTIC ACCURACY OF THE EQUILIBRIUM DIFFUSION APPROXIMATION AND SEMI-ANALYTIC SOLUTIONS OF RADIATING SHOCKS

A Dissertation

by

JIM MICHAEL FERGUSON

Submitted to the Office of Graduate and Professional Studies of
Texas A&M University
in partial fulfillment of the requirements for the degree of

DOCTOR OF PHILOSOPHY

Chair of Committee,	George Kattawar
Co-Chair of Committee,	Jim Morel
Committee Members,	Vitaly Kocharovsky
	Marv Adams
	Alexey Zheltikov
Head of Department,	George Welch

May 2014

Major Subject: Applied Physics

ABSTRACT

Radiation hydrodynamics (RH) provides a theoretical description for many astrophysical events spanning a wide range of observable phenomena. It is the goal of high-energy-density laboratory astrophysics (HEDLA) to reproduce some of these events in terrestrial settings. Computational models exist to aide our understanding by simulating astrophysical observations and laboratory experiments, and by making predictions which guide both experiments and observations. It is the goal of this dissertation to contribute to our understanding of computational models in RH. Two problems are solved that aide this understanding: 1) we showed that the asymptotic equilibrium diffusion limit (EDL) of the RH equations reproduces the equilibrium diffusion approximation (EDA), through first-order in the asymptotic expansion, in agreement with previous transport models that neglect material motion; and, 2) we produced semi-analytic radiative shock solutions using grey, angularly discretized (S_n) transport. The first problem establishes the asymptotic limits of the EDA in RH, which will have direct applications to discretizations of RH models. The second problem extends previous semi-analytic solution methods for radiative shocks to include grey S_n transport. Previous semi-analytic methods relied on nonequilibrium diffusion theory to describe the radiation, which assumes that while the radiation is out of equilibrium with the material, the angular dependence of the radiation field is isotropic over the extended spatial domain of the radiative shock, and that the radiation energy density is monotonic over the shock's spatial domain. The purpose of using grey S_n transport is to determine the angular dependence of the radiation field. It is shown that the anisotropy of the radiation field can cause the radiation energy density to be nonmonotonic and exhibit a local maximum if a spike in the

material temperature, called a Zel'dovich spike, near the shock discontinuity exists. This local maximum of the radiation energy density is termed "anti-diffusive" radiation because the radiation flux and the gradient of the radiation energy density may have the same sign in this region, which is in stark contrast to diffusion theory wherein the radiation flux is proportional to the *negative* gradient of the radiation energy density.

DEDICATION

This thesis is dedicated to my wife, Kimberly Rae Ferguson. You have been my constant champion, and every aspect of my life is better because you are in it.

You are the wife of my youth, and I love You!

ACKNOWLEDGEMENTS

This dissertation is the end-product, over many years, and with the help of many different people, of a single pursuit: a Ph.D. in the applied sciences.

Jon Hartgraves and Gaye-Lynn Seawright personally ensured that I received the best education they could provide, and just as importantly, they provided patient support and encouragement when I was still a child. Gaye-Lynn and Jimmy have provided an anchor to my past that is invaluable, and I cannot sufficiently express my gratitude.

Christine Ehlig-Economides has become a true friend, and I am grateful for everything that she has taken the time to teach me.

Bruce Freeman introduced me to research, and true scientific curiousity. He was the first to teach me that saying "I don't know", can be the right answer. Jim Morel taught me to learn what "I don't know" before I got to his office. He has had the largest affect on how I think about physics, always pushing me to understand the details, and their consequences. George Kattawar showed me a quiet forcefulness that impressed on me how much power can be wielded by silent contemplation. While George has retired, Marv Adams similarly shows all of his students this same quiet forcefulness. I am humbled, and grateful, to have been guided by these men along my scientific path.

My committee has been exceedingly patient and helpful: George, Jim, Marv, Vi-

taly, and Alexey, thank you for your support and patience!

Rob Lowrie, Bryan Johnson, and Nick Gentile made various contributions to the work in this dissertation, and my understanding. I look forward to continuing our collaborations.

I have enjoyed many day-to-day conversations, and sundry distractions, with friends and colleagues alike. Jason Cezeaux, Erich Fruchtnicht, and Brent Lindeburg knew me before I knew myself. Jianwei Mei and Chris Bertinato helped me learn everything I needed to know about black-holes, and high-energy theoretical physics: That studying these subjects wouldn't allow me to support a family! Adam "Eeyore" Hetzler, Hayes Stripling, Jarrod Edwards, and Paul and Jenny Bruillard have gone before me; Don Bruss, Marco Delchini, Akansha Kumar, Alex Long, Peter Maginot, Carolyn McGraw, Andrew Till, I look forward to seeing you finish. I am grateful for these relationships!

My wife has shown me exceeding patience and support; I'm still trying to learn. Ken and LouEllen have been similarly patient, and have provided me with many examples I didn't have before. I have learned, and will continue to learn, from you both, the most important lessons in life. My sweet Evelyn Grace will no longer appreciate being called "baby-girl" long before she can understand the words written here. You are a Blessing, and I give thanks to my God every time I think of you.

TABLE OF CONTENTS

Page

Page

LIST OF FIGURES

Page

Page

Page

Page

Page

Page

CHAPTER I

INTRODUCTION

Radiation hydrodynamics (RH) provides a theoretical description for many astrophysical events spanning a wide range of observable phenomena. It is the goal of high-energy-density laboratory astrophysics (HEDLA) to reproduce some of these events in terrestrial settings. Computational models exist to aide our understanding by simulating astrophysical observations and laboratory experiments, and by making predictions which guide both experiments and observations.

It is the goal of this dissertation to contribute to our understanding of computational models in RH. Two problems are solved that aide this understanding: 1) we showed that the asymptotic equilibrium diffusion limit (EDL) of the RH equations reproduces the equilibrium diffusion approximation (EDA), through first-order in the asymptotic expansion, in agreement with previous transport models that neglect material motion; and, 2) we produced semi-analytic radiative shock solutions using grey, angularly discretized (S_n) transport. The first problem establishes the asymptotic limits of the EDA in RH, which will have direct applications to discretizations of RH models. The second problem extends the semi-analytic solution method of Lowrie and Edwards [1] for radiative shocks to include grey S_n transport. Previous semi-analytic methods relied on nonequilibrium diffusion theory to describe the radiation, which assumes that while the radiation is out of equilibrium with the material, the angular dependence of the radiation field is isotropic over the extended spatial domain of the radiative shock, and that the radiation energy density is monotonic

over the shock's spatial domain. The purpose of using grey S_n transport is to determine the angular dependence of the radiation field. It is shown that the anisotropy of the radiation field can cause the radiation energy density to be nonmonotonic and exhibit a local maximum if a spike in the material temperature, called a Zel'dovich spike, near the shock discontinuity exists. This local maximum of the radiation energy density has been termed "anti-diffusive" radiation by McClarren and Drake [2] because the radiation flux and the gradient of the radiation energy density may have the same sign in this region, which is in stark contrast to diffusion theory wherein the radiation flux is proportional to the *negative* gradient of the radiation energy density.

It is the goal of this chapter to introduce some of the physical concepts and observations which are important and interesting in RH, and pertinent to the problems solved in this dissertation. In Chapter II, the elements of radiation transport and RH that pertain to this dissertation are briefly reviewed. Specifically, the lab-frame formulations of both theories are derived, and specific equations that are needed in Chapters III - V are collected. In Chapter III, an asymptotic analysis is performed in the EDL of the RH equations, and the results are discussed. In Chapter IV, a review of past-work on analytic and semi-analytic radiative shocks is made. The reviewed work includes the standard treatises by Zel'dovich and Raizer [3], and Mihalas and Mihalas [4], for analytic nonequilibrium diffusion theory, recent work by Drake [5, 6], and McClarren and Drake [2], wherein radiation transport models are considered and computational results are predicted, and the recent work by Lowrie and collaborators [1, 7] which describe semi-analytic radiative shock solutions with the EDA and with nonequilibrium diffusion theory, respectively. This review represents the current state-of-the-art in analytic and semi-analytic radiative shock solutions. Codes that use discretization methods to solve the RH equations and then model radiative

shocks are mentioned for the purposes of code-verification, but not discussed as comparative alternatives. In Chapter V, a semi-analytic radiative shock solution method using grey S_n transport is described, and standard results are presented. Distinctions between these results and those obtained from nonequilibrium diffusion theory are discussed, then the method is used for code-verification, and finally new results are analyzed. A concluding chapter summarizes the results presented in this dissertation.

The rest of this chapter is meant to provide an overview of important topics in RH. In Section I.1, a brief description of the physical domain of RH is given. In Section I.2, the EDA in RH is briefly described and a historical background to the EDL, in general, is given. In Section I.3, astrophysical and laboratory observations of radiative shocks are discussed, along with a brief account of some computational attempts to model the astrophysical origins of radiative shocks. This chapter concludes, in Section I.4, with an overview of current state-of-the-art computational methods which solve the RH equations. The purpose of this dissertation is to aide such computational methods.

I.1 Background

The appropriate purview of RH is to kinetic and dynamic responses of a material-radiation system. Kinetic effects are those in which the thermodynamic state of the fluid is altered. For example, changes to the internal energy state by exciting translational, rotational and/or vibrational degrees of freedom. This potentially leads to a significant departure in the fluid from local thermodynamic equilibrium (LTE), and is responsible for shock waves, and ionization and disassociation fronts, along with other observable phenomena. Dynamic effects are those in which the energy

and/or momentum deposition rates to the fluid from the radiation are significant. In these cases, the radiation represents a considerable fraction of the total momentum density, for example, stellar winds, and may represent a considerable fraction of the content in the stress-energy tensor, which results in, for example, effective changes to the speed of sound. Novae and supernovae represent phenomena in which both the kinetics and dynamics of the system are largely affected by the radiation field, and also by the more weakly interacting neutrino field, which is not considered here. It is the study of these effects, in HEDLA experiments and in astrophysical observations, which make the theory of RH useful and interesting.

The canonical work by Mihalas and Mihalas, "Foundations of Radiation Hydrodynamics" [4], is the time-honored place to begin learning RH. But perhaps the best place to begin understanding the extent of its astrophysical applications is in a lesser-known Lecture Notes in Physics publication, edited by Mihalas and Winkler, "Radiation Hydrodynamics in Stars and Compact Objects" [8]. The table of contents in this publication covers a vast expanse of astrophysical phenomena: protostellar objects; normal stars; supernovae; stellar x-ray sources; novae and accretion disks; x-ray and gamma-ray bursters; active galactic nuclei; stellar and extragalactic jets. The texts by Shapiro and Teukolsky, "Black Holes, White Dwarfs, and Neutron Stars" [9], and Zel'dovich and Novikov, "Relativistic Astrophysics", are devoted to studying truly compact astrophysical objects where relativistic effects are relevant. While the latter two books never explicitly mention RH, the basic concepts are continuously used: equilibrium and nonequilibrium phases within the *local* fluid, and the *non-local* transport of energy and momentum, by radiation and other fields.

I.2 Equilibrium diffusion in radiation hydrodynamics

Stellar and compact astrophysical objects have in common that their interiors, assumed to be composed of some bulk material and radiation, are largely in thermal equilibrium (TE), which is not to be confused with LTE which is a statement about electron level populations. Much of the local radiation is strongly interacting with the interior material, and the radiation energy transported by the photon-field has a diffusive character. Simultaneous TE and diffusive coupling between the fluid and the radiation defines the EDA, and is of significant interest in many astrophysical applications because it reduces the system in a way that allows analysis or even a physical solution. In certain physical situations, it is not clear *a priori* whether the EDA reasonably applies to the problem, but, in the interest of describing the system and obtaining a solution, the system may be assumed to obey the EDA. The EDA, and its physical limits of validity, are well covered in the classic texts by Mihalas and Mihalas [4] and Zel'dovich and Raizer [3].

It is typically assumed that the physical system, whether an astrophysical object or a portion of a laboratory experiment, can be decomposed into two spatially separable parts, the interior and the boundary, where the boundary is a "few" photon mean-free-paths thick. In the EDA, the radiation energy and momentum deposited in the fluid is dominantly due to photon absorption in the interior region, where this energy is isotropically re-emitted, and slowly approaches the boundary of the system. As the radiation approaches the boundary-layer there is a significant probability that it will escape the system, and potentially be observed by the astronomer or experimentalist. As such, the EDA is not directly observable, but, it is also not possible to observe exactly how far the system is from satisfying the EDA, unless it is obviously

nowhere near it. So for many problems, on heuristic grounds, the EDA is reasonable.

An open question that has been discussed in the literature for several decades [4, 10, 11] is, "What level of material-motion corrections are required in the radiation transport equation, when coupled to the RH equations, such that the EDA is satisfied?" This is the first question this dissertation rigorously answers. A subtle rejoinder might be, "If the EDA can not be observed, then why is it important to resolve this question?", and the answer is "Because we expect computational models to accurately simulate the interior regions of stellar objects, compact objects, and laboratory experiments." Thus, it is necessary to know which terms are required in the analytic equations of the model which may then be discretized, and solved computationally. Previous work has shown that once the necessary terms to describe diffusion processes in neutron transport [12, 13], and radiative transfer [14, 15], are known rigorously, then specific discretizations can be meaningfully tested to determine whether a given discretization 1) rigorously preserves the EDA, and 2) produces accurate solutions to analytic problems. Work by Lowrie, Morel and Hittinger [11] began the rigorous analytic extension to the equations of RH, but stopped short of determining which terms were necessary and sufficient for the EDA. This question is addressed in Chapter III, but only to the extent of establishing which terms are necessary in the radiation transport equation to satisfy the EDA in RH. The problem of testing specific RH discretizations will be a complex challenge due to the severe complexity of consistent RH codes, even in one-dimension, and also due to the fact that novel codes are currently being developed and released.

Figure I.1: Simeis 147, the remnant of SN185. A neutron star is in the center of the figure. The red filaments represent color enhancement of hydrogen recombination at the front of the expanding shock. Adapted from the March 24, 2005, Astronomy Picture of the Day [16].

I.3 Radiative shocks

The canonical work by Zel'dovich and Raizer, "Physics of Shock Waves and High-Temperature Hydrodynamic Phenomena" [3], provides a clear explanation of the kinetic and dynamic processes between the radiation and the fluid mentioned above. Before this publication, both authors, and many other contributors to the field, performed extensive research attempting to understand the theoretical and experimental aspects of radiative shocks associated with myriad phenomena. Much of this work continues today.

While the process of equilibrium diffusion erases all traces of its existence, radiating shocks typically have explosive signatures. Supernovae represent the earliest observations of radiating shocks with estimated dates of observation going back to the year 185AD when Chinese astronomers recorded a "guest star" in the Book of Later Han,

which is labelled Simeis 147. Simeis 147 is a supernova remnant whose supernova is estimated to have occurred in the year 38,000BCE. It was featured as an Astronomy Picture of the Day on March 24, 2005, and is shown in Figure (I.1). Part of the Figure's caption [16] reads:

> It covers a width of 150 light-years. The color composite image includes eight hours of exposure time with an H-alpha filter, transmitting only the light from recombining hydrogen atoms in the expanding nebulosity and tracing the regions of shocked, glowing gas.

Perhaps the most well known supernova in recent history is SN1987A, which was observed from earth on February 23, 1987, and is shown in Figure (I.2). One of the first models of SN1987A was made by Ensman and Burrows [17] wherein they investigate the physics of shock breakout using the two-temperature, one-dimensional, Lagrangian, LTE, RH code VISPHOT, which includes a variable Eddington closure of the radiation transport angular moments. They computationally observe both kinetic and dynamic affects to the shock regime during shock breakout, and present simulated evidence of a radiative precursor. The radiative precursor was first predicted in 1957, by Sen and Guess [18], when reporting semi-analytic radiative shock solutions. The radiative precursor is predicted to have two classifications, subcritical and supercritical, depending on whether the material temperature ahead of the shock is less than (subcritical), or greater than (supercritical), the material's final post-shock temperature.

HEDLA is relatively young compared to observational astronomy, and there is considerable overlap between the two fields; excellent reviews can be found in [20–24]. In

Figure I.2: SN1987A was viewed from earth on February 23, 1987. Only 168,000 light-years away, it is one of the most well-studied supernovae. The brightly lit inner-ring and the two fainter outer-rings were blown off long before the supernova event, and the cause of their formation is still discussed. The inner-ring is *currently* glowing due to the supernova shocked gas which is travelling through the ring exciting local matter. Adapted from the February 26, 2012, Astronomy Picture of the Day [19].

2002, Keiter, et. al. [25], using the OMEGA laser, reported observing the radiative precursor created due to a hydrodynamic shock. In 2004, Bouquet et. al. [26], using the LULI laser, reported observing supercritical radiative shock precursors. Blast wave development of a radiation precursor was observed in 2005 by Hansen [27]; see Figure (I.3). Radiatively collapsed shocks were reported in 2006 by Reighard, et. al. [28] which are of observational interest in the regime of thin shocks. These papers all used their experimental tests as validation for the simulation code of their choice. But as mentioned at the end of the previous paragraph, many of these observations were originally predicted using semi-analytic methods.

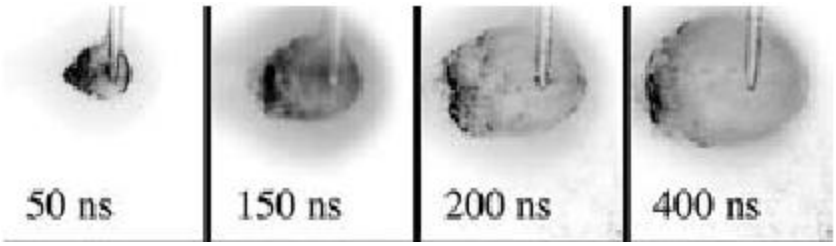

Figure I.3: An ablative laser pulse (10 J for 5 ns), from the left, is focused on a solid pin. The super-critical radiating shock preheats the ambient gas as seen in the faint glow. Adapted from [27].

I.4 State-of-the-art computational methods

One of the first modern multi-dimensional radiation (magneto-)hydrodynamic codes, ZEUS-2D, was the work of Stone, Mihalas and Norman [29]. In 1994, Ensman published a suite of test problems for RH codes [30], which she used to test VISPHOT. Two of the tests reported in Ensman's suite are for a subcritical radiative shock and a supercritical radiative shock. This is not to say that Ensman generated semi-analytic solutions to radiating shocks, but the importance of such solutions, for code comparison, was recognized, and it appears that many of the semi-analytic solution methods developed in the 1960's had been forgotten, or ignored. TITAN was released in 1994 by Gehmeyr and Mihalas as a one-dimensional adaptive grid RH code. They used Ensman's test suite as part of their verification process. The papers by Sincell, Gehmeyr and Mihalas [31, 32] focused TITAN specifically on the time-dependent structure of radiating shocks, and again, Ensman's test-suite was used for code comparison. Analytic results described in Zel'dovich and Raizer, and reviewed in their paper [31], disagreed with their computational results, which were explained as being due to terms second-order in the gas compression ratio. Drake [5, 6] made the poignant comment that discretized computational results must be in agreement

with analytic methods. High-resolution Godunov and discontinuous Galerkin methods were addressed by Lowrie and Morel [33, 34], but little progress was made in the way of advanced numerical methods. It would take almost a decade before a hybrid-Godunov RH solver would be published. It seems appropriate that it was produced by Jim Stone and his student [35], almost 20 years after Stone introduced ZEUS-2D.

While code development in the 1990's was focused largely on methods in one-dimension, with the early exception of Stone's work on ZEUS-2D [29], the last decade-and-a-half has seen a number of advances in physical developments in 3-D RH. The 2003 paper by Hayes and Norman [36] presents physical and numerical extensions of Stone's ZEUS-2D code, including time-dependent transport and the ability to run the code on massively parallel architectures. In 2007 Krumholz et. al. [37] introduced an operator-splitting flux-limited diffusion 3-D algorithm coupled to the base code ORION. In 2009, Klein and Stone [38] co-wrote a conference proceedings on the numerical methods used in their separate codes. Their review is a stout reminder of the complexity of modelling astronomical observations and HEDLA experiments. The vast amount of chemical physics involved in astrophysical processes is packaged in the code by Reynolds, et. al., [39], which was published in 2009. In 2010, Sekora and Stone [35] developed the first one-dimensional hybrid-Godunov RH algorithm. In 2011, John Bell's group [40] added a grey flux-limited diffusion solver to their compressible astrophysics code, CASTRO. In 2012, Stone's [41] group extended Sekora's one-dimensional hybrid-Godunov solver to multiple dimensions using a variable Eddington tensor treatment for the radiation transport. Bell's group [42] extended their work, in 2013, by incorporating a multigroup solver for the radiation frequency.

CHAPTER II

RADIATION TRANSPORT AND RADIATION HYDRODYNAMICS

As mentioned in Chapter I, RH describes the kinetic and dynamic responses between radiation and a fluid. When kinetic effects are dominant, the radiation mainly effects the internal state of the fluid via (de)excitation of atomic electron levels and local thermal properties. When dynamic effects are also important, the radiation significantly affects the trajectory of the fluid and other hydrodynamic characteristics.

We begin the study of radiation-material interactions by considering the radiation transport equation, without material motion, which is represented by the Boltzmann transport equation,

$$\frac{1}{c}\partial_t I_\nu + \Omega_i \partial_i I_\nu = -\sigma_t I_\nu + \frac{\sigma_s}{4\pi}\phi_\nu + \sigma_a B_\nu(T)\,. \tag{II.1}$$

The left-hand side (LHS) of equation (II.1) represents the time and space rates of change of the frequency dependent radiation intensity, I_ν $[energy/length^2 - time - steradian - frequency]$, where c $[length/time]$ is the speed of light, and the derivatives are with respect to the lab-frame space-time coordinates. These derivatives are referred to as the transport terms. Latin subscripts are integer valued, with domain $i \in \{1, 2, 3\}$. A repeated Latin subscript represents Einstein summation, and since the distinction between covariant and contravariant tensors will not be needed in this dissertation, all indices will be written as subscripts. The right-hand side (RHS) represents the interaction of the radiation with the fluid, where σ_t $[length^{-1}]$ is the total

cross-section analogous to the extinction coefficient, σ_s $[length^{-1}]$ is the scattering cross-section which is assumed to be isotropic (denoted by dividing by 4π) acting on the angle-integrated radiation intensity ϕ_ν $[energy/length^2 - time - frequency]$, and σ_a $[length^{-1}]$ is the absorption cross-section acting on the Planck function $B_\nu(T)$ $[energy/length^2 - time - steradian - frequency]$. The total cross-section is the sum of the scattering and absorption cross-sections, $\sigma_t = \sigma_s + \sigma_a$. All the cross-sections are assumed to depend on the material temperature and density, and the absorption and total cross-sections are assumed to be frequency-dependent.

The three terms on the RHS of equation (II.1) are the extinction of photons with frequency ν $[time^{-1}]$, the isotropic net in-scatter of photons with frequency ν, and the isotropic Planck emission of photons with frequency ν. The Planck function,

$$B_\nu(T) = \frac{2h\nu^3}{c^2}\left[\exp\left(\frac{h\nu}{k_B T}\right) - 1\right]^{-1}, \tag{II.2}$$

represents the radiation intensity emitted by a black-body in thermal equilibrium with its surroundings (TE), where h $[energy - time]$ is Planck's constant and k_B $[energy/Kelvin]$ is Boltzmann's constant. It is generally assumed in RH that materials at temperature T $[Kelvin]$ radiate according to the Planck function, and thus that the material is in LTE with its surroundings. Even though it is known that this is a weak assumption at best, it allows the use of standard thermodynamic relationships. This makes it important in many studies of stellar environments to correctly determine the effective material temperature, such that the correct Planck distribution is used, and the correct radiation emission is modeled. Figure (II.1) shows the accuracy of assuming that the sun is a black-body at an effective temperature, $T_{\text{eff}} = 5777\text{K}$.

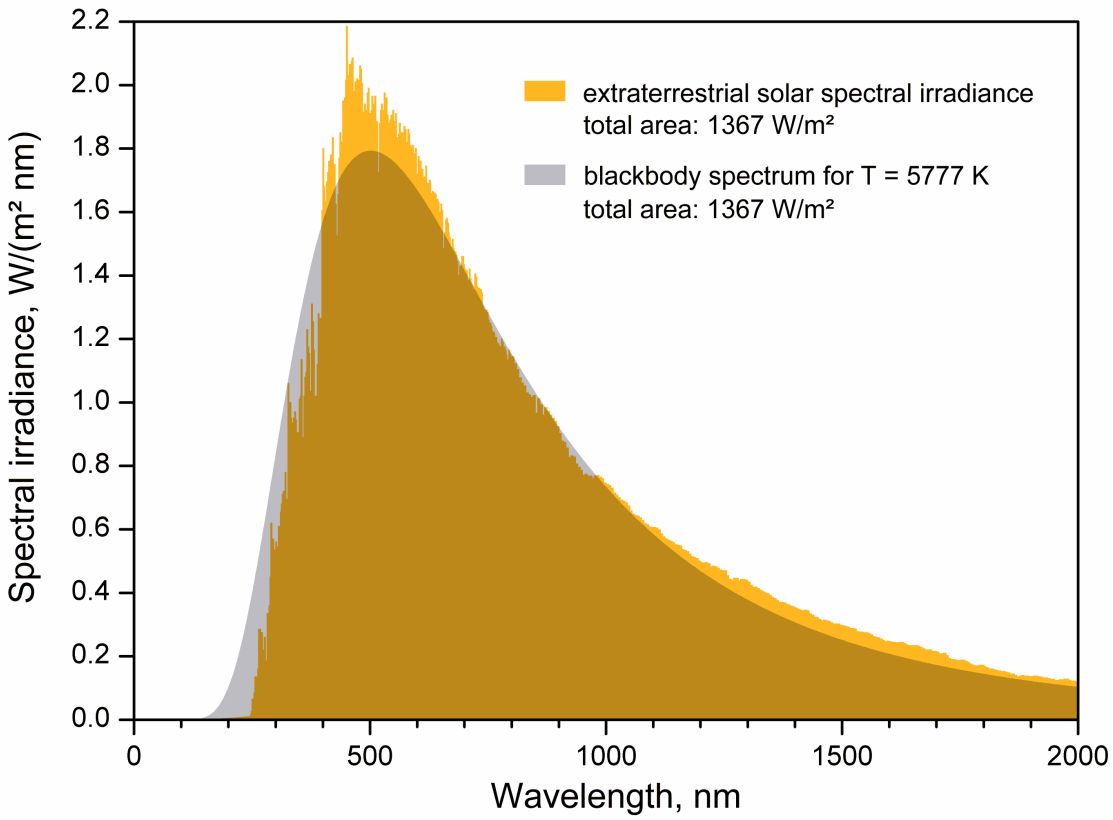

Figure II.1: Spectral irradiance of the sun overlayed on the blackbody spectrum for an object with temperature value $\sim$ 5777K. It is seen that the sun's spectrum very nearly fits the blackbody spectrum. Adapted from Wikipedia [43].

The Planck function may be frequency-integrated to obtain the temperature-dependent Planck function

$$B(T) = \int_0^\infty B_\nu(T)\, d\nu = \frac{a_r c T^4}{4\pi} = \sigma_{SB} T^4\,, \tag{II.3}$$

where a_r $[energy/Kelvin^4 - length^3]$ is the radiation constant and σ_{SB} $[energy/Kelvin^4 - length^2 - time - steradian]$ is the Stefan-Boltzmann constant. The frequency-

integrated Planck function is isotropic and its zeroth angular-moment is

$$\int_{4\pi} B(T) d\Omega = a_r c T^4 \,. \tag{II.4}$$

The LHS of equation (II.4) is the spectral irradiance for a body emitting radiation according to the Planck-function. It is this integrated value, measured for the sun, which determines the sun's effective temperature via the RHS of equation (II.4).

II.1 Radiation transport without material motion

Since the radiation transport equation is effectively a kinetic theory for photons, the zeroth, first, and second angular-moments of the radiation intensity are physically meaningful

$$\phi_\nu \equiv \int_{4\pi} I_\nu \, d\Omega \,, \tag{II.5a}$$

$$F_{i,\nu} \equiv \int_{4\pi} \Omega_i I_\nu \, d\Omega \,, \tag{II.5b}$$

$$P_{ij,\nu} \equiv \int_{4\pi} \Omega_i \Omega_j I_\nu \, d\Omega \,, \tag{II.5c}$$

and represent the angle-integrated radiation intensity ϕ_ν, the frequency-dependent radiation flux $F_{i,\nu}$, and the frequency-dependent radiation pressure $P_{ij,\nu}$. These terms may be frequency-integrated

$$\mathcal{E} \equiv \frac{1}{c} \int_0^\infty \int_{4\pi} I_\nu \, d\nu d\Omega \,, \tag{II.6a}$$

$$\mathcal{F}_i \equiv \int_0^\infty \int_{4\pi} \Omega_i I_\nu \, d\nu d\Omega \,, \tag{II.6b}$$

$$\mathcal{P}_{ij} \equiv \frac{1}{c} \int_0^\infty \int_{4\pi} \Omega_i \Omega_j I_\nu \, d\nu d\Omega \,, \tag{II.6c}$$

and represent the radiation energy density $\mathcal{E}$, the radiation flux $\mathcal{F}_i$, and the radiation pressure $\mathcal{P}_{ij}$. The zeroth and first angular-moments of the frequency-integrated transport equation (II.1),

$$\int_0^\infty \int_{4\pi} \left[\frac{1}{c} \partial_t I_\nu + \Omega_i \partial_i I_\nu \right] d\nu d\Omega \equiv \partial_t \mathcal{E} + \partial_i \mathcal{F}_i = \int_0^\infty \int_{4\pi} Q_\nu d\nu d\Omega \equiv S_{re} \,, \quad \text{(II.7a)}$$

$$\frac{1}{c} \int_0^\infty \int_{4\pi} \Omega_i \left[\frac{1}{c} \partial_t I_\nu + \Omega_j \partial_j I_\nu \right] d\nu d\Omega \equiv \frac{1}{c^2} \partial_t \mathcal{F}_i + \partial_j \mathcal{P}_{ij} = \frac{1}{c} \int_0^\infty \int_{4\pi} \Omega_i Q_\nu d\nu d\Omega \equiv S_{i,rp} \,, \quad \text{(II.7b)}$$

represent the rate at which radiation energy and radiation momentum enter the radiation field, such that the radiation energy and momentum source rates, S_{re} and $S_{i,rp}$, are represented on the RHS. The factor of c dividing the momentum source rate is required to obtain the correct units since a photon's momentum is defined as its energy divided by the speed of light: $p_\gamma = E_\gamma / c$. Since the interaction terms on the RHS of equation (II.1), which are written as Q_ν in equations (II.7), are frequency-dependent they do not immediately simplify, and including these terms does not clarify the meaning of equations (II.7). Now that the necessary angular moments have been defined, it is appropriate to talk about the P_1 approximation, the diffusion approximation, and the EDA.

II.1.1 The P_1 approximation

The radiation energy and momentum equations (II.7) represent two equations containing three radiation variables. These are the first two angular-moments of the radiation transport equation (II.1) and each new angular-moment would simply introduce a new radiation variable of one higher angular-moment. Thus the angular-

moments method of solving the transport equation is always an under-determined system of n-equations in $(n+1)$-unknowns. One way to solve this hierarchy problem, which is physically reasonable in certain circumstances, is to invoke the P_1 approximation and stipulate that the radiation intensity is weakly anisotropic, i.e., $|F_{i,\nu}| \ll \phi_\nu$,

$$I_\nu = \frac{1}{4\pi}\left(\phi_\nu + 3\Omega_i F_{i,\nu}\right) . \tag{II.8}$$

Thus, the radiation intensity is dominantly isotropic since ϕ_ν dominates $F_{i,\nu}$, and the angular-dependence of the radiation intensity is allowed to come from the weak radiation flux. The name P_1 is a reference to the first-order Legendre polynomial expansion in the angular variable Ω_i. The zeroth, first, and second angular-moments of the weakly anisotropic radiation intensity, equation (II.8), produce

$$\phi_\nu = \frac{1}{4\pi}\int_{4\pi}\left(\phi_\nu + 3\Omega_i F_{i,\nu}\right)\, d\Omega = \phi_\nu \,, \tag{II.9a}$$

$$F_{i,\nu} = \frac{1}{4\pi}\int_{4\pi}\Omega_i\left(\phi_\nu + 3\Omega_i F_{i,\nu}\right)\, d\Omega = F_{i,\nu} \,, \tag{II.9b}$$

$$P_{ij,\nu} = \frac{1}{4\pi}\int_{4\pi}\Omega_i\Omega_j\left(\phi_\nu + 3\Omega_i F_{i,\nu}\right)\, d\Omega = \frac{1}{3}\phi_\nu \,, \tag{II.9c}$$

where the first and second expressions are consistency checks, and the third expression relates the frequency-dependent radiation pressure to the angle-integrated radiation intensity. The frequency-integrated expressions are

$$\mathcal{E} = \frac{h}{4\pi}\int_0^\infty\int_{4\pi}\left(\phi_\nu + 3\Omega_i F_{i,\nu}\right)\, d\nu d\Omega = \mathcal{E} \,, \tag{II.10a}$$

$$\mathcal{F}_i = \frac{h}{4\pi}\int_0^\infty\int_{4\pi}\Omega_i\left(\phi_\nu + 3\Omega_i F_{i,\nu}\right)\, d\nu d\Omega = \mathcal{F}_i \,, \tag{II.10b}$$

$$\mathcal{P}_{ij} = \frac{h}{4\pi}\int_0^\infty\int_{4\pi}\Omega_i\Omega_j\left(\phi_\nu + 3\Omega_i F_{i,\nu}\right)\, d\nu d\Omega = \frac{1}{3}\mathcal{E}\delta_{ij} \,, \tag{II.10c}$$

where, again, the first two expressions are consistency conditions and the third expression relates the radiation pressure to the radiation energy density. In the astrophysical literature, this relation between the radiation pressure and the radiation energy density is termed the Eddington approximation, after Sir Arthur Eddington. The assumption that the radiation field is weakly anisotropic has the effect of making the radiation pressure isotropic. The radiation energy and momentum equations (II.7), in the P_1 approximation, take the form of a 2×2 system of equations with two variables in two equations:

$$\partial_t \mathcal{E} + \partial_i \mathcal{F}_i = S_{re}\,, \tag{II.11a}$$

$$\frac{1}{c^2}\partial_t \mathcal{F}_i + \frac{1}{3}\partial_i \mathcal{E} = S_{i,rp}\,. \tag{II.11b}$$

The physical grounds for the P_1 approximation are that, in many problems of interest, the radiation intensity is *nearly* isotropic such that the radiation flux is weak and the radiation pressure is effectively isotropic. Isotropy of the radiation pressure, equation (II.10c), implies that the net radiation forces acting across a perpendicular plane are zero, which represent the off-diagonal components of the radiation pressure. As for the diagonal components, the trace of the radiation pressure tensor is the radiation energy density

$$\begin{aligned}
\mathrm{Tr}(\mathcal{P}_{ij}) &= \mathcal{P}_{xx} + \mathcal{P}_{yy} + \mathcal{P}_{zz} \\
&= \int_0^\infty \int_{4\pi} \left(\Omega_x^2 + \Omega_y^2 + \Omega_z^2\right) I_\nu \, d\nu d\Omega \\
&= \int_0^\infty \int_{4\pi} I_\nu \, d\nu d\Omega \\
&= \mathcal{E},
\end{aligned} \tag{II.12}$$

and due to the isotropy of the radiation pressure the three diagonal terms are equal such that

$$\mathcal{P}_{xx} = \mathcal{P}_{yy} = \mathcal{P}_{zz} = \frac{1}{3}\mathcal{E}\,. \tag{II.13}$$

II.1.2 The diffusion approximation

The diffusion approximation incorporates the P_1 approximation in equations (II.7), as written in equations (II.11a), and imposes on them that the radiation diffuses through the material. Diffusion theory says that the radiation flux should be proportional to the negative gradient of the radiation energy density: $\mathcal{F}_i \sim -\partial_i \mathcal{E}$. Assuming that the interaction terms on the RHS of the transport equation (II.1) are isotropic and frequency-independent, then the first-angular moment of the frequency-integrated transport equation can be extended to the RHS,

$$\frac{1}{c^2}\partial_t \mathcal{F}_i + \frac{1}{3}\partial_i \mathcal{E} = -\frac{\sigma_t}{c}\mathcal{F}_i\,, \tag{II.14}$$

and it is apparent that the time-derivative of the radiation flux must be set to zero to obtain an expression in which the radiation flux is the gradient of the radiation energy density:

$$\mathcal{F}_i = -\frac{c}{3\sigma_t}\partial_i \mathcal{E}\,. \tag{II.15}$$

In Chapter III, it will be shown that the time-derivative in the radiation momentum equation, in the EDL, is $\mathcal{O}(\epsilon^2)$, and therefore negligible. Thus, the diffusion approximation requires, beyond the P_1 approximation, that the time derivative in the radiation momentum equation be zero.

II.1.3 The equilibrium diffusion approximation

The EDA extends the diffusion approximation in such a way that the radiation and material are in TE such that they acquire the same temperature, T, the radiation energy density is $\mathcal{E} \equiv a_r T^4$, and the radiation flux is *approximately* zero, $\mathcal{F}_i \approx 0$. Physically, the EDA stipulates that the absorption mean-free-path for the radiation in the material, $\lambda_a = \sigma_a^{-1}$, is very small compared to the size of the material-system, L: $\lambda_a \ll L$. Then the material, at temperature T, isotropically emits photons in accordance with the Planck function, and these photons travel, on average, one mean-free-path before being reabsorbed by the material. The isotropy of radiation emission by the material is responsible for the vanishing of the radiation flux. The absorption mean-free-path is assumed to be very small compared to the physical size of the material system, $\lambda_a \ll L$, such that the radiation energy is reabsorbed in a neighborhood near its emission. In this way the radiation energy density is a manifestation of the local material temperature, and the material temperature from point to point is tightly coupled locally via radiation emission and absorption. Thus the radiation-material system is in TE.

II.2 Invariants and transformations

It is known from special relativity that certain physical characteristics of a system are invariant under transformations between different reference frames. These frame-independent terms help determine how to transform other important terms that are not invariant, and thus the special importance of the frame-invariants. It is worth commenting that the photon is treated in this dissertation as a conserved particle. While this does not hold in quantum electrodynamics, it is a reasonable assumption

in nonrelativistic quantum mechanics and much of quantum statistics, and it is a reasonable assumption for the problems of interest here. Much of this Section, and Appendix A, follow directly from Section 1.6 of Jeremy Goodman's High-Energy Astrophysics lecture notes [44] and section 4.9 of Rybicki and Lightman [45].

Four invariants are needed in this chapter: the intensity invariant, the absorption or cross-section invariant, the emission invariant, and the invariant of the momentum-space volume. While their derivations are interesting, they divert from the necessary course of discussion, and are relegated to Appendix A. The respective expressions for these invariants are:

$$\mathfrak{I} = \frac{I_\nu}{\nu^3}\,, \tag{II.16a}$$

$$\mathfrak{a} = \nu\sigma_a\,, \tag{II.16b}$$

$$\mathfrak{e} = \frac{\sigma_a B_\nu(T)}{\nu^2}\,, \tag{II.16c}$$

$$\nu\, d\nu d\Omega = \nu_o\, d\nu_o d\Omega_o\,, \tag{II.16d}$$

where the subscript-$_o$ denotes a comoving-frame quantity. The second and third invariants are familiar from the first and third interaction terms on the RHS of the radiation transport equation (II.1), and since that equation is written without considering material motion, such that the comoving- and lab-frames are the same, their importance is more obvious. The first and fourth invariants are necessary for the isotropic in-scatter source on the RHS of equation (II.1), which is the second interaction term.

While Lorentz invariants are helpful, they are not the full story. Many "objects"

in special relativity cannot be viewed simply as Lorentz invariants without losing a considerable amount of the information they carry. A simple example is the space-time four-vector; a more useful one is the four-momentum of a particle. A Lorentz invariant can be defined for both, individually, as the square of the four-vector, but at the cost of losing the information contained in the coordinates.

The Lorentz transformation from the lab-frame to the comoving-frame, $\boldsymbol{x}$ going to $\boldsymbol{x}_o$, is written

$$\boldsymbol{x}_o = \begin{pmatrix} \gamma_u & -\gamma_u \boldsymbol{\beta}^\intercal \\ -\gamma_u \boldsymbol{\beta} & \mathbf{I} + (\gamma_u - 1)\,\beta^{-2} \boldsymbol{\beta}\boldsymbol{\beta}^\intercal \end{pmatrix} \boldsymbol{x}\,, \tag{II.17}$$

where $\gamma_u = (1-\beta^2)^{-1}$ is the Lorentz factor, $\boldsymbol{\beta} \equiv \mathbf{u}/c$ is a column-vector, and $\boldsymbol{\beta}^\intercal$ is its transpose, $\mathbf{I}$ is the 3-by-3 identity matrix, and $\boldsymbol{x} = (ct, \mathbf{x})^\intercal$ represents the space-time four-vector. A photon's four-momentum may similarly be Lorentz transformed between the two frames of reference

$$\boldsymbol{p}_o = \begin{pmatrix} \gamma_u & -\gamma_u \boldsymbol{\beta}^\intercal \\ -\gamma_u \boldsymbol{\beta} & \mathbf{I} + (\gamma_u - 1)\,\beta^{-2} \boldsymbol{\beta}\boldsymbol{\beta}^\intercal \end{pmatrix} \boldsymbol{p}\,, \tag{II.18}$$

where $\boldsymbol{p} = (E/c, \mathbf{p}) = (h\nu/c)(1, \boldsymbol{\Omega})^\intercal$ is the photon four-momentum, and $\boldsymbol{\Omega}$ represents the photon's unit-normalized direction of travel. The transformation of the photon frequency,

$$\nu_o = \nu \gamma_u \left(1 - \boldsymbol{\beta} \cdot \boldsymbol{\Omega}\right)\,, \tag{II.19}$$

corresponds to the E/c term of the photon four-momentum in equation (II.18).

II.3 Radiation transport in the lab-frame with material motion

The radiation transport equation, as written in equation (II.1), is for a material at rest in the lab-frame. The question is then, "How should this equation change when the material is in motion but the radiation and the fluid are viewed from the lab-frame?" The cross-sections and the Planck function are experimentally measured in the comoving-frame, and so the comoving-frame is the physically correct frame from which to reference the interaction terms and the Planck function. For notational convenience, the subscript-$_o$ will be omitted from all cross-sections and the Planck function with the understanding that they reference their comoving-frame values.

Every term in equation (II.1) is a lab-frame quantity, so it is necessary to transform the interaction and source terms to the comoving-frame. Thus, every term on the LHS is an innate lab-frame quantity since there are no interaction nor source terms there, and the LHS will be left alone. The first term on the RHS contains the material total cross-section and the lab-frame measured radiation intensity. The cross-section must be correctly transformed to the comoving-frame according to equation (II.16b)

$$-\sigma_t I_\nu \mapsto -\frac{\nu_o}{\nu}\sigma_t I_\nu \,. \tag{II.20}$$

The second term on the RHS is fairly involved since, as the in-scatter source, it represents a source term and must be treated on the same footing as the invariant emission in equation (II.16c). Ultimately, this means transforming the in-scatter source to the comoving-frame, and then transforming the radiation intensity and the momentum-space volume back to the lab-frame. Its derivation is left to Appendix

B, and the result is presented here:

$$\frac{\sigma_s}{4\pi}\phi_\nu \mapsto \left(\frac{\nu}{\nu_o}\right)^2 \frac{\sigma_s}{4\pi}\int_{4\pi}\frac{\nu_o}{\nu'}I_{\nu'}(\Omega')\,d\Omega'\,. \tag{II.21}$$

The third term is the emission source, the invariance of which is defined in equation (II.16c),

$$\sigma_a B_\nu(T) \mapsto \left(\frac{\nu}{\nu_o}\right)^2 \sigma_a B_\nu(T)\,. \tag{II.22}$$

Thus, the lab-frame radiation transport equation correct through all orders in β, with interaction terms appropriately transformed to their comoving-frame values, is

$$\begin{aligned}\frac{1}{c}\partial_t I_\nu + \Omega_i \partial_i I_\nu \\ = -\frac{\nu_o}{\nu}\sigma_t I_\nu + \left(\frac{\nu}{\nu_o}\right)^2 \frac{\sigma_s}{4\pi}\int_{4\pi}\frac{\nu_o}{\nu'}I_{\nu'}(\Omega')\,d\Omega' + \left(\frac{\nu}{\nu_o}\right)^2 \sigma_a B_\nu(T)\,.\end{aligned} \tag{II.23}$$

It is worth calling attention to the primed-$'$ angular variable and frequency in the second interaction term on the RHS, which can be considered from equation (II.19),

$$\nu_o = \nu'\gamma_u\left(1-\boldsymbol{\beta}\cdot\boldsymbol{\Omega}'\right)\,. \tag{II.24}$$

The primed angular variable and frequency reside in the same frame as the unprimed variables, and hence have the same velocity and β. The frequency dependence of the radiation intensity in the integrand is with respect to the primed frequency variable.

II.4 Radiation hydrodynamics

Now that the correct lab-frame radiation transport equation has been derived, the rates at which radiation energy and momentum are deposited into the fluid can be determined, and these values can be coupled to the Euler equations of hydrodynamics. In this way, the radiation informs the hydrodynamics about the appropriate kinetic and dynamic effects and the equations of radiation hydrodynamics are formed.

The radiation energy and momentum source rates represent radiation source rates to the radiation field due to interactions between the material-radiation system. Since the total energy and momentum of the material-radiation system must be conserved during these interactions, it is necessary to couple these sources to the Euler equations of hydrodynamics as deposition rates into the material:

$$\partial_t \rho + \partial_i \left(\rho u_i\right) = 0 \,, \tag{II.25a}$$

$$\partial_t \left(\rho u_i\right) + \partial_j \left(\rho u_i u_j + p_{ij}\right) = -S_{i,rp} \,, \tag{II.25b}$$

$$\partial_t \left(\frac{1}{2}\rho u^2 + \rho e\right) + \partial_i \left[u_j \left(\frac{1}{2}\rho u_i u_j + \rho e \delta_{ij} + p_{ij}\right)\right] = -S_{re} \,, \tag{II.25c}$$

$$\begin{aligned} &\frac{1}{c}\partial_t I_\nu + \Omega_i \partial_i I_\nu \\ &\quad = -\frac{\nu_o}{\nu}\sigma_t I_\nu + \left(\frac{\nu}{\nu_o}\right)^2 \frac{\sigma_s}{4\pi}\int_{4\pi} \frac{\nu_o}{\nu'} I_{\nu'}(\Omega')\, d\Omega' + \left(\frac{\nu}{\nu_o}\right)^2 \sigma_a B_\nu(T) \equiv Q_\nu \,, \end{aligned} \tag{II.25d}$$

where

$$S_{re} \equiv \int_0^\infty \int_{4\pi} Q_\nu d\nu d\Omega = \partial_t \mathcal{E} + \partial_i \mathcal{F}_i \,, \tag{II.25e}$$

$$S_{i,rp} \equiv \frac{1}{c}\int_0^\infty \int_{4\pi} \Omega_i Q_\nu d\nu d\Omega = \frac{1}{c^2}\partial_t \mathcal{F}_i + \partial_j \mathcal{P}_{ij} \,. \tag{II.25f}$$

These equations represent the conservation of mass, material momentum and material energy coupled to the radiation momentum and energy source rates, the lab-frame radiation transport equation with comoving-frame cross-sections and Planck function, and the source rates of radiation energy and momentum to the radiation field. Photons are massless so there is no contribution to the mass conservation equation. The minus signs on the RHS of the fluid equations are necessary because S_{re} and $S_{i,rp}$ represent sources for the radiation field, i.e., they are sinks for the fluid, but the RHS is expected to represent sources for the fluid, thus the minus signs. These four equations represent a closed set of equations which correctly describe the radiation-material system. The range of physical applications of these four equations was briefly discussed in Chapter I.

It is worth noting that the Navier-Stokes equations of hydrodynamics, which incorporate fluid viscosity and thermal conductivity, could have been coupled to the radiation energy and momentum source rates instead of the Euler equations. However, these effects are 1) often too computationally expensive and produce potentially small corrections, and 2) Traugott [46] showed that in radiating shocks the radiation length scale dominates the fluid length scale, which controls viscosity and thermal conductivity. More importantly, the effects of viscosity and conductivity are not important to the problems solved in this dissertation. If another problem demanded it, then the pertinent Navier-Stokes terms could be implemented without affecting the radiation variables.

CHAPTER III

ASYMPTOTIC ACCURACY OF THE EQUILIBRIUM DIFFUSION APPROXIMATION IN RADIATION HYDRODYNAMICS

Asymptotic analysis provides a rigorous mathematical framework from which to derive the behaviour of a set of equations in the limit that certain terms are dominant. This dominance generally corresponds to the manifestation of some physical approximations, which define asymptotic scalings. The equations being analyzed can be either the analytic equations of a theory, an associated model, or a specific discretization. If the asymptotic solutions of the scaled analytic equations exhibit a physical approximation, through some order in the scaling, then we say that the solutions of the (unscaled) analytic equations "satisfy" the approximation through this asymptotic order. When the associated model, or discretization, also exhibits the physical approximation, in the asymptotic limit, we say that they "preserve" the limit. Even if the analytic equations asymptotically satisfy the physical approximation it is possible that the associated model, or discretization, may not preserve the limit, or perhaps not to the same asymptotic order. Those models, and discretizations, that do preserve the approximations that the analytic equations satisfy are generally more accurate, and less computationally expensive due to less severe meshing requirements.

III.1 Example: asymptotic analysis of the neutron transport equation

As a specific but simple example, we will generate the analytic neutron diffusion equation by performing an asymptotic analysis of the analytic neutron transport

equation. This requires nondimensionalizing the neutron transport equation, and determining the appropriate scalings. For convenience, we will work in 1-D, and focus on asymptotic expansions of the neutron variables that appear in the neutron transport equation, which are the angular flux ψ, and the scalar flux ϕ.

Before the asymptotic analysis, we derive the neutron diffusion equation from the neutron transport equation. Consider the 1-D neutron transport equation

$$\frac{1}{v}\partial_t\psi + \mu\partial_x\psi + \sigma_t\psi = \frac{\sigma_s}{4\pi}\phi + \frac{Q}{4\pi}\,, \tag{III.1}$$

whose zeroth and first angular moments are:

$$\frac{1}{v}\partial_t\phi + \partial_x J + \sigma_a\phi = Q\,, \tag{III.2a}$$

$$\frac{1}{v}\partial_t J + \frac{1}{3}\partial_x\phi + \sigma_t J = 0\,. \tag{III.2b}$$

A diffusion equation is constructed by dropping the time derivative in the first angular moment, solving for the neutron flux

$$J = -\frac{1}{3\sigma_t}\partial_x\phi\,, \tag{III.3}$$

and inserting this into the zeroth angular moment

$$\frac{1}{v}\partial_t\phi - \partial_x\left(\frac{1}{3\sigma_t}\partial_x\phi\right) + \sigma_a\phi = Q. \tag{III.4}$$

This is the neutron diffusion equation, which we now derive asymptotically. The following nondimensionalization decomposes dimensional variables into the product of a variable containing the dimension with subscript-$_\infty$, and a hatted-$\hat{}$ variable

containing a characteristic value of the variable:

$$t = t_\infty \hat{t}\,, \tag{III.5a}$$

$$x = l_\infty \hat{x}\,, \tag{III.5b}$$

$$\psi = \psi_\infty \hat{\psi}\,, \tag{III.5c}$$

$$\phi = \phi_\infty \hat{\phi} = 4\pi\psi_\infty \hat{\phi}\,, \quad \text{where} \quad \hat{\phi} \equiv \frac{1}{4\pi}\int_{4\pi} \hat{\psi} d\Omega\,, \tag{III.5d}$$

$$Q = Q_\infty \hat{Q}. \tag{III.5e}$$

Therefore, t_∞ contains units of $[time]$, x_∞ contains units of $[length]$, ψ_∞ contains units of $[energy/length^2 - time - steradian - energy]$, and ϕ_∞ contains units of $[energy/length^2 - time - energy]$. Implementing this nondimensionalization in the neutron transport equation (III.1), and dividing through by $\sigma_t\psi_\infty$, produces the nondimensional neutron transport equation

$$\frac{1}{t_\infty v\sigma_t}\partial_{\hat{t}}\hat{\psi} + \frac{1}{\sigma_t l_\infty}\mu\partial_{\hat{x}}\hat{\psi} + \hat{\psi} = \left(1 - \frac{\sigma_a}{\sigma_t}\right)\frac{\hat{\phi}}{\psi_\infty} + \frac{\hat{Q}}{4\pi\sigma_t\psi_\infty}\,, \tag{III.6}$$

where the scattering cross-section has been split into the difference between the total and absorption cross-sections: $\sigma_s = \sigma_t - \sigma_a$. The equation above indicates that the transport operators, and source terms, are associated with specific nondimensional ratios:

$$\frac{1}{v}\partial_t \to \frac{1}{t_\infty v\sigma_t}\partial_{\hat{t}}\,, \tag{III.7a}$$

$$\mu\partial_x \to \frac{1}{\sigma_t l_\infty}\mu\partial_{\hat{x}}\,, \tag{III.7b}$$

$$\phi \to \frac{\hat{\phi}}{\psi_\infty}\,, \tag{III.7c}$$

$$Q \to \frac{\hat{Q}}{\sigma_t \psi_\infty} \,. \tag{III.7d}$$

This information is used to nondimensionalize the neutron diffusion equation (III.4)

$$\frac{1}{t_\infty v \sigma_t} \partial_t \phi - \frac{1}{3} \left(\frac{1}{\sigma_t l_\infty} \right) \partial_x \left(\frac{1}{\sigma_t l_\infty} \right) \partial_x \phi + \frac{\sigma_a}{\sigma_t} \phi = \frac{Q}{4\pi \sigma_t} \,, \tag{III.8}$$

where the hats-ˆ have been dropped for notational convenience, and the common factor of ψ_∞ has been removed. The diffusion solution ϕ, must be invariant to the scaling (neglecting boundary conditions), and since the diffusive term is quadratic in $(\sigma_t l_\infty)^{-1}$, a reasonable scaling is to multiply all terms by ϵ^2

$$\frac{\epsilon^2}{t_\infty v \sigma_t} \partial_t \phi - \frac{1}{3} \left(\frac{\epsilon}{\sigma_t l_\infty} \right) \partial_x \left(\frac{\epsilon}{\sigma_t l_\infty} \right) \partial_x \phi + \frac{\epsilon^2 \sigma_a}{\sigma_t} \phi = \epsilon^2 \frac{Q}{4\pi \sigma_t} \,. \tag{III.9}$$

The following scalings are thus defined,

$$\frac{1}{t_\infty v \sigma_t} \to \frac{\epsilon^2}{t_\infty v \sigma_t} \,, \tag{III.10a}$$

$$\frac{1}{\sigma_t l_\infty} \to \frac{\epsilon}{\sigma_t l_\infty} \,, \tag{III.10b}$$

$$\frac{\sigma_a}{\sigma_t} \to \frac{\epsilon^2 \sigma_a}{\sigma_t} \,, \tag{III.10c}$$

$$Q \to \epsilon^2 Q \,, \tag{III.10d}$$

and used to define the scaled, redimensionalized, neutron transport equation (III.1)

$$\epsilon^2 \frac{1}{v} \partial_t \psi + \epsilon \mu \partial_x \psi + \sigma_t \psi = \frac{(\sigma_t - \epsilon^2 \sigma_a)}{4\pi} \phi + \epsilon^2 \frac{Q}{4\pi} \,. \tag{III.11}$$

The scalings in equations (III.10) define the neutron diffusion limit. The angular flux and scalar flux in equation (III.11) are now asymptotically expanded in powers

of ϵ,

$$\psi = \sum_{n=0}^{\infty} \psi^{(n)} \epsilon^n \,, \tag{III.12a}$$

$$\phi = \sum_{n=0}^{\infty} \phi^{(n)} \epsilon^n \,, \tag{III.12b}$$

generating a hierarchical set of equations. The leading-, first-, second-, and third-order asymptotic neutron transport equations of this hierarchical set are:

$\underline{\mathcal{O}(\epsilon^{(0)})}$

$$\psi^{(0)} = \frac{\phi^{(0)}}{4\pi} \,, \tag{III.13a}$$

$\underline{\mathcal{O}(\epsilon^{(1)})}$

$$\mu \partial_x \psi^{(0)} + \sigma_t \psi^{(1)} = \frac{\sigma_t}{4\pi} \phi^{(1)} \,, \tag{III.13b}$$

$\underline{\mathcal{O}(\epsilon^{(2)})}$

$$\frac{1}{v} \partial_t \psi^{(0)} + \mu \partial_x \psi^{(1)} + \sigma_t \psi^{(2)} = \frac{\sigma_t}{4\pi} \phi^{(2)} - \frac{\sigma_a}{4\pi} \phi^{(0)} + \frac{Q}{4\pi} \,, \tag{III.13c}$$

$\underline{\mathcal{O}(\epsilon^{(3)})}$

$$\frac{1}{v} \partial_t \psi^{(1)} + \mu \partial_x \psi^{(2)} + \sigma_t \psi^{(3)} = \frac{\sigma_t}{4\pi} \phi^{(3)} - \frac{\sigma_a}{4\pi} \phi^{(1)} \,. \tag{III.13d}$$

The zeroth angular moment of the second- and third-order asymptotic equations (III.13c) - (III.13d) represent balance equations of the neutron transport equation,

$\underline{\mathcal{O}(\epsilon^{(2)})}$

$$\frac{1}{v}\partial_t\phi^{(0)} + \partial_x J^{(1)} = -\sigma_a\phi^{(0)} + Q\,, \tag{III.14a}$$

$\underline{\mathcal{O}(\epsilon^{(3)})}$

$$\frac{1}{v}\partial_t\phi^{(1)} + \partial_x J^{(2)} = -\sigma_a\phi^{(1)}\,, \tag{III.14b}$$

and also define which asymptotic terms must be evaluated: $\phi^{(0)}$, $\phi^{(1)}$, $J^{(1)}$, and $J^{(2)}$. To obtain the expressions for these asymptotic variables the zeroth and first angular moments must be taken of $\psi^{(0)}$, $\psi^{(1)}$, and $\psi^{(2)}$, which are determined from equations (III.13a) - (III.13c):

$\underline{\mathcal{O}(\epsilon^{(0)})}$

$$\psi^{(0)} = \frac{\phi^{(0)}}{4\pi}\,, \tag{III.15a}$$

$\underline{\mathcal{O}(\epsilon^{(1)})}$

$$\psi^{(1)} = -\frac{\mu}{\sigma_t}\partial_x\psi^{(0)} + \frac{1}{4\pi}\phi^{(1)}\,, \tag{III.15b}$$

$\underline{\mathcal{O}(\epsilon^{(2)})}$

$$\psi^{(2)} = -\frac{1}{v\sigma_t}\partial_t\psi^{(0)} - \frac{\mu}{\sigma_t}\partial_x\psi^{(1)} + \frac{1}{4\pi}\phi^{(2)} - \frac{\sigma_a}{4\pi\sigma_t}\phi^{(0)} + \frac{Q}{4\pi\sigma_t}\,. \tag{III.15c}$$

The necessary zeroth and first angular moments of these angular flux solutions are:

$\underline{\mathcal{O}(\epsilon^{(0)})}$

$$\phi^{(0)} = \phi^{(0)}\,, \tag{III.16a}$$

$$J^{(0)} = 0\,, \tag{III.16b}$$

$\underline{\mathcal{O}(\epsilon^{(1)})}$

$$\phi^{(1)} = \phi^{(1)}\,, \tag{III.16c}$$

$$J^{(1)} = -\frac{1}{3\sigma_t}\partial_x\phi^{(0)}\,, \tag{III.16d}$$

$\underline{\mathcal{O}(\epsilon^{(2)})}$

$$J^{(2)} = -\frac{1}{3\sigma_t}\partial_x\phi^{(1)}\,. \tag{III.16e}$$

Using these results in equations (III.14) produces the leading- and first-order asymptotic neutron diffusion equations,

$\underline{\mathcal{O}(\epsilon^{(0)})}$

$$\frac{1}{v}\partial_t\phi^{(0)} - \partial_x\frac{1}{3\sigma_t}\partial_x\phi^{(0)} + \sigma_a\phi^{(0)} = Q\,, \tag{III.17a}$$

$\underline{\mathcal{O}(\epsilon^{(1)})}$

$$\frac{1}{v}\partial_t\phi^{(1)} - \partial_x\frac{1}{3\sigma_t}\partial_x\phi^{(1)} + \sigma_a\phi^{(1)} = 0\,. \tag{III.17b}$$

For notational convenience we write the first-order expansion of a variable as

$$\phi^{[1]} \equiv \phi^{(0)} + \epsilon\phi^{(1)}\,, \tag{III.18}$$

such that the term in brackets represents the order of expansion. Then, equations (III.17) can be summed

$$\frac{1}{v}\partial_t\phi^{[1]} - \partial_x\frac{1}{3\sigma_t}\partial_x\phi^{[1]} + \sigma_a\phi^{[1]} = Q\,, \tag{III.19}$$

and the asymptotic neutron transport equation (III.11) has been used to reproduce the neutron diffusion equation through first-order, and we say that the asymptotic neutron transport solutions satisfy the neutron diffusion equation (III.4) through first-order. This is the highest-order at which the asymptotic solutions of the neutron transport equation satisfy the neutron diffusion approximation. Thus, for a physical model, or a valid discretization, associated with the neutron transport equation to fully preserve the neutron diffusion limit their asymptotic solutions must preserve the neutron diffusion equation through first-order. Then, we say that the model, or the discretization, preserves the diffusion limit. In this case, the diffusion approximation is valid under the discretization. If two different physical models independently preserve the diffusion limit, then we say that these models are equivalent in the diffusion limit.

The various discretizations used to computationally solve the neutron transport equation give quantitatively different solutions to the diffusion equation, and some of the solutions are even qualitatively different, especially near the boundaries. Larsen, Morel and Miller [12] and Larsen and Morel [13] used asymptotic analysis to predict

when and which discretizations preserve the neutron diffusion limit; some discretizations preserve the diffusion limit in certain limiting circumstances and to certain orders in the expansion parameter. They then presented computational results from the discretized solutions of the neutron diffusion equation. The asymptotic analysis predictions are in agreement with the computational results, and provided guidance to understand the distinctions between, and weaknesses, of the individual discretizations.

Similar asymptotic analysis work was performed for the equations of radiative transfer, which manifest the equilibrium diffusion approximation (EDA), and defined the scalings of the equilibrium diffusion limit (EDL). This coupled, non-linear, set of differential equations does not simplify to a single diffusion equation, but various discretizations of these equations have been used to solve diffusive problems, again, with quantitatively and sometimes qualitatively different solutions. Morel used asymptotic analysis to show that the coupled equations satisfy the EDA through first-order. Morel then applied asymptotic analysis to various discretizations to predict which preserved the EDL and under what circumstances, or at what order a discretization failed to preserve the EDL. Olson, Auer and Hall computationally tested the accuracy of these discretizations against the analytic time-dependent Su-Olson radiative transfer problem [47], which uses a constant opacity, and against a problem in which the opacity varies with temperature as T^{-3} and the heat capacity is constant, analogous to an ideal gas. The S_8 transport solution with a variable Eddington factor was used as the exact answer for this problem. While these two problems do not have an analytic equilibrium-diffusion solution, and they pose boundary limits, they do test similar important physics. Invariably, the discretizations which preserved the EDL were more accurate in both problems.

The EDA of RH was considered by Lowrie, Morel and Hittinger [11], but they only presented results showing that it was satisfied through leading-order, and left for future work whether the EDL was fully satisfied through first-order. The work by Sekora and Stone [35], which describes a 1-D hybrid Godunov scheme for RH, performed self-similar convergence tests, analogous to the work of Larsen, Morel and Miller [12], to ensure that their scheme preserved the EDL to the level presented in [11]. The results in this Chapter extend the work in [11].

The RH equations, used in this chapter, are

$$\partial_t \rho + \partial_i \left(\rho u_i\right) = 0 \tag{III.20a}$$

$$\partial_t \left(\rho u_i + \frac{1}{c^2}\mathcal{F}_i\right) + \partial_j \left(\rho u_i u_j + p_{ij} + \mathcal{P}_{ij}\right) = 0 \tag{III.20b}$$

$$\partial_t \left(\frac{1}{2}\rho u^2 + \rho e + \mathcal{E}\right) + \partial_i \left[u_j \left(\frac{1}{2}\rho u_i u_j + \rho e \delta_{ij} + p_{ij}\right) + \mathcal{F}_i\right] = 0 \tag{III.20c}$$

$$\begin{aligned}
&\frac{1}{c}\partial_t I_\nu + \Omega_i \partial_i I_\nu = \sigma_t B_\nu - \sigma_t I_\nu + \frac{\sigma_s}{4\pi}\left(\phi_\nu - 4\pi B_\nu\right) \\
&+ \beta_i \Omega_i \left(\sigma_t I_\nu + I_\nu \nu \partial_\nu \sigma_t + 2\sigma_t B_\nu - \nu \partial_\nu \left(\sigma_t B_\nu\right)\right) \\
&+ \frac{\sigma_s}{4\pi}\beta_i \left(\Omega_i \left(2\phi_\nu - 8\pi B_\nu - \nu \partial_\nu \phi_\nu + \nu \partial_\nu B_\nu\right) - F_{i,\nu} + \nu \partial_\nu F_{i,\nu}\right) \\
&- \frac{1}{2}\beta_i \beta_j \left(\sigma_t \delta_{ij} I_\nu + \delta_{ij} I_\nu \nu \partial_\nu \sigma_t + \Omega_i \Omega_j I_\nu \nu^2 \partial_\nu^2 \sigma_t\right) \\
&+ \beta_i \beta_j \left(\left(3\Omega_i \Omega_j - \delta_{ij}\right)\sigma_t B_\nu + \left(\frac{1}{2}\delta_{ij} - 3\Omega_i \Omega_j\right)\nu \partial_\nu \left(\sigma_t B_\nu\right) + \frac{1}{2}\Omega_i \Omega_j \nu^2 \partial_\nu^2 \left(\sigma_t B_\nu\right)\right) \\
&+ \frac{\sigma_s}{4\pi}\beta_i \beta_j \left(\left(3\Omega_i \Omega_j - \frac{1}{2}\delta_{ij}\right)\phi_\nu - 2\Omega_i \Omega_j \nu \partial_\nu \phi_\nu - 2\Omega_i F_{j,\nu} + 2\Omega_i \nu \partial_\nu F_{j,\nu}\right) \\
&- \sigma_s \beta_i \beta_j \left(\left(3\Omega_i \Omega_j - \delta_{ij}\right) B_\nu - \left(\frac{1}{2}\delta_{ij} - 3\Omega_i \Omega_j\right)\nu \partial_\nu B_\nu + \frac{1}{2}\Omega_i \Omega_j \nu^2 \partial_\nu^2 B_\nu\right).
\end{aligned} \tag{III.20d}$$

In Section III.2, the equations are nondimensionalized, and nondimensional scaling ratios are defined. In Section III.3, the asymptotic expansion of the RH equations is

performed, and it is shown that the asymptotic solutions of the RH equations satisfy the EDA through $\mathcal{O}(\epsilon)$. In Section III.4, the validity of the lab- and comoving-frame P_1 and diffusion models, in the EDL, are compared.

III.2 Nondimensional variables and scaling ratios

It is useful, before beginning the asymptotic expansion, to nondimensionalize the RH equations, group the dimensional variables, and define scaling ratios with respect to the asymptotically small parameter ϵ. Each dimensional variable is decomposed into the product of a variable containing the dimension with subscript-∞, and a hatted-$\hat{}$ variable containing a characteristic value of the variable. This decomposition for the RH variables is

$$x = \hat{x}\, l_\infty \,, \tag{III.21a}$$

$$u = \hat{u}\, u_\infty \,, \tag{III.21b}$$

$$t = \hat{t}\, \frac{l_\infty}{u_\infty} \,, \tag{III.21c}$$

$$\rho = \hat{\rho}\, \rho_\infty \,, \tag{III.21d}$$

$$p = \hat{p}\, \rho_\infty u_\infty^2 \,, \tag{III.21e}$$

$$e = \hat{e}\, u_\infty^2 \,, \tag{III.21f}$$

$$\sigma_t = \hat{\sigma}_t\, \sigma_{t,\infty} \,, \tag{III.21g}$$

$$\sigma_s = \hat{\sigma}_s\, \sigma_{s,\infty} \,, \tag{III.21h}$$

$$I_\nu = \hat{I}_\nu\, \frac{a_r c h T_\infty^3}{k_B} \,, \tag{III.21i}$$

$$\nu = \hat{\nu}\, \frac{k_B T_\infty}{h} \,, \tag{III.21j}$$

where l_∞ is a reference length, u_∞ is a reference speed typically assumed to be the speed of sound, ρ_∞ is a reference density, $\sigma_{t,\infty}$ and $\sigma_{s,\infty}$ are reference total and scattering cross-sections, respectively, T_∞ is a reference temperature, a_r is the radiation constant, c is the speed of light, h is Planck's constant, and k_B is Boltzmann's constant. The definition of the radiation intensity, and the frequency, are chosen such that the definitions for the radiation energy density, radiation flux, and radiation pressure are sensible:

$$\mathcal{E} = \frac{1}{c}\int_0^\infty \int_{4\pi} \hat{I}_\nu \frac{a_r c h T_\infty^3}{k_B} \frac{k_B T_\infty}{h} d\hat{\nu} d\Omega = \hat{\mathcal{E}}\, a_r T_\infty^4 \,, \tag{III.22a}$$

$$\mathcal{F}_i = \int_0^\infty \int_{4\pi} \Omega_i \hat{I}_\nu \frac{a_r c h T_\infty^3}{k_B} \frac{k_B T_\infty}{h} d\hat{\nu} d\Omega = \hat{\mathcal{F}}_i\, a_r c T_\infty^4 \,, \tag{III.22b}$$

$$\mathcal{P}_{ij} = \frac{1}{c}\int_0^\infty \int_{4\pi} \Omega_i \Omega_j \hat{I}_\nu \frac{a_r c h T_\infty^3}{k_B} \frac{k_B T_\infty}{h} d\hat{\nu} d\Omega = \hat{\mathcal{P}}_{ij}\, a_r T_\infty^4 \,. \tag{III.22c}$$

The nondimensional RH equations, with the reference variables collected, and the hats dropped for notational convenience, are

$$\partial_t \rho + \partial_i \left(\rho u_i\right) = 0 \,, \tag{III.23a}$$

$$\partial_t \left(\rho u_i + \frac{u_\infty}{c}\frac{a_r T_\infty^4}{\rho_\infty u_\infty^2}\mathcal{F}_i\right) + \partial_j \left(\rho u_i u_j + p_{ij} + \frac{a_r T_\infty^4}{\rho_\infty u_\infty^2}\mathcal{P}_{ij}\right) = 0 \,, \tag{III.23b}$$

$$\begin{aligned} &\frac{u_\infty}{c}\partial_t \left(\frac{1}{2}\rho u^2 + \rho e + \frac{a_r T_\infty^4}{\rho_\infty u_\infty^2}\mathcal{E}\right) \\ &\qquad + \partial_i \left(\frac{u_\infty}{c} u_j \left(\frac{1}{2}\rho u_i u_j + \rho e \delta_{ij} + p_{ij}\right) + \frac{a_r T_\infty^4}{\rho_\infty u_\infty^2}\mathcal{F}_i\right) = 0 \,, \end{aligned} \tag{III.23c}$$

$$\begin{aligned} &\frac{1}{l_\infty \sigma_{t,\infty}}\left(\frac{u_\infty}{c}\partial_t I_\nu + \Omega_i \partial_i I_\nu\right) = \sigma_t B_\nu - \sigma_t I_\nu + \frac{\sigma_{s,\infty}}{\sigma_{t,\infty}}\frac{\sigma_s}{4\pi}\left(\phi_\nu - 4\pi B_\nu\right) \\ &+ \frac{u_\infty}{c} u_i \Omega_i \left(\sigma_t I_\nu + I_\nu \nu \partial_\nu \sigma_t + 2\sigma_t B_\nu - \nu \partial_\nu \left(\sigma_t B_\nu\right)\right) \\ &+ \frac{\sigma_{s,\infty}}{\sigma_{t,\infty}}\frac{\sigma_s}{4\pi}\frac{u_\infty}{c} u_i \left(\Omega_i \left(2\left(\phi_\nu - 4\pi B_\nu\right) - \nu \partial_\nu \phi_\nu + 4\pi \nu \partial_\nu B_\nu\right) - F_{i,\nu} + \nu \partial_\nu F_{i,\nu}\right) \\ &- \frac{1}{2}\left(\frac{u_\infty}{c}\right)^2 u_i u_j \left(\sigma_t \delta_{ij} I_\nu + \delta_{ij} I_\nu \nu \partial_\nu \sigma_t + \Omega_i \Omega_j I_\nu \nu^2 \partial_\nu^2 \sigma_t\right) \end{aligned}$$

$$+\left(\frac{u_\infty}{c}\right)^2 u_i u_j \left(\left(3\Omega_i\Omega_j - \delta_{ij}\right)\sigma_t B_\nu + \left(\frac{1}{2}\delta_{ij} - 3\Omega_i\Omega_j\right)\nu\partial_\nu\left(\sigma_t B_\nu\right) + \frac{1}{2}\Omega_i\Omega_j\nu^2\partial_\nu^2\left(\sigma_t B_\nu\right)\right)$$
$$+\frac{\sigma_{s,\infty}}{\sigma_{t,\infty}}\frac{\sigma_s}{4\pi}\left(\frac{u_\infty}{c}\right)^2 u_i u_j \left(\left(3\Omega_i\Omega_j - \frac{1}{2}\delta_{ij}\right)\phi_\nu - 2\Omega_i\Omega_j\nu\partial_\nu\phi_\nu - 2\Omega_i F_{j,\nu} + 2\Omega_i\nu\partial_\nu F_{j,\nu}\right)$$
$$-\frac{\sigma_{s,\infty}}{\sigma_{t,\infty}}\sigma_s\left(\frac{u_\infty}{c}\right)^2 u_i u_j \left(\left(3\Omega_i\Omega_j - \delta_{ij}\right)B_\nu - \left(\frac{1}{2}\delta_{ij} - 3\Omega_i\Omega_j\right)\nu\partial_\nu B_\nu + \frac{1}{2}\Omega_i\Omega_j\nu^2\partial_\nu^2 B_\nu\right). \tag{III.23d}$$

Four ratios of dimensional reference variables occur in the equations above,

$$\frac{u_\infty}{c}, \tag{III.24a}$$
$$\frac{a_r T_\infty^4}{\rho_\infty u_\infty^2}, \tag{III.24b}$$
$$\frac{\sigma_{s,\infty}}{\sigma_{t,\infty}}, \tag{III.24c}$$
$$\frac{1}{l_\infty\sigma_{t,\infty}}, \tag{III.24d}$$

such that the dimensionless scaling ratios, and their scalings with the asymptotically small parameter ϵ, are defined as:

$$\mathcal{U} = \frac{u_\infty}{c} = \mathcal{O}(\epsilon), \tag{III.25a}$$
$$P_0 = \frac{a_r T_\infty^4}{\rho_\infty u_\infty^2} = \mathcal{O}(1), \tag{III.25b}$$
$$\mathcal{L}_s = \frac{\sigma_{s,\infty}}{\sigma_{t,\infty}} = \mathcal{O}(\epsilon), \tag{III.25c}$$
$$\mathcal{L} = l_\infty\sigma_{t,\infty} = \mathcal{O}\left(\frac{1}{\epsilon}\right). \tag{III.25d}$$

The first scaling is appropriate to nonrelativistic physics, and says that the material reference velocity is small compared to the speed of light, and hence scales as ϵ. The second scaling is a measure of the strength of the radiation energy compared to the material kinetic energy, and scaling it as a constant means that no assumptions are

made as to its size. This scaling may be chosen to be small, in which case radiation effects are expected to be negligible, or it may be chosen to be large and radiation effects are expected to dominate fluid flow. The third scaling is a measure of the ratio of the scattering cross-section to the total cross-section, which is assumed to be small; thus absorption dominates scattering. It is this scaling that is traditionally used in physical considerations of diffusion [48, 49], and since diffusion is correct through a linear-power of this ratio it is necessary to expand the RH equations at least through $\mathcal{O}(\epsilon)$. The fourth scaling is a measure of the system reference length compared to the radiation mean-free-path for interaction. It is assumed that the radiation travels a very short distance between each interaction, such that the ratio of the system size to the mean-free-path is very large, and scales inversely to ϵ. These scalings define the EDL.

III.3 Asymptotic expansion of the radiation hydrodynamic equations

Upon implementing the scaling ratios (III.24), and their scalings (III.25), in the nondimensional RH equations (III.23), it is helpful to consider the first three RH equations separately from the radiation transport equation (III.23d), which will be considered shortly. The scaled, redimensionalized, equations of mass, momentum, and energy conservation, are

$$\partial_t \rho + \partial_i \left(\rho u_i\right) = 0 \,, \tag{III.26a}$$

$$\partial_t \left(\rho u_i\right) + \partial_j \left(\rho u_i u_j + p_{ij}\right) = -\epsilon \partial_t \mathcal{F}_i - \partial_j \mathcal{P}_{ij} \,, \tag{III.26b}$$

$$\epsilon \left[\partial_t \left(\frac{1}{2}\rho u^2 + \rho e\right) + \partial_i \left(u_j \left(\frac{1}{2}\rho u_i u_j + \rho e \delta_{ij} + p_{ij}\right)\right)\right] = -\epsilon \partial_t \mathcal{E} - \partial_i \mathcal{F}_i \,. \tag{III.26c}$$

The energy conservation equation, at $\mathcal{O}(\epsilon^0)$, implies that the leading-order radiation flux should be zero when calculated from the radiation transport equation since the radiation flux is the only variable at $\mathcal{O}(\epsilon^0)$. It is known from the work of Lowrie, Morel and Hittinger [11] that this is correct. This corresponds to a state *near* equilibrium. Using this information in the momentum conservation equation, through $\mathcal{O}(\epsilon)$, implies that the time derivative of the radiation flux disappears, in agreement with a diffusion approximation.

An asymptotic power-series expansion is assumed for the RH variables:

$$\rho = \sum_{n=0}^{\infty} \rho^{(n)} \epsilon^n \,, \tag{III.27a}$$

$$u_i = \sum_{n=0}^{\infty} u_i^{(n)} \epsilon^n \,, \tag{III.27b}$$

$$p_{ij} = \sum_{n=0}^{\infty} p_{ij}^{(n)} \epsilon^n \,, \tag{III.27c}$$

$$e = \sum_{n=0}^{\infty} e^{(n)} \epsilon^n \,, \tag{III.27d}$$

$$T = \sum_{n=0}^{\infty} T^{(n)} \epsilon^n \,, \tag{III.27e}$$

$$T^4 = \sum_{n=0}^{\infty} T^{(n),4} \epsilon^n \,, \tag{III.27f}$$

$$\sigma_t = \sum_{n=0}^{\infty} \sigma_t^{(n)} \epsilon^n \,, \tag{III.27g}$$

$$\sigma_s = \sum_{n=0}^{\infty} \sigma_s^{(n)} \epsilon^n \,, \tag{III.27h}$$

$$I_\nu = \sum_{n=0}^{\infty} I_\nu^{(n)} \epsilon^n \,, \tag{III.27i}$$

$$B_\nu = \sum_{n=0}^{\infty} B_\nu^{(n)} \epsilon^n \,. \tag{III.27j}$$

In accordance with the comment above that asymptotic solutions of the diffusion equation only satisfy the diffusion approximation through $\mathcal{O}(\epsilon)$, the leading- and first-order expansions of the conservation RH equations are:

$\underline{\mathcal{O}(\epsilon^{(0)})}$

$$\left[\partial_t \rho + \partial_i \left(\rho u_i\right)\right]^{(0)} = 0\,, \tag{III.28a}$$

$$\left[\partial_t \left(\rho u_i\right) + \partial_j \left(\rho u_i u_j + p_{ij}\right)\right]^{(0)} = -\partial_j \mathcal{P}_{ij}^{(0)}\,, \tag{III.28b}$$

$$\left[\partial_t \left(\frac{1}{2}\rho u^2 + \rho e\right) + \partial_i \left(u_j \left(\frac{1}{2}\rho u_i u_j + \rho e \delta_{ij} + p_{ij}\right)\right)\right]^{(0)} = -\partial_t \mathcal{E}^{(0)} - \partial_i \mathcal{F}_i^{(1)}\,, \tag{III.28c}$$

$\underline{\mathcal{O}(\epsilon^{(1)})}$

$$\left[\partial_t \rho + \partial_i \left(\rho u_i\right)\right]^{(1)} = 0\,, \tag{III.28d}$$

$$\left[\partial_t \left(\rho u_i\right) + \partial_j \left(\rho u_i u_j + p_{ij}\right)\right]^{(1)} = -\partial_t \mathcal{F}_i^{(0)} - \partial_j \mathcal{P}_{ij}^{(1)}\,, \tag{III.28e}$$

$$\left[\partial_t \left(\frac{1}{2}\rho u^2 + \rho e\right) + \partial_i \left(u_j \left(\frac{1}{2}\rho u_i u_j + \rho e \delta_{ij} + p_{ij}\right)\right)\right]^{(1)} = -\partial_t \mathcal{E}^{(1)} - \partial_i \mathcal{F}_i^{(2)}\,. \tag{III.28f}$$

The asymptotic terms of $\mathcal{E}$, $\mathcal{F}$ and $\mathcal{P}$ on the RHS of equations (III.28) are evaluated in Appendix D. The results are:

$\underline{\mathcal{O}(\epsilon^{(0)})}$

$$\mathcal{E}^{(0)} = a_r T^{(0),4}\,, \tag{III.29a}$$

$$\mathcal{F}_i^{(0)} = 0\,, \tag{III.29b}$$

$$\mathcal{P}_{ij}^{(0)} = \frac{1}{3}\mathcal{E}^{(0)}\,, \tag{III.29c}$$

$\underline{\mathcal{O}(\epsilon^{(1)})}$

$$\mathcal{E}^{(1)} = a_r T^{(1),4}\,, \tag{III.29d}$$

$$\mathcal{F}_i^{(1)} = \left[-\frac{a_r c}{3\sigma_{t,R}}\partial_i T^4 + \frac{4}{3}a_r u_i T^4\right]^{(0)}\,, \tag{III.29e}$$

$$\mathcal{P}_{ij}^{(1)} = \frac{1}{3}\mathcal{E}^{(1)}\,, \tag{III.29f}$$

$\underline{\mathcal{O}(\epsilon^{(2)})}$

$$\mathcal{F}_i^{(2)} = \left[-\frac{a_r c}{3\sigma_{t,R}}\partial_i T^4 + \frac{4}{3}a_r u_i T^4\right]^{(1)}\,, \tag{III.29g}$$

where $\sigma_{t,R}$ is the Rosseland mean opacity, defined in Appendix D. The radiation variables can now be written through $\mathcal{O}(\epsilon)$, according to equation (III.27), and recalling equation (III.18):

$$\mathcal{E}^{[1]} = \mathcal{E}^{(0)} + \mathcal{E}^{(1)}\epsilon = a_r T^{(0),4} + a_r T^{(1),4}\epsilon = a_r T^{[1],4}\,, \tag{III.30a}$$

$$\begin{aligned}\mathcal{F}_i^{[1]} = \mathcal{F}_i^{(0)} + \mathcal{F}_i^{(1)}\epsilon &= \left[-\frac{a_r c}{3\sigma_{t,R}}\partial_i T^4 + \frac{4}{3}a_r u_i T^4\right]^{(0)} + \left[-\frac{a_r c}{3\sigma_{t,R}}\partial_i T^4 + \frac{4}{3}a_r u_i T^4\right]^{(1)}\epsilon \\ &= \left[-\frac{a_r c}{3\sigma_{t,R}}\partial_i T^4 + \frac{4}{3}a_r u_i T^4\right]^{[1]}\,,\end{aligned} \tag{III.30b}$$

$$\mathcal{P}_{ij}^{[1]} = \mathcal{P}_{ij}^{(0)} + \mathcal{P}_{ij}^{(1)}\epsilon = \frac{1}{3}a_r T^{(0),4} + \frac{1}{3}a_r T^{(1),4}\epsilon = \frac{1}{3}a_r T^{[1],4}\,. \tag{III.30c}$$

Similarly, the three RH conservation equations, through $\mathcal{O}(\epsilon)$, are:

$$\left\{\partial_t \rho + \partial_i\left(\rho u_i\right)\right\}^{[1]} = 0\,, \tag{III.31a}$$

$$\left\{\partial_t\left(\rho u_i\right) + \partial_j\left(\rho u_i u_j + p_{ij} + \frac{1}{3}a_r T^4 \delta_{ij}\right)\right\}^{[1]} = 0\,, \tag{III.31b}$$

$$\left\{\partial_t\left(\frac{1}{2}\rho u^2 + \rho e + a_r T^4\right)\right.$$

$$+\partial_i \left[u_j \left(\frac{1}{2}\rho u_i u_j + \left(\rho e + \frac{4}{3} a_r T^4 \right) \delta_{ij} + p_{ij} \right) - \frac{a_r c}{3\sigma_{t,R}} \partial_i T^4 \right] \Bigg\}^{[1]} = 0 \quad \text{(III.31c)}$$

The radiation variables have been returned to the LHS to make obvious the conservative nature of the equations. In the momentum conservation equation, there is no time-derivative of a radiation flux, which is representative of a diffusion approximation. The terms containing T^4 represent either the radiation pressure $\mathcal{P}_{ij} = \frac{1}{3} a_r T^4 \delta_{ij}$, the radiation energy density $\mathcal{E} = a_r T^4$, or their dyadic sum $\mathcal{P}_{ij} + \mathcal{E}\delta_{ij} = \frac{4}{3} a_r T^4 \delta_{ij}$. Thus, the radiation pressure takes on the *lab-frame* P_1 approximation, which was defined in Chapter II for radiation interacting with a material *at rest*, recall that the P_1 approximation is typically assumed in the diffusion approximation, and the radiation energy density is in equilibrium with material at temperature T. The material pressure and the radiation pressure, as well as the material internal energy density and the radiation energy density, can be written as a total pressure and a total internal energy density,

$$p^*_{ij} = p_{ij} + \frac{1}{3} a_r T^4 \delta_{ij} \,, \quad \text{(III.32a)}$$

$$e^* = e + \frac{a_r T^4}{\rho} \,. \quad \text{(III.32b)}$$

Finally, two special cases of diffusion are considered, which are defined for particular values of the product $\beta\tau$, when the individual terms are held to the limits, $\beta \ll 1$ and $\tau \gg 1$:

$$\beta\tau = \frac{u_\infty}{c} \frac{l_\infty}{\lambda_{t,\infty}} \ll 1 \,, \quad \text{static diffusion,} \quad \text{(III.33a)}$$

$$\beta\tau = \frac{u_\infty}{c} \frac{l_\infty}{\lambda_{t,\infty}} \gtrsim 1 \,, \quad \text{dynamic diffusion,} \quad \text{(III.33b)}$$

where $\tau \equiv l_\infty \sigma_{t,\infty} = l_\infty/\lambda_\infty$ represents the optical depth of the system. Based on the scaling ratios (III.25), the product $\beta\tau = \mathcal{UL} = \mathcal{O}(\epsilon)/\mathcal{O}(\epsilon)$ scales as $\mathcal{O}(1)$ in the EDL, such that the analysis above holds both limits. Formally, these ratios are represented as the ratio of the diffusion time-scale to the fluid time-scale, t_d/t_f. The diffusion time-scale is set by the average number of diffusive interactions such that a photon will travel a distance l_∞, multiplied by the time between two interactions, $t_d \sim (l_\infty^2/\lambda_t^2)(\lambda_t/c)$. The fluid time-scale is set by the size of the system and some reference fluid speed, $t_f \sim l_\infty/u_\infty$. Static diffusion holds when the material velocity, as a fraction of the speed of light, is significantly less than the photon mean-free-path compared to the system size; that is, when the diffusion time-scale is small compared to the fluid time-scale. This is the situation most often associated with diffusion. The radiation is locally trapped in the fluid and develops on its own time-scale. Dynamic diffusion holds when the *non-relativistic* material velocity, as a fraction of the speed of light, is slightly larger than the ratio of the photon mean-free-path to the system size; that is, when the diffusion time-scale is slightly larger than fluid time-scale. In this case the radiation is advected by the fluid, and the fluid can dynamically drive local changes in the radiation field on a time-scale faster than the radiation's diffusion time-scale.

III.4 P_1 and diffusion models in the lab- and comoving-frames in the equilibrium diffusion limit

In this section, the lab-frame and comoving-frame variants of two physical models are compared in the EDL. First, the radiation energy and momentum equations are Lorentz transformed, as a four-vector, to the comoving-frame, then the physical model is imposed, and the equations are Lorentz transformed back to the lab-frame.

We call this the comoving-frame approximation of the physical model. To obtain the lab-frame approximation of the physical model, we simply impose the physical model on the lab-frame radiation energy and momentum equations. The comoving-frame and lab-frame approximations are compared in the EDL, and it is shown that the comoving-frame and lab-frame physical models are equivalent in the EDL. The two physical models we consider, in the next two subsections, are the P_1 approximation and the grey-diffusion approximation, which were introduced in Chapter II.

The lab-frame radiation energy and momentum equations are:

$$\partial_t \mathcal{E} + \partial_i \mathcal{F}_i = S_{re}\,, \tag{III.34a}$$

$$\partial_t \mathcal{F}_i + \partial_j \mathcal{P}_{ij} = S_{rp,i}\,. \tag{III.34b}$$

To Lorentz transform the radiation source rate equations to the comoving-frame, it is not enough to Lorentz transform the individual radiation variables, because the individual equations of radiation energy and momentum are not Lorentz scalars. Instead, the one radiation energy equation, and the three radiation momentum equations, are combined to give a set of four equations, the radiation energy-momentum four-vector, $S_\mu = (S_{re}/c, S_{rp,i})^\intercal$, which is Lorentz transformed, via the Lorentz matrix defined in equation (A.13), from the lab-frame to the comoving-frame, $(S_o)_\nu = \Lambda^\mu{}_\nu S_\mu$. Similarly, the radiation variables can be combined to form the radiation stress-energy tensor

$$P_{\mu\nu} = \begin{pmatrix} \mathcal{E} & \frac{1}{c}\mathcal{F}_i^\intercal \\ \frac{1}{c}\mathcal{F}_i & \mathcal{P}_{ij} \end{pmatrix}\,, \tag{III.35}$$

which is Lorentz transformed in an analogous manner to the energy-momentum four-vector $(P_o)_{\mu\nu} = \Lambda^{\sigma}{}_{\nu} P_{\rho\sigma} \Lambda_{\mu}{}^{\rho}$, where $\Lambda_{\mu}{}^{\rho} \equiv (\Lambda^{\mu}{}_{\rho})^{\intercal} = \Lambda^{\mu}{}_{\rho}$ due to the symmetry of the Lorentz transformations. The Lorentz matrix, through $\mathcal{O}(\beta)$, is:

$$\mathbf{\Lambda} = \begin{pmatrix} 1 & -\beta_i^{\intercal} \\ -\beta_i & 1 \end{pmatrix} . \tag{III.36}$$

The comoving-frame radiation energy and momentum source rates, written with lab-frame radiation variables, are:

$$S_{o,re} = S_{re} - u_i S_{i,rp} = \partial_t \mathcal{E} + \partial_i \mathcal{F}_i - \frac{u_i}{c^2} \partial_t \mathcal{F}_i - u_i \partial_j \mathcal{P}_{ij} \, , \tag{III.37a}$$

$$S_{o,i,rp} = -\frac{u_i}{c^2} S_{re} + S_{i,rp} = -\frac{u_i}{c^2} \partial_t \mathcal{E} - \frac{u_i}{c^2} \partial_j \mathcal{F}_j + \frac{1}{c^2} \partial_t \mathcal{F}_i + \partial_j \mathcal{P}_{ij} \, . \tag{III.37b}$$

The Lorentz transformations of the lab-frame radiation variables to the comoving-frame are:

$$\mathcal{E} = \mathcal{E}_o + 2 \frac{u_i}{c^2} \mathcal{F}_{o,i} \, , \tag{III.38a}$$

$$\mathcal{F}_i = \mathcal{F}_{o,i} + u_j \left(\mathcal{E}_o \delta_{ij} + \mathcal{P}_{o,ij} \right) \, , \tag{III.38b}$$

$$\mathcal{P}_{ij} = \mathcal{P}_{o,ij} + \frac{u_i}{c^2} \mathcal{F}_{o,j} + \frac{u_j}{c^2} \mathcal{F}_{o,i} \, . \tag{III.38c}$$

The Lorentz transformations of the radiation variables can be quickly reversed by simply reversing the direction of the velocity, i.e., $u_i \rightarrow -u_i$. The comoving-frame radiation energy and momentum source rate equations can now be written in terms of the comoving-frame radiation variables, through $\mathcal{O}(\beta)$,

$$S_{o,re} = \partial_t \mathcal{E}_o + \frac{1}{c^2} \partial_t \left(u_i \mathcal{F}_{o,i} \right) + \frac{a_i}{c^2} \mathcal{F}_{o,i} + \partial_i \mathcal{F}_{o,i} + \partial_i \left(u_i \mathcal{E}_o \right) + \mathcal{P}_{o,ij} \partial_j u_i \, , \tag{III.39a}$$

$$S_{o,i,rp} = \frac{1}{c^2}\partial_t \mathcal{F}_{o,i} + \frac{a_i}{c^2}\mathcal{E}_o + \frac{1}{c^2}\partial_t \left(u_j \mathcal{P}_{o,ij}\right) + \partial_j \mathcal{P}_{o,ij} + \frac{1}{c^2}\mathcal{F}_{o,j}\partial_j u_i + \frac{1}{c^2}\partial_j \left(u_j \mathcal{F}_{o,i}\right) , \quad \text{(III.39b)}$$

where $a_i = \partial_t u_i$. These equations agree with Castor's equations (6.47) and (6.48) [49], and represent the comoving-frame radiation energy and momentum equations to which the comoving-frame P_1 and diffusion approximations will be applied in the next two sections.

III.4.1 The comoving- and lab-frame P_1 models

In this subsection, the comoving- and lab-frame P_1 approximations are applied to the comoving- and lab-frame radiation energy and momentum source rate equations, (III.34) and (III.39), respectively, and compared. The comoving-frame equations are Lorentz transformed to the lab-frame, and the effect of the comoving-frame approximation on the lab-frame radiation pressure is determined. The EDL is applied to this lab-frame radiation pressure, and it is determined that, in the EDL, the comoving-frame P_1 approximation implies the lab-frame P_1 approximation. The lab-frame P_1 approximation is also investigated, and it is determined that the difference between it and the lab-frame radiation pressure, due to the comoving-frame P_1 approximation, is a traceless symmetric dyad, which is $\mathcal{O}(\epsilon^2)$. Thus, in the EDL, the comoving- and lab-frame P_1 approximations produce identical models through $\mathcal{O}(\epsilon)$.

The comoving-frame P_1 approximation assumes that the comoving-frame radiation intensity is weakly anisotropic, $|F_{o,i,\nu}| \ll \phi_{o,\nu}$, and linear in the comoving-frame angle,

$$I_{o,\nu} = \frac{1}{4\pi}\left(\phi_{o,\nu} + 3\Omega_{o,i}F_{o,i,\nu}\right) , \quad \text{(III.40)}$$

where $\phi_{o,\nu}$ and $F_{o,i,\nu}$ are the zeroth and first angular-moments of the radiation intensity as defined in Chapter II. The result of angle- and frequency-integrating this comoving-frame radiation intensity is that the radiation pressure is related to the radiation energy density via the comoving-frame Eddington approximation,

$$\mathcal{P}_{o,ij} = \frac{1}{3}\mathcal{E}_o\delta_{ij}\,. \tag{III.41}$$

Applying the comoving-frame P_1 approximation to the comoving-frame radiation source rate equations (III.39), produces

$$S_{o,re} = \partial_t\mathcal{E}_o + \frac{1}{c^2}\partial_t\left(u_i\mathcal{F}_{o,i}\right) + \frac{a_i}{c^2}\mathcal{F}_{o,i} + \partial_i\mathcal{F}_{o,i} + \partial_i\left(u_i\mathcal{E}_o\right) + \frac{1}{3}\mathcal{E}_o\partial_i u_i\,, \tag{III.42a}$$

$$\begin{aligned} S_{o,i,rp} = {} & \frac{1}{c^2}\partial_t\mathcal{F}_{o,i} + \frac{a_i}{c^2}\mathcal{E}_o + \frac{1}{3c^2}\partial_t\left(u_i\mathcal{E}_o\right) \\ & + \frac{1}{3}\partial_i\mathcal{E}_o + \frac{1}{c^2}\mathcal{F}_{o,j}\partial_j u_i + \frac{1}{c^2}\partial_j\left(u_j\mathcal{F}_{o,i}\right)\,, \end{aligned} \tag{III.42b}$$

and transforming the equations, and their radiation variables, back to the lab-frame produces

$$S_{re} = \partial_t\mathcal{E} + \partial_i\mathcal{F}_i + \partial_i\left(\frac{1}{3}u_i\mathcal{E} - u_j\mathcal{P}_{ij}\right)\,, \tag{III.43a}$$

$$\begin{aligned} S_{i,rp} = {} & \frac{1}{c^2}\partial_t\left(\mathcal{F}_i + u_j\left(\frac{1}{3}\mathcal{E}\delta_{ij} - \mathcal{P}_{ij}\right)\right) \\ & + \partial_j\left(\frac{1}{3}\mathcal{E}\delta_{ij} + \frac{1}{c^2}u_i\mathcal{F}_j + \frac{1}{c^2}u_j\mathcal{F}_i - \frac{2}{3c^2}u_k\mathcal{F}_k\delta_{ij})\right)\,. \end{aligned} \tag{III.43b}$$

In further reducing the above equations, it is helpful to consider the effect of the comoving-frame P_1 approximation on the lab-frame radiation pressure. Transforming the comoving-frame radiation energy density, due to the comoving-frame P_1 ap-

proximation, to the lab-frame gives

$$\mathcal{P}_{o,ij} = \frac{1}{3}\mathcal{E}_o\delta_{ij} = \frac{1}{3}\left(\mathcal{E} - \frac{2u_k}{c^2}\mathcal{F}_k\right)\delta_{ij}\,, \tag{III.44}$$

and the comoving-frame radiation pressure written in terms of lab-frame variables is

$$\mathcal{P}_{o,ij} = \mathcal{P}_{ij} - \frac{u_i}{c^2}\mathcal{F}_j - \frac{u_j}{c^2}\mathcal{F}_i\,. \tag{III.45}$$

Therefore, by equating these last two expressions for the comoving-frame radiation pressure, the effect of the comoving-frame P_1 approximation on the lab-frame radiation pressure is that the lab-frame radiation pressure is now decomposed into a symmetric diagonal term and a symmetric traceless dyad,

$$\mathcal{P}_{ij} = \frac{1}{3}\mathcal{E}\delta_{ij} + \frac{1}{c^2}\left(u_i\mathcal{F}_j + u_j\mathcal{F}_i - \frac{2}{3}u_k\mathcal{F}_k\delta_{ij}\right)\,, \tag{III.46a}$$

and further,

$$u_i\left(\frac{1}{3}\mathcal{E}\delta_{ij} - \mathcal{P}_{ij}\right) = \mathcal{O}(\beta^2) \sim \mathcal{O}(\epsilon^2)\,. \tag{III.46b}$$

Recalling the effect of the comoving-frame P_1 approximation on the lab-frame radiation source rate equations (III.43), it is seen that the last term in the radiation momentum source rate equation is the lab-frame radiation pressure under the comoving-frame P_1 approximation (III.46a), and the two terms which are the difference between the lab-frame P_1 approximation multiplied by a velocity are $\mathcal{O}(\epsilon)$, and thus negligible. Thus, the comoving-frame radiation source rate equations (III.39), under the comoving-frame P_1 approximation, transformed to the lab-frame, equa-

tions (III.43), take the form

$$\partial_t \mathcal{E} + \partial_i \mathcal{F}_i = S_{re}\,, \tag{III.47a}$$

$$\frac{1}{c^2}\partial_t \mathcal{F}_i + \partial_j \mathcal{P}_{ij} = S_{i,rp}\,, \tag{III.47b}$$

which are identical to the lab-frame radiation source rate equations (III.34), and where the radiation pressure in the radiation momentum equation assumes the Eddington approximation, through $\mathcal{O}(\epsilon^2)$, as written in equation (III.46a). Finally, the effect of the comoving-frame P_1 approximation on the lab-frame radiation pressure can be asymptotically expanded in the EDL

$$\mathcal{P}_{ij}^{[1]} = \frac{1}{3}\mathcal{E}^{(0)}\delta_{ij} + \epsilon\frac{1}{3}\mathcal{E}^{(1)}\delta_{ij} + \epsilon\frac{1}{c^2}\left[u_i\mathcal{F}_j + u_j\mathcal{F}_i - \frac{2}{3}u_k\mathcal{F}_k\delta_{ij}\right]^{(0)} = \frac{1}{3}\mathcal{E}^{[1]}\delta_{ij}\,, \tag{III.48}$$

where it must be recalled that $\mathcal{F}_i^{(0)} = 0$. Therefore, the comoving-frame P_1 approximation not only preserves the lab-frame source rate equations, it also reproduces the lab-frame P_1 approximation, in the EDL.

Now that the effect of the comoving-frame P_1 approximation on the lab-frame radiation pressure is known, it is worth considering how this is different from the lab-frame P_1 approximation $\mathcal{P}_{ij} = \frac{1}{3}\mathcal{E}\delta_{ij}$. Comparing the lab-frame P_1 approximation to equation (III.46a), the difference is the symmetric traceless dyad $\frac{1}{c^2}\left(u_i\mathcal{F}_j + u_j\mathcal{F}_i - \frac{2}{3}u_k\mathcal{F}_k\delta_{ij}\right)$. As mentioned previously, in the EDL, this tensor is zero through $\mathcal{O}(\epsilon)$. Thus, the comoving-frame P_1 approximation, and the lab-frame P_1 approximation, preserve the EDL.

III.4.2 The comoving- and lab-frame grey-diffusion models

In this context the word "grey" means that the cross-sections are assumed to be frequency-independent. Typically, this is not a terribly valid physical assumption, but it is common and often necessary for practical reasons. The analysis in this subsection for the grey-diffusion approximation largely imitates that of the previous subsection. The comoving- and lab-frame grey-diffusion approximations are applied to the comoving- and lab-frame radiation energy and momentum source rate equations, (III.34) and (III.39), and compared. The EDL is applied to the lab-frame results of these comoving- and lab-frames models, and it is shown that both models preserve the EDL through $\mathcal{O}(\epsilon)$. This subsection concludes the chapter with a discussion on the importance of the results presented in this section.

The grey radiation transport equation through $\mathcal{O}(\beta)$ is taken from Appendix D:

$$\frac{1}{c}\partial_t I_\nu + \Omega_i \partial_i I_\nu = \sigma_t \left(B_\nu - I_\nu\right) + \beta_i \Omega_i \left(\sigma_t I_\nu + 2\sigma_t B_\nu - \sigma_t \nu \partial_\nu B_\nu\right) + \frac{\sigma_s}{4\pi}\left(\phi_\nu - 4\pi B_\nu\right) . \quad \text{(III.49)}$$

The radiation energy and momentum equations, derived from equation (III.49) as the frequency-integrated zeroth and first angular-moments, are

$$\partial_t \mathcal{E} + \partial_i \mathcal{F}_i = \sigma_a c \left(a_r T^4 - \mathcal{E}\right) + \beta_i \sigma_t \mathcal{F}_i \,, \quad \text{(III.50a)}$$

$$\frac{1}{c^2}\partial_t \mathcal{F}_i + \partial_j \mathcal{P}_{ij} = -\frac{\sigma_t}{c}\mathcal{F}_i + \beta_j \sigma_t \left(\mathcal{P}_{ij} + a_r T^4 \delta_{ij}\right) . \quad \text{(III.50b)}$$

Lorentz transforming these equations to the comoving-frame yields:

$$\partial_t \mathcal{E}_o + \frac{1}{c^2}\partial_t \left(u_i \mathcal{F}_{o,i}\right) + \frac{a_i}{c^2}\mathcal{F}_{o,i} + \partial_i \mathcal{F}_{o,i} + \partial_i \left(u_i \mathcal{E}_o\right) + \mathcal{P}_{o,ij}\partial_j u_i$$
$$= \sigma_a c \left(a_r T^4 - \mathcal{E}_o\right) + 2\beta_i \sigma_s \mathcal{F}_{o,i} \,, \quad \text{(III.51a)}$$

$$\frac{1}{c^2}\partial_t \mathcal{F}_{o,i} + \frac{a_i}{c^2}\mathcal{E}_o + \frac{1}{c^2}\partial_t \left(u_j \mathcal{P}_{o,ij}\right) + \partial_j \mathcal{P}_{o,ij} + \frac{1}{c^2}\mathcal{F}_{o,j}\partial_j u_i + \frac{1}{c^2}\partial_j \left(u_j \mathcal{F}_{o,i}\right)$$
$$= -\frac{\sigma_t}{c}\mathcal{F}_{o,i} + \beta_i \sigma_s \left(a_r T^4 - \mathcal{E}_o\right) \,. \quad \text{(III.51b)}$$

The comoving-frame diffusion approximation requires the comoving-frame P_1 approximation, $\mathcal{P}_{o,ij} = \frac{1}{3}\mathcal{E}_o \delta_{ij}$, setting the time-derivative in the radiation momentum equation to zero, and dropping the velocity terms in that equation, which yields a comoving-frame diffusion equation for the radiation flux,

$$\mathcal{F}_{o,i} = -\frac{c}{3\sigma_t}\partial_i \mathcal{E}_o \,. \quad \text{(III.52)}$$

The comoving-frame radiation energy and momentum equations, under the comoving-frame grey-diffusion approximation, are:

$$\partial_t \mathcal{E}_o - \partial_t \frac{1}{3\sigma_t}\beta_i \partial_i \mathcal{E}_o - \frac{a_i}{3c\sigma_t}\partial_i \mathcal{E}_o - \partial_i \frac{c}{3\sigma_t}\partial_i \mathcal{E}_o + \partial_i \left(u_i \mathcal{E}_o\right) + \frac{1}{3}\mathcal{E}_o \partial_i u_i$$
$$= \sigma_a c \left(a_r T^4 - \mathcal{E}_o\right) + 2\beta_i \sigma_s \mathcal{F}_{o,i} \,, \quad \text{(III.53a)}$$

$$\frac{1}{3}\partial_i \mathcal{E}_o = -\frac{\sigma_t}{c}\mathcal{F}_{o,i} \,. \quad \text{(III.53b)}$$

Since the time-derivative in the radiation momentum equation is neglected these equations are not in conservative form. Lorentz transformation of these equations to the lab-frame yields:

$$\partial_t \mathcal{E} - \frac{2}{c}\partial_t \left(\beta_i \mathcal{F}_i\right) - \partial_t \frac{1}{3\sigma_t}\beta_i \partial_i \mathcal{E} - \frac{a_i}{3c\sigma_t}\partial_i \mathcal{E} - \partial_i \frac{c}{3\sigma_t}\partial_i \mathcal{E} + \partial_i \frac{1}{3\sigma_t}\partial_i \left(\beta_j \mathcal{F}_j\right) + \frac{4}{3}\partial_i \left(u_i \mathcal{E}\right)$$

$$= \sigma_a c \left(a_r T^4 - \mathcal{E}\right) + \beta_i \sigma_t \mathcal{F}_i \,, \quad \text{(III.54a)}$$

$$\beta_i \left(\frac{1}{c}\partial_t \mathcal{E} - \partial_j \frac{1}{3\sigma_t}\partial_j \mathcal{E}\right) + \frac{1}{3}\partial_i \mathcal{E} - \frac{1}{3c}\partial_i \left(\beta_j \mathcal{F}_j\right)$$
$$= \beta_i \sigma_a \left(a_r T^4 - \mathcal{E}\right) - \frac{\sigma_t}{c}\mathcal{F}_i + \sigma_t \left(\beta_i \mathcal{E} + \beta_j \mathcal{P}_{ij}\right) \,. \quad \text{(III.54b)}$$

It is helpful to consider the effect of the comoving-frame grey-diffusion approximation on the lab-frame radiation flux, and to recall that the comoving-frame P_1 approximation induces the P_1 approximation in the lab-frame through $\mathcal{O}(\beta) \sim \mathcal{O}(\epsilon)$. Since the only appearance of the lab-frame radiation flux is as the product with the velocity, $u_i \mathcal{F}_i$, and to $\mathcal{O}(\beta)$ this product does not distinguish between the comoving- and lab-frame radiation fluxes, $u_i \mathcal{F}_i = u_i \mathcal{F}_{o,i} + \mathcal{O}(\beta^2)$, then we have the following relation:

$$-\frac{u_i}{3\sigma_t}\partial_i \mathcal{E}_o = \beta_i \mathcal{F}_{o,i} = \beta_i \mathcal{F}_i = -\frac{u_i}{3\sigma_t}\partial_i \mathcal{E} \,. \quad \text{(III.55)}$$

Therefore, the lab-frame radiation energy and momentum equations, under the comoving-frame grey-diffusion approximation, are:

$$\partial_t \mathcal{E} + \beta_i \partial_t \frac{1}{3\sigma_t}\partial_i \mathcal{E} - \partial_i \frac{c}{3\sigma_t}\partial_i \mathcal{E} - \partial_i \frac{2}{3\sigma_t}\partial_i \left(\frac{u_j}{3\sigma_t}\partial_j \mathcal{E}\right) + \frac{4}{3}\partial_i \left(u_i \mathcal{E}\right)$$
$$= \sigma_a c \left(a_r T^4 - \mathcal{E}\right) - \frac{1}{3}u_i \partial_i \mathcal{E} \,, \quad \text{(III.56a)}$$

$$\frac{1}{c}\beta_i \partial_t \mathcal{E} - \beta_i \partial_j \frac{1}{3\sigma_t}\partial_j \mathcal{E} + \frac{1}{3}\partial_i \mathcal{E} + \frac{1}{3}\partial_i \frac{1}{3\sigma_t}\beta_j \partial_j \mathcal{E}$$
$$= \beta_i \sigma_a \left(a_r T^4 - \mathcal{E}\right) - \frac{\sigma_t}{c}\mathcal{F}_i + \frac{4}{3}\sigma_t \beta_i \mathcal{E} \,. \quad \text{(III.56b)}$$

Again, these lab-frame radiation energy and momentum equations are not conservative. In the EDL, the scaled equations are:

$$\epsilon^2\partial_t\mathcal{E}+\epsilon^4\beta_i\partial_t\frac{1}{3\sigma_t}\partial_i\mathcal{E}-\epsilon^2\partial_i\frac{c}{3\sigma_t}\partial_i\mathcal{E}-\epsilon^4\partial_i\frac{2}{3\sigma_t}\partial_i\left(\frac{u_j}{3\sigma_t}\partial_j\mathcal{E}\right)+\epsilon^2\frac{4}{3}\partial_i\left(u_i\mathcal{E}\right)$$
$$=\sigma_t c\left(a_rT^4-\mathcal{E}\right)-\epsilon\sigma_s c\left(a_rT^4-\mathcal{E}\right)-\epsilon\frac{1}{3}u_i\partial_i\mathcal{E}\,, \quad \text{(III.57a)}$$

$$\epsilon^3\frac{1}{c}\beta_i\partial_t\mathcal{E}-\epsilon^3\beta_i\partial_j\frac{1}{3\sigma_t}\partial_j\mathcal{E}+\epsilon\frac{1}{3}\partial_i\mathcal{E}+\epsilon^3\frac{1}{3}\partial_i\frac{1}{3\sigma_t}\beta_j\partial_j\mathcal{E}$$
$$=\epsilon\beta_i\sigma_t\left(a_rT^4+\frac{1}{3}\mathcal{E}\right)-\epsilon^2\beta_i\sigma_s\left(a_rT^4-\mathcal{E}\right)-\frac{\sigma_t}{c}\mathcal{F}_i\,. \quad \text{(III.57b)}$$

The leading-, first, and second-order results can be read from the equations above:

$\underline{\mathcal{O}(\epsilon^{(0)})}$

$$\mathcal{E}^{(0)}=a_rT^{(0),4}\,, \quad \text{(III.58a)}$$

$$\mathcal{F}_i^{(0)}=0\,, \quad \text{(III.58b)}$$

$$\mathcal{P}_{ij}^{(0)}=\frac{1}{3}\mathcal{E}^{(0)}\delta_{ij}\,, \quad \text{(III.58c)}$$

$\underline{\mathcal{O}(\epsilon^{(1)})}$

$$\mathcal{E}^{(1)}=a_rT^{(1),4}\,, \quad \text{(III.58d)}$$

$$\mathcal{F}_i^{(1)}=\left[-\frac{c}{3\sigma_t}\partial_i\mathcal{E}+\frac{4}{3}u_ia_rT^4\right]^{(0)}\,, \quad \text{(III.58e)}$$

$$\mathcal{P}_{ij}^{(1)}=\frac{1}{3}\mathcal{E}^{(1)}\delta_{ij}\,, \quad \text{(III.58f)}$$

$\underline{\mathcal{O}(\epsilon^{(2)})}$

$$\mathcal{F}_i^{(2)}=\left[-\frac{c}{3\sigma_t}\partial_i\mathcal{E}+\frac{4}{3}u_ia_rT^4\right]^{(1)}\,, \quad \text{(III.58g)}$$

where, at first-order in the energy equation, it was used that $u_i\partial_i\mathcal{E}^{(0)} \sim \beta_i\mathcal{F}_i^{(0)} = 0$, and the lab-frame P_1 approximation is induced from the comoving-frame P_1 approximation.

The lab-frame grey-diffusion approximation can be applied to the original lab-frame source rate equations, (III.50), wherein the time-derivative in the momentum equation is set to zero, and the lab-frame P_1 approximation is made, which yields a lab-frame diffusion approximation,

$$\mathcal{F}_i = -\frac{c}{3\sigma_t}\partial_i\mathcal{E} + u_i\left(\frac{1}{3}\mathcal{E} + a_rT^4\right), \tag{III.59}$$

such that the lab-frame radiation energy and momentum equations are:

$$\partial_t\mathcal{E} - \partial_i\frac{c}{3\sigma_t}\partial_i\mathcal{E} = \sigma_a c\left(a_rT^4 - \mathcal{E}\right) - \frac{1}{3}u_i\partial_i\mathcal{E}\,, \tag{III.60a}$$

$$\frac{1}{3}\partial_i\mathcal{E} = -\frac{\sigma_t}{c}\mathcal{F}_i + \beta_i\sigma_t\left(\frac{1}{3}\mathcal{E} + a_rT^4\right). \tag{III.60b}$$

Once again, these equations do not take a conservative form, which is appropriate for the diffusion approximation. Scaling them with the EDL yields,

$$\epsilon^2\partial_t\mathcal{E} - \epsilon^2\partial_i\frac{c}{3\sigma_t}\partial_i\mathcal{E} = \sigma_t c\left(a_rT^4 - \mathcal{E}\right) - \epsilon\sigma_s c\left(a_rT^4 - \mathcal{E}\right) - \epsilon^2\frac{1}{3}u_i\partial_i\mathcal{E}\,, \tag{III.61a}$$

$$\epsilon\frac{1}{3}\partial_i\mathcal{E} = -\frac{\sigma_t}{c}\mathcal{F}_i + \epsilon\beta_i\sigma_t\left(\frac{1}{3}\mathcal{E} + a_rT^4\right). \tag{III.61b}$$

Again, the leading-, first-, and second-order results can be read from the equations above:

$\underline{\mathcal{O}(\epsilon^{(0)})}$

$$\mathcal{E}^{(0)} = a_r T^{(0),4}\,, \tag{III.62a}$$

$$\mathcal{F}_i^{(0)} = 0\,, \tag{III.62b}$$

$$\mathcal{P}_{ij}^{(0)} = \frac{1}{3}\mathcal{E}^{(0)}\delta_{ij}\,, \tag{III.62c}$$

$\underline{\mathcal{O}(\epsilon^{(1)})}$

$$\mathcal{E}^{(1)} = a_r T^{(1),4}\,, \tag{III.62d}$$

$$\mathcal{F}_i^{(1)} = \left[-\frac{c}{3\sigma_t}\partial_i\mathcal{E} + \frac{4}{3}u_i a_r T^4\right]^{(0)}\,, \tag{III.62e}$$

$$\mathcal{P}_{ij}^{(1)} = \frac{1}{3}\mathcal{E}^{(1)}\delta_{ij}\,, \tag{III.62f}$$

$\underline{\mathcal{O}(\epsilon^{(2)})}$

$$\mathcal{F}_i^{(2)} = \left[-\frac{c}{3\sigma_t}\partial_i\mathcal{E} + \frac{4}{3}u_i a_r T^4\right]^{(1)}\,. \tag{III.62g}$$

It must be recalled that the diffusion approximation subsumes the P_1 approximation. These results come from quite different equations than the analysis in Section III.3, where the complete asymptotic analysis was performed. There, the lab-frame RH equations, with no further approximations, were scaled via the EDL, and the asymptotic results were obtained from the radiation transport equation: specifically, the lab-frame P_1 approximation, lab-frame radiation diffusion, and lab-frame equilibrium between the radiation and material. In this Section, the comoving- and lab-frame grey-diffusion approximations were independently applied to the frequency-integrated zeroth and first angular-moments of the radiation transport equation, and the same results were obtained.

The EDA is an important physical concept that guides our understanding of the natural world, especially as it relates to astrophysical observations and terrestrial experiments, c.f., Chapter I. The EDA is a set of approximations that describe the kinetic and dynamic interactions of radiation with matter, which are typically claimed to be true only in the comoving-frame. However, the RH equations that describe these kinetic and dynamic interactions are best written, for reasons of expressing total conservation, in the lab-frame. The EDL scaling of the RH equations shows that the solutions of the RH equations will satisfy the EDA through $\mathcal{O}(\epsilon)$, in agreement with the order accuracy of previous asymptotic analyses of the radiative transfer and neutron transport equations. What the EDL scaling of the RH equations says is, the EDA may be made in *either frame* and the *correct* results are expected through $\mathcal{O}(\beta) \sim \mathcal{O}(\epsilon)$. In the asymptotic analysis given in Section III.3, neither the P_1, nor the grey-diffusion models were assumed. In Section III.4, the P_1 and grey-diffusion models were imposed in the comoving- and lab-frames, individually, and it was shown that their results preserve the EDA. In this sense, *in the EDL*, we consider the comoving-frame P_1 model to be equivalent to the lab-frame P_1 model, and the comoving-frame grey-diffusion model to be equivalent to the lab-frame grey-diffusion model. It is not obvious that there should exist any limit, with material motion, in which these models should be frame invariant.

CHAPTER IV

PREVIOUS ANALYTIC AND SEMI-ANALYTIC RADIATIVE SHOCK SOLUTIONS

There have been few successful attempts to find analytic solutions of the hydrodynamic equations. One solution was obtained by Becker [50] for the steady-state Navier-Stokes equations (Euler equations plus viscosity and heat-conduction) in one planar dimension, with constant viscosity and a Prandtl number P_r, of 3/4. The Prandtl number is proportional to the ratio of viscosity to heat-conduction. Another solution was discovered by Noh [51], for a fluid assuming the ideal-gas equation-of-state with $\gamma = 5/3$, constant velocity flow with infinite strength, moving toward a rigid wall. Coggeshall discovered many distinct solutions using Lie group theory, including solutions with hydrodynamic shocks, and equilibrium diffusion radiative shocks [52]. More recently, Johnson [53] has obtained analytic solutions for $P_r \to 0$ and $P_r \to \infty$. The solutions for $P_r \to 0$ correspond to a solution of the radiation hydrodynamic equations with $P_0 \to 0$. Analytic solutions are critical in aiding code verification, and furthering our understanding of the equations and their results.

Despite the more recent analytic solutions, the theoretical development of RH provided by Zel'dovich and Raizer [3], and Mihalas and Mihalas [4], is fundamental to understanding analytic solutions in RH. These two books are now 50 and 30 years old, respectively, though, and it is expected that their content, while classic, should become dated. Only recently, however, have the ideas expressed in these books been challenged, and extensions beyond the nonequilibrium diffusion model, including the

effect of incorporating radiation transport into RH calculations, been made.

The goal in this Chapter is to review the current state-of-the-art analytic, and semi-analytic, solution methods in 1-D RH. In Section IV.1, physical approximations are assumed of the nonequilibrium diffusion model, resulting in analytic solutions for subcritical ("weak") and supercritical ("strong") shocks [3, 4]. The results show that the radiation energy density is monotonic across the shock profile, and provide a graphical representation of T, $\mathcal{F}$, and p, versus $\eta \equiv 1/\rho$, which is supposed to provide an analytic check on computational solutions of radiative shocks. In Section IV.2, recent work by Drake [5, 6], and McClarren and Drake [2], describing a three-layer model of RH, and anti-diffusive transport in radiative shocks, respectively, is outlined. Anti-diffusion will be discussed in greater depth in Chapter V. In Section IV.3, a historical review of semi-analytic solution methods for radiative shocks is given, and some results from the multi-physics package, KULL [54], developed at Lawrence Livermore National Lab (LLNL), are presented for code-verification purposes. Semi-analytic solutions of various shocks was an active research area during the 1960's and, after a dormant period, was rejuvenated in 2007 by Lowrie and collaborators [1, 7]. The nonequilibrium diffusion radiative shock solutions by Lowrie and Edwards [1] are now a common measure of a RH code's ability to accurately simulate radiative shocks [35, 39–42, 55–58].

IV.1 Nonequilibrium diffusion analytic results

In this Section, the steady-state grey nonequilibrium diffusion model of RH is used to derive analytic results found in [3] and [4]. The steady-state nondimensional RH equations are collected from equations (II.25) and equation (C.21), and rewritten

here for convenience:

$$\partial_x \left(\rho u\right) = 0\,, \tag{IV.1a}$$

$$\partial_x \left(\rho u^2 + p + P_0 \mathcal{P}_r\right) = 0\,, \tag{IV.1b}$$

$$\partial_x \left[\beta \left(\frac{1}{2}\rho u^2 + p + \rho e\right) + P_0 \mathcal{F}\right] = 0\,, \tag{IV.1c}$$

$$\mu \partial_x I = -\sigma_t I + \frac{\sigma_s}{4\pi}\mathcal{E} + \frac{\sigma_a}{4\pi}T^4 - 2\frac{\sigma_s}{4\pi}\beta\mathcal{F} + \beta\mu\left(\sigma_t I + \frac{3\sigma_s}{4\pi}\mathcal{E} + \frac{3\sigma_a}{4\pi}T^4\right)\,. \tag{IV.1d}$$

The first three equations represent the conservation of total mass, total momentum and total energy of Eulerian fluid mechanics coupled to radiation. These equations represent an approximation to the fully relativistic RH equations, and are correct through $\mathcal{O}(\beta)$. The fourth equation is the grey lab-frame radiation transport equation, which is also correct through $\mathcal{O}(\beta)$. The grey approximation assumes that all frequencies of radiation interact with the material in the same way. This is physically wrong, but the approximation makes the analytic solution tractable.

IV.1.1 Derivation of the nonequilibrium diffusion equations

In this subsection, the nonequilibrium diffusion model is derived from the RH equations with the goal of making the required assumptions to obtain the analytic results explicit. The analytic results describe the general shape expected for radiative shocks, but not the exact shape of any given radiative shock, and they give a functional dependence of T, $\mathcal{F}$, and p, on $\eta \equiv 1/\rho$ the inverse compression ratio, which can be checked graphically.

The nonequilibrium diffusion model, discussed in the books by Zel'dovich and Raizer [3], and Mihalas and Mihalas [4], imposes the following assumptions on the RH equa-

tions (IV.1):

- the material obeys an ideal gas equation-of-state (EOS) and maintains LTE throughout the shock profile, for all particle species, such that there is only one material temperature;
- the radiative shock is propagating into a cold material, such that the upstream internal energy density and material pressure are negligible;
- the radiation is considered weak, such that the radiation energy density, and radiation pressure, are negligible compared to their material counterparts;
- the radiation may be out of equilibrium with the material, but still obeys a diffusive law;
- the material is optically thick upstream and downstream of the shock.

The first assumption establishes the functional form of the internal energy density and material pressure, which are assumed to depend on the material density and temperature:

$$e = \frac{T}{\gamma\left(\gamma-1\right)}\,, \tag{IV.2a}$$

$$p = \rho e\left(\gamma-1\right) = \frac{\rho T}{\gamma}\,. \tag{IV.2b}$$

The second assumption drops the radiation pressure from total momentum conservation equation (IV.1b). The three conservation equations represent first-integrals. Mass conservation can be used to simplify the other two first-integrals by defining $\mathcal{M}_0 = \rho u$. For notational convenience, $\mathcal{M}_c = \rho\beta$ is analogously defined. Integrating

the other two conservation equations over the domain $(-\infty, x)$ gives:

$$\mathcal{M}_0 u + p = \mathcal{M}_0 u_0 \,, \tag{IV.3a}$$

$$\frac{1}{2}\mathcal{M}_c u^2 + \frac{\mathcal{M}_c T}{\gamma - 1} + P_0 \mathcal{F} = \frac{1}{2}\mathcal{M}_c u_0^2 \,. \tag{IV.3b}$$

The third assumption has the effect of dropping the velocity-dependent terms from the radiation transport equation (IV.1d), such that the zeroth and first angular moments are:

$$\partial_\tau \mathcal{F} = T^4 - \mathcal{E} \,, \tag{IV.4a}$$

$$\mathcal{F} = -\frac{1}{3}\partial_\tau \mathcal{E} \,, \tag{IV.4b}$$

where the opacity has been absorbed into the derivative to form a derivative with respect to the optical depth, $\tau = \sigma_t x$. Their combination produces

$$\partial_\tau^2 \mathcal{F} = 3\mathcal{F} + 4T^3 \partial_\tau T \,. \tag{IV.4c}$$

The fourth assumption is satisfied by the radiation diffusion equation (IV.4b). The fifth assumption imposes a closed thermodynamic system.

The zeroth and first angular-moments, presented in equations (IV.4), are solved subject to the boundary conditions at $\tau = \pm\infty$:

$$T\left(\tau = -\infty\right) = 0 \qquad T\left(\tau = \infty\right) = T_f \,, \tag{IV.5}$$

$$\mathcal{E}\left(\tau = -\infty\right) = 0 \qquad \mathcal{E}\left(\tau = \infty\right) = T_f^4 \,, \tag{IV.6}$$

$$\mathcal{F}\left(\tau = -\infty\right) = 0 \qquad \mathcal{F}\left(\tau = \infty\right) = 0 \,. \tag{IV.7}$$

The material pressure, from the first-integral of the momentum conservation equation (IV.3a), can be solved for in terms of the inverse compression ratio, $\eta = \rho_0/\rho = u/u_0$:

$$\begin{aligned} p &= \mathcal{M}_0 \left(u_0 - u\right) \\ &= \mathcal{M}_0 u_0 \left(1 - \frac{u}{u_0}\right) \\ &= \mathcal{M}_0 u_0 \left(1 - \eta\right) , \end{aligned} \tag{IV.8}$$

and using the ideal gas EOS (IV.2), the material temperature is:

$$\begin{aligned} \frac{p}{p_f} &= \frac{\rho T}{\rho_f T_f} \\ \Rightarrow \frac{T}{T_f} &= \frac{p \rho_f}{p_f \rho} \\ &= \frac{\left(1-\eta\right) \rho_f}{\left(1-\eta_f\right) \rho} \frac{\rho_0}{\rho_0} \\ &= \frac{\eta \left(1-\eta\right)}{\eta_f \left(1-\eta_f\right)} , \end{aligned} \tag{IV.9}$$

where $\eta_f = \rho_0/\rho_f$ is defined to be the maximum compression ratio, taking the form $\left(\gamma - 1\right) / \left(\gamma + 1\right)$, which is $1/4$ for $\gamma = 5/3$. Strictly speaking, this value of the maximum compression ratio is only valid when the radiation is very weak, as assumed in this case. The radiation flux may now be written in terms of η, using equations (IV.2b), (IV.3b), (IV.8) and (IV.9):

$$\mathcal{F} = -\frac{\mathcal{M}_c T}{2\gamma P_0} \frac{\left(\eta - \eta_f\right)}{\eta \eta_f} = -\frac{\mathcal{M}_c T_f}{2\gamma P_0} \frac{\left(1-\eta\right)\left(\eta - \eta_f\right)}{\eta_f^2 \left(1-\eta_f\right)} . \tag{IV.10}$$

As $\tau \to -\infty$, which is the unheated precursor state, $T = 0$ such that $\mathcal{F} = 0$, as required by the boundary conditions. Similarly, as $\tau \to \infty$, the compression ratio reaches its maximum value, $\eta = \eta_f$, such that $\mathcal{F} = 0$, as required, again, by the

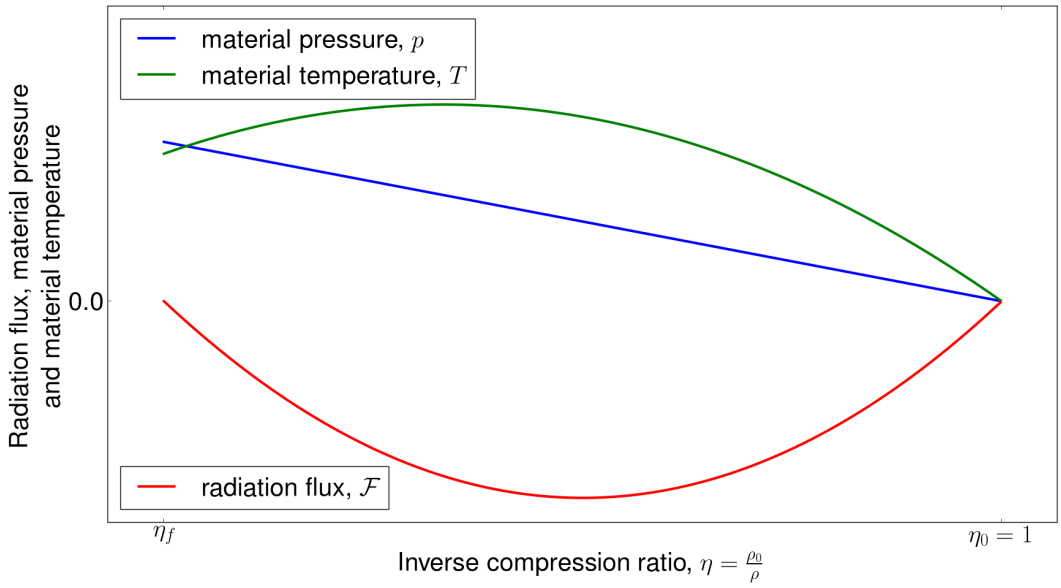

Figure IV.1: Radiation flux, material pressure and material temperature as functions of the inverse compression ratio. The upstream precursor region begins at $\eta_0 = 1$, the solution traverses the radiative shock wave as η decreases, until $\eta = \eta_f$, when the fluid and radiation have returned to their equilibrium values, as noted by the radiation flux returning to zero. Adapted from [3].

boundary conditions. Figure IV.1 shows p, T, and $\mathcal{F}$ versus η.

IV.1.2 Subcritical radiating shocks

Subcritical and supercritical radiating shocks are distinguished by the value of the material temperature, T_p, immediately upstream of the shock discontinuity. In subcritical shocks, $T_p < T_f$, whereas in supercritical shocks, $T_p = T_f$. The value of the material temperature immediately downstream of the shock is labelled T_s, and an embedded hydrodynamic shock is defined between state-$_p$ and state-$_s$. In radiative shocks, the material density is largely unaffected in the precursor region, and most of the compression takes place inside the embedded hydrodynamic shock. See Figure

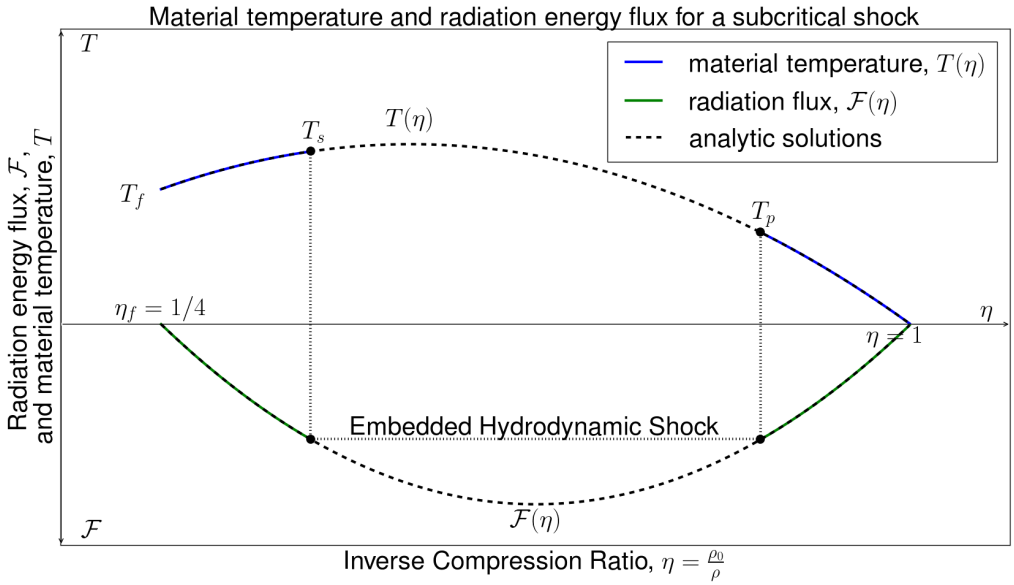

Figure IV.2: Radiation flux and material temperature as functions of the inverse compression ratio for a subcritical radiative shock. The upstream precursor region begins at $\eta_0 = 1$ and ends at η_p, where $T = T_p$. Continuity of the radiation flux between state-$_p$ and state-$_s$ defines the embedded hydrodynamic shock, and determines the value of the material temperature at state-$_s$, T_s. The downstream relaxation region is defined between η_s and η_f. Adapted from [4].

IV.2. Subsequently, it is reasonable to assume that no compression takes place before the shock, and $\eta \approx 1$. Therefore, in the precursor region, the radiation flux takes the form

$$\begin{aligned} \mathcal{F} &= -\frac{\mathcal{M}_c T}{2\gamma P_0}\frac{(1-\eta_f)}{\eta_f} \\ &= -\frac{\mathcal{M}_c T}{\gamma\,(\gamma-1)\,P_0} \\ &= -\frac{\mathcal{M}_c}{P_0} e\,, \end{aligned} \tag{IV.11}$$

such that the upstream flow of radiation from the shock is offset by the downstream

flow of internal energy, which is due to the material being heated by the radiation. Referring to equation (IV.3b), this implies that the speed profile in the precursor region is largely unaffected, which is verified by the semi-analytic solutions. The radiation emitted into the precursor region can be assumed to radiate from an opaque wall with material temperature, T_f, such that, at state-$_p$, $\mathcal{E}_p \sim T_f^4$ and $\mathcal{F}_p \sim T_f^4$. It is now assumed that $T_p^4 \ll T_f^4$ and equations (IV.4) can be considered near the precursor shock state-$_p$,

$$\partial\tau\mathcal{F}\big|_p = T_p^4 - \mathcal{E}_p \approx -\mathcal{E}_p\,, \tag{IV.12a}$$

$$\partial_\tau^2\mathcal{F} = 3F_p + \partial_\tau T^4\big|_p \approx 3F_p\,, \tag{IV.12b}$$

and solved for in the precursor region

$$\mathcal{F} = \mathcal{F}_p e^{-\sqrt{3}\tau}\,, \tag{IV.13a}$$

$$\mathcal{E} = -\sqrt{3}\mathcal{F}_p e^{-\sqrt{3}\tau}\,. \tag{IV.13b}$$

Given this solution for the radiation flux (IV.13a), and the relation between the radiation flux and the flow of internal energy, per equation (IV.11), the material temperature solution is:

$$T = -\frac{2\gamma P_0 \eta_f}{\mathcal{M}_c\,(1-\eta_f)}\mathcal{F}_p e^{-\sqrt{3}\tau} = T_p e^{-\sqrt{3}\tau}\,. \tag{IV.14}$$

While the hydrodynamic variables may be discontinuous across the shock, the radiation variables must be continuous. This is because the radiation variables are angular moments of a Boltzmann equation, which is a continuity equation for the radiation intensity. If either of the radiation variables were discontinuous, then equa-

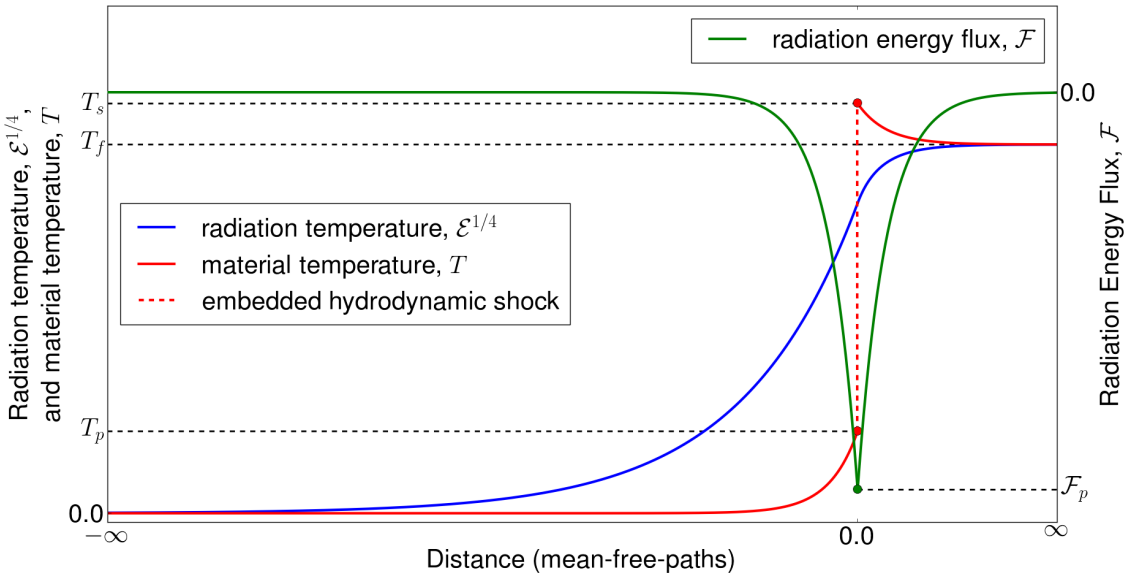

Figure IV.3: Analytic profiles for the material temperature, radiation temperature and radiation energy flux for a subcritical radiative shock with $\mathcal{M}_0 = 2$ and $P_0 = 1.e-4$. The embedded hydrodynamic shock defined between state-$_p$ and state-$_s$ is represented by the dashed red line. The temperatures equilibrate far from the embedded hydrodynamic shock. The radiation energy flux is continuous at the shock discontinuity, and exponentially relaxes to zero far from the embedded hydrodynamic shock. Adapted from [4].

tions (IV.4a) and (IV.4b) would force the other variable to be infinite at some point, which is physically nonsensical.

In the downstream post-shock relaxation region, it is assumed that the material temperature is constant, taking its final value, $T \approx T_f$. Then the second term in (IV.4c) is zero, and again the radiation flux takes the form

$$\mathcal{F} = \mathcal{F}_p e^{-\sqrt{3}\tau}\,, \tag{IV.15}$$

where continuity at $\tau = 0$ is used to show that this $\mathcal{F}_p$ is the same as in the precursor region. To determine the radiation energy density in the downstream region it helps to remove the derivative with respect to τ by multiplying equations (IV.4a) and (IV.4b), and working through the ordinary differentials:

$$\begin{aligned}
\mathcal{F}\partial_\tau\mathcal{F} &= -\frac{1}{3}\left(T_f^4 - \mathcal{E}\right)\partial_\tau\mathcal{E} \\
\mathcal{F}d\mathcal{F} = -\frac{1}{3}\left(T_f^4 - \mathcal{E}\right)d\mathcal{E} &= \frac{1}{3}\left(\mathcal{E} - T_f^4\right)d\left(\mathcal{E} - T_f^4\right) \\
d\mathcal{F}^2 &= \frac{1}{3}d\left(\mathcal{E} - T_f^4\right)^2 \\
\mathcal{F} &= \frac{1}{\sqrt{3}}\left(\mathcal{E} - T_f^4\right) \\
\mathcal{E} &= \sqrt{3}\mathcal{F} + T_f^4\,. \qquad \text{(IV.16)}
\end{aligned}$$

Enforcing continuity of the radiation energy density at $\tau = 0$ produces the following values of $\mathcal{F}_p$, $\mathcal{E}_p$ and T_p:

$$\begin{aligned}
\mathcal{E}_p = -\sqrt{3}\mathcal{F}_p &= \sqrt{3}\mathcal{F}_p + T_f^4\,, \\
\Rightarrow \mathcal{F}_p &= -\frac{1}{2\sqrt{3}}T_f^4\,, \qquad \text{(IV.17a)} \\
\Rightarrow \mathcal{E}_p &= \frac{1}{2}T_f^4\,, \qquad \text{(IV.17b)} \\
\Rightarrow T_p &= \frac{\gamma\mathcal{P}_0\eta_f}{\mathcal{M}_c\left(1-\eta_f\right)\sqrt{3}}T_f^4\,. \qquad \text{(IV.17c)}
\end{aligned}$$

Additionally, Mihalas and Mihalas claim that the following two relations for the material temperature, on the relaxation side of the embedded hydrodynamic shock, can be derived from the radiation flux:

$$\begin{aligned}
T - T_f &= \left(T_s - T_f\right)e^{-\sqrt{3}\tau}\,, \qquad \text{(IV.18a)} \\
T_s - T_f &= \frac{3-\gamma}{\gamma+1}T_p\,. \qquad \text{(IV.18b)}
\end{aligned}$$

The spatial-profiles of the radiation energy density, radiation flux, and material temperature are:

$$\mathcal{E}(x) = \begin{cases} \frac{1}{2}e^{-\sqrt{3}\tau}T_f^4\,, & x < 0\,, \\ -\frac{1}{2}T_f^4 e^{-\sqrt{3}\tau} + T_f^4\,, & x > 0\,, \end{cases} \tag{IV.19a}$$

$$\mathcal{F}(x) = -\frac{1}{2\sqrt{3}}e^{-\sqrt{3}\tau}\,, \qquad \forall x\,, \tag{IV.19b}$$

$$T(x) = \begin{cases} \frac{\gamma P_0 \eta_f}{\mathcal{M}_c\left(1-\eta_f\right)\sqrt{3}}e^{-\sqrt{3}\tau}T_f^4\,, & x < 0\,, \\ T_f + \frac{(3-\gamma)\gamma P_0 \eta_f}{(\gamma+1)\mathcal{M}_c\left(1-\eta_f\right)\sqrt{3}}e^{-\sqrt{3}\tau}T_f^4\,, & x > 0\,, \end{cases} \tag{IV.19c}$$

and are plotted in Figure IV.3. An immediate problem with the material temperature profile presented in equation (IV.19c) is that the material temperature always exhibits a Zel'dovich spike, since $T_s > T_f$ in equation (IV.18b).

IV.1.3 Supercritical radiating shocks

As mentioned at the beginning of the previous subsection, supercritical radiating shocks are defined as having $T_p = T_f$. See Figure IV.4. The value of the material temperature at the final equilibrium state, T_f, increases proportionally with the Mach number. It is claimed that the increasing radiant energy emitted from the embedded hydrodynamic shock, $\sim T_f^4$, does not cause $T_p > T_f$, but instead drives the radiation precursor deeper into the unshocked material. Since $T_p = T_f$ at the shock front, then as the Mach number increases and the radiation precursor extends further from the shock discontinuity, there exists a zone of equilibrium between the radiation and the material. This equilibrium zone extends a depth τ_c into the precursor region before the material and radiation are not in equilibrium. The material temperature at this point is prescribed to be T_c. The analysis for the precursor region of the

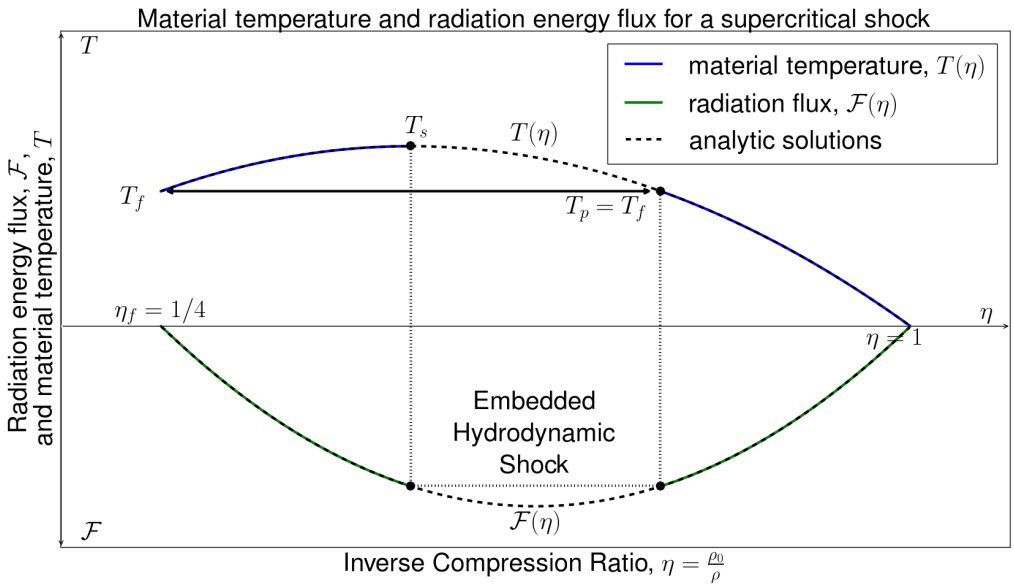

Figure IV.4: Radiation flux and material temperature as functions of the inverse compression ratio for a supercritical radiating shock. The upstream precursor region begins at $\eta_0 = 1$ and ends at η_p, where $T_p = T_f$. Continuity of the radiation flux between state-$_p$ and state-$_s$ defines the embedded hydrodynamic shock, and determines the value of the material temperature at state-$_s$, T_s. The downstream relaxation region is defined between η_s and η_f. Adapted from [4].

previous subsection can be applied here to the nonequilibrium domain, but with $|\tau| \to |\tau - \tau_c|$, yielding:

$$\mathcal{F} = \mathcal{F}_c e^{-\sqrt{3}|\tau-\tau_c|}\,, \tag{IV.20a}$$

$$\mathcal{E} = -\sqrt{3}\mathcal{F}_c e^{-\sqrt{3}|\tau-\tau_c|}\,. \tag{IV.20b}$$

For the purpose of illustration in Figure IV.5, the material temperature is fored to decay as

$$T = T_c e^{-3|\tau-\tau_c|/4}\,. \tag{IV.21}$$

According to [4], the values of $\mathcal{F}_c = -T_c^4/\sqrt{3}$ and $\mathcal{E}_c = T_c^4$ contain a multiplicative factor of 2 that was missing from the previous analysis. Since the comparison of the radiation flux to the internal energy flux in equation (IV.11) is still valid, the value of T_c can be determined:

$$\begin{aligned} \mathcal{F}_c &= -\frac{P_0 T_c^4}{\sqrt{3}} = -\frac{\mathcal{M}_c T_c}{\gamma\left(\gamma-1\right)} \\ \Rightarrow T_c^3 &= \frac{\sqrt{3}\mathcal{M}_c}{P_0\gamma\left(\gamma-1\right)}. \end{aligned} \tag{IV.22}$$

In the equilibrium domain, $\mathcal{E} = T^4$, and radiation diffusion takes on the form of heat-conduction:

$$\mathcal{F} = -\frac{4}{3}T^3\partial_\tau T\,. \tag{IV.23}$$

The differentials of material temperature and optical depth can be related by equations (IV.11), (IV.1.3) and (IV.23):

$$\begin{aligned} \mathcal{F} = -\frac{4}{3}T^3\partial_\tau T &= -\frac{\mathcal{M}_c T}{P_0\gamma\left(\gamma-1\right)} \\ \frac{4}{3}T^2 dT = \frac{\mathcal{M}_c}{P_0\gamma\left(\gamma-1\right)}d\tau &= \frac{T_c^3}{\sqrt{3}}d\tau \\ \Rightarrow T^2 dT &= \frac{\sqrt{3}}{4}T_c^3 d\tau\,. \end{aligned} \tag{IV.24}$$

Integrating from $|\tau_c|$, into the equilibrium zone, toward the shock, to $|\tau|$, produces the ratio of the material temperatures:

$$\begin{aligned} \int_{T_c}^{T} T^2 dT &= \frac{\sqrt{3}}{4}T_c^3\int_0^{|\tau-\tau_c|} d\tau \\ \frac{1}{3}\left(T^3 - T_c^3\right) &= \frac{\sqrt{3}}{4}T_c^3\left|\tau-\tau_c\right| \end{aligned}$$

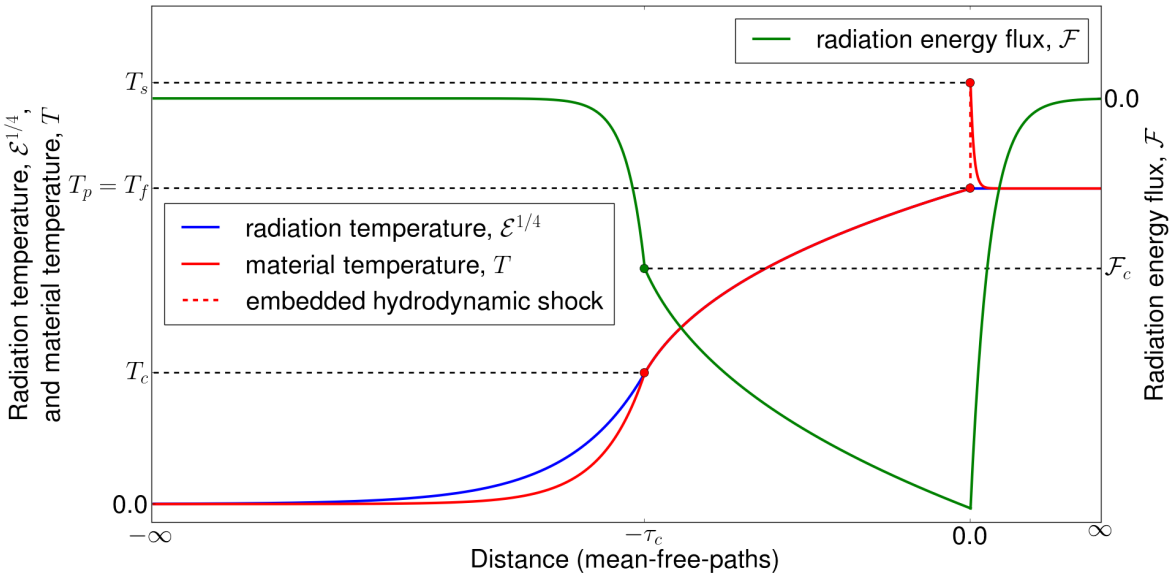

Figure IV.5: Analytic profiles for the material temperature, radiation temperature and radiation energy flux for a supercritical radiating shock with $\mathcal{M}_0 = 5$ and $P_0 = 1.e-4$. The nonequilibrium region spans the domain $\tau \in (-\infty, -\tau_c)$, and the equilibrium region spans the domain $\tau \in [-\tau_c, 0]$. An embedded hydrodynamic shock exists between state-$_p$ and state-$_s$. The material temperature shows a Zel'dovich spike in the relaxation region, downstream of the shock discontinuity, while the radiation temperature maintains a constant value equal to the final equilibrium temperature. Adapted from [4].

$$\frac{T^3 - T_c^3}{T_c^3} = \frac{3\sqrt{3}}{4}\left|\tau - \tau_c\right|$$
$$\Rightarrow \frac{T}{T_c} = \left(1 + \frac{3\sqrt{3}}{4}\left|\tau - \tau_c\right|\right)^{1/3}, \tag{IV.25}$$

and extending this result to the shock, and recalling that $T_p = T_f$, allows $|\tau_c|$ to be solved for:

$$|\tau_c| = \frac{4}{3\sqrt{3}}\left(\left(\frac{T_f}{T_c}\right)^3 - 1\right). \tag{IV.26}$$

According to [3] and [4], the relaxation region cannot be solved, or approximately solved, with any satisfaction via simple analytic models. However, the Zel'dovich spike can be superposed if T_s is known, and using the knowledge that the optical thickness of the spike is less than one photon mean-free-path. Mihalas and Mihalas [4] claim T_s can be ascertained by using equations (IV.9) and (IV.10), and forcing $T_p = T_f$, which is supposed to result in:

$$T_s = (3 - \gamma)T_f \,. \tag{IV.27}$$

Since the material and radiation are out of equilibrium in the relaxation region, in Figure IV.5 the radiation energy flux is forced to decay as

$$\mathcal{F} = \mathcal{F}_p e^{-\sqrt{3}\tau} \,, \tag{IV.28}$$

in agreement with the nonequilibrium region of the precursor, and where $\mathcal{F}_p$ is taken from the derivation of equation (IV.24), with $T = T_p = T_f$. The spatial profiles of the radiation temperature, radiation energy flux, and the material temperature are displayed in Figure IV.5.

IV.2 Analytic work of Drake, and McClarren and Drake

In this Section, the theory of the three-layer model, developed by Drake [5, 6], is discussed, as is the prediction of anti-diffusive radiative shocks, developed by McClarren and Drake [2]. Both descriptions of radiative shocks make predictions that are discussed in the next Chapter.

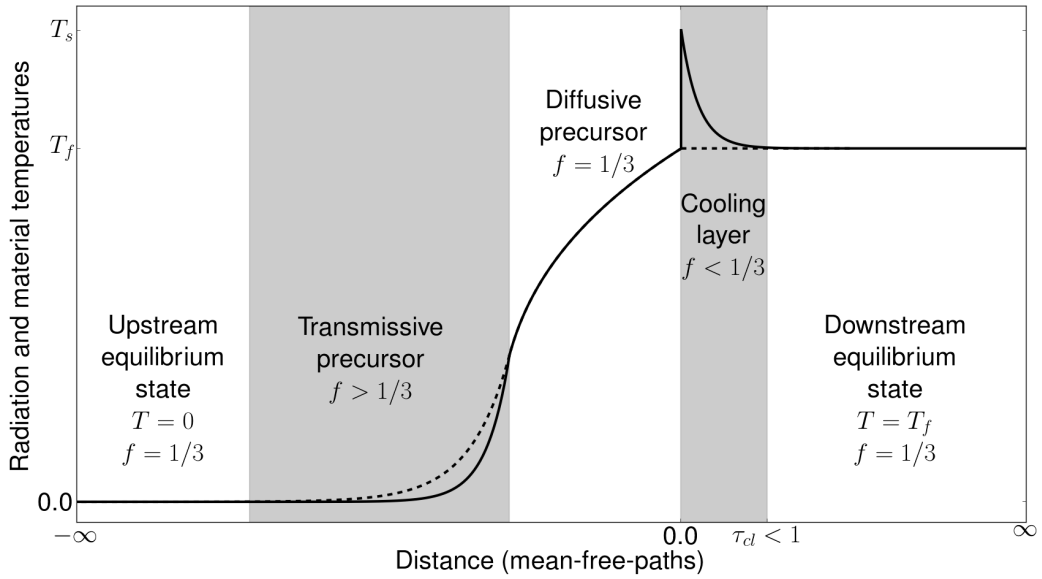

Figure IV.6: The three-layer model as described by Drake [5, 6] for a supercritical radiative shock. The first layer defines the precursor region, and contains the upstream equilibrium state, the transmissive precursor and the diffusive precursor. The second layer is the cooling layer, often referred to as the relaxation region, which is considered to be optically thin, with $\tau_{cl} < 1$. The third layer is the downstream equilibrium state. The first and third layers are assumed to be optically thick. Adapted from [5, 6].

IV.2.1 The three-layer model

Drake's three-layer model focuses on supercritical radiating shocks and consists of the precursor region, the relaxation region, which he terms the cooling layer, and the final downstream region. The precursor region is claimed to be composed of two regions: the transmissive precursor near the upstream equilibrium state, and the diffusive precursor which sits between the transmissive precursor and the embedded hydrodynamic shock. See Figure IV.6. As such, the three-layer model builds on the nonequilibrium diffusion theory as described in the previous section, but avoids

describing each region analytically. Instead, emphasis is placed on analyzing the fluid equations, and considering appropriate transport descriptions. Essentially, the three-layer model represents a semi-analytic solution procedure, but without making this solution procedure explicit.

The fluid equations are the integrated Euler equations, in the flux-dominated regime:

$$\rho u = \rho_0 u_0 \,, \tag{IV.29a}$$

$$\rho u^2 + p = \rho_0 u_0 u + p = \rho_0 u_0^2 \,, \tag{IV.29b}$$

$$\frac{1}{2}\rho u^3 + (\rho e + p)\, u + \mathcal{F} = \frac{1}{2}\rho_0 u_0^3 \,. \tag{IV.29c}$$

These equations represent the conservation of mass, material momentum, and material energy, coupled to the energy flux of radiation. The radiation energy density, and radiation pressure, are assumed to be negligible compared to their material counterparts, and only the radiation energy flux is assumed to contribute substantially to the material dynamics.

Normalization constants can be introduced for the pressure, temperature, and radiation energy flux, which simplify the analysis of the Euler fluid equations:

$$p_n = \frac{p}{\rho_0 u_0^2} \,, \tag{IV.30a}$$

$$T_n = \frac{T}{u_0^2} \,, \tag{IV.30b}$$

$$\mathcal{F}_n = \frac{2\mathcal{F}}{\rho_0 u_0^3} \,. \tag{IV.30c}$$

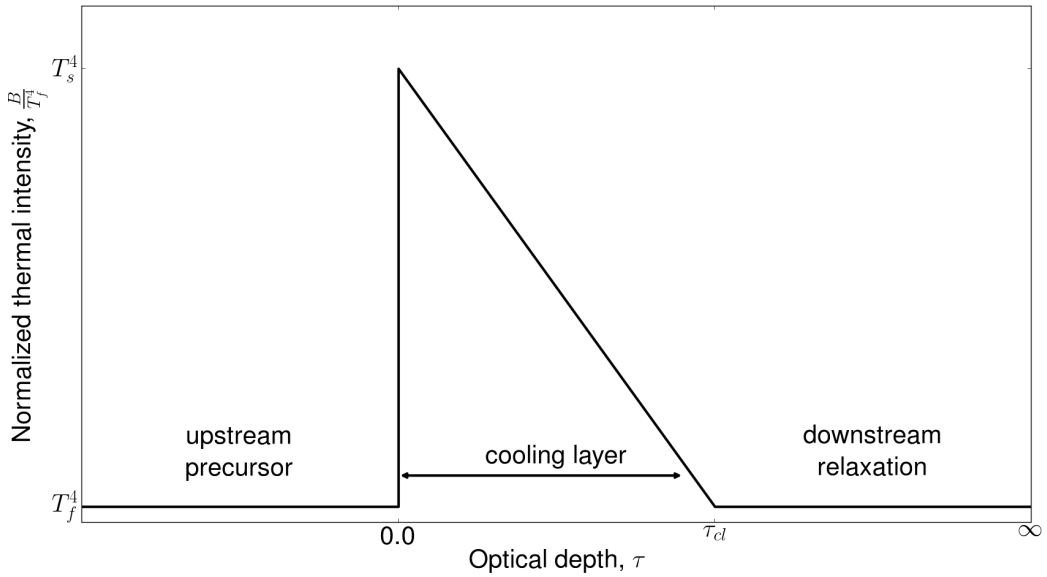

Figure IV.7: Simplified model of the Zel'dovich spike proposed by Drake [5, 6]. For a supercritical radiating shock the upstream precursor region approaches the shock discontinuity with temperature, T_f. The embedded hydrodynamic shock and the Zel'dovich spike are defined as the region where $T > T_f$ and has an optical depth of τ_{cl}. The cooling layer represents the Zel'dovich spike and the relaxation region. Downstream of the cooling layer the shock is in its final equilibrium state. Adapted from [5, 6].

Recalling the inverse compression ratio $\eta = \rho_0/\rho$, the conservation equations of mass and momentum can be combined to give an equation for the normalized pressure

$$p_n = (1 - \eta) \ , \tag{IV.31}$$

assuming an ideal gas, where $p = \rho RT$, provides an equation for the normalized temperature

$$T_n = \eta\,(1 - \eta) \ . \tag{IV.32}$$

Assuming a γ-law EOS,

$$p = \rho e \left(\gamma - 1\right) , \tag{IV.33a}$$

$$e = \frac{T}{\gamma \left(\gamma - 1\right)} , \tag{IV.33b}$$

provides an equation for the normalized radiation flux

$$\mathcal{F}_n = 1 - \frac{2\gamma}{\gamma - 1}\eta + \frac{\gamma + 1}{\gamma - 1}\eta^2 . \tag{IV.34}$$

Thus, a complete understanding of the hydrodynamic variables and the radiation flux rest only on the inverse compression ratio, and results in the same illustration given in Figure IV.1. This much was discussed in [3] and [4]. Drake goes further by considering how to couple the hydrodynamics to the radiation, without initially assuming that the nonequilibrium diffusion model suffices.

The spatial derivative of $\mathcal{F}_n$ provides an expression for the spatial derivative of the inverse compression:

$$\partial_x \mathcal{F}_n = \left(\frac{2\gamma - 2\eta \left(\gamma + 1\right)}{\gamma - 1} \right) \partial_x \eta . \tag{IV.35}$$

The radiation transport equation is now introduced

$$\frac{1}{c}\partial_t I + \mu \partial_x I = -\sigma_t I + \frac{\sigma_a}{4\pi}\alpha_R c T^4 + \frac{\sigma_s}{4\pi} c\mathcal{E} , \tag{IV.36}$$

and the time-derivative is dropped with the explanation that the radiation equilibrates with the material on time-scales sufficiently small compared to the hydrodynamic time-scale. This was discussed at the end of Section III.3 when the diffusive

time-scale was compared to the fluid time-scale, and this particular situation was termed "static diffusion". The zeroth angular-moment is

$$\partial_x \mathcal{F}_n = \sigma_a c \left(\alpha_R T^4 - \mathcal{E} \right) , \tag{IV.37}$$

which provides an expression for the gradient of the radiation flux at the expense of introducing a new variable. Drake resolves this by introducing the diffusion approximation with a quasi-static variable Eddington factor (VEF),

$$\partial_x \mathcal{P} = f \partial_x \mathcal{E} = -\frac{\sigma_t}{c} \mathcal{F}_n \, . \tag{IV.38}$$

Drake immediately addresses the assumed quasi-static nature of the VEF, claiming that integrating the precursor region with it is fine, where the gradients of $\mathcal{P}$ and $\mathcal{E}$ are "parallel", but "this method proves to be qualitatively incorrect for the cooling layer in a radiative shock". What is meant by the gradients being parallel is made clear in the next Subsection. Equations (IV.34) and (IV.38) can now be coupled, as can equations (IV.35) and (IV.37), such that the precursor region is governed by two spatial ordinary differential equations (ODEs):

$$\frac{c}{\sigma_t} f \partial_x \mathcal{E} - 1 + \frac{2\gamma}{\gamma - 1} \eta - \frac{\gamma + 1}{\gamma - 1} \eta^2 \, , \tag{IV.39a}$$

$$2\pi \sigma_a c \left(\mathcal{E} - \frac{\alpha_R T^4}{4\pi} \right) = \left(\frac{\eta \left(\gamma + 1 \right) - \gamma}{\gamma - 1} \right) \partial_x \eta \, . \tag{IV.39b}$$

The simultaneous integration of these two ODEs provides a complete solution of the precursor region. In this sense, Drake's solution method is semi-analytic.

For the relaxation region, a simple model of the Zel'dovich spike is assumed, see

Figure IV.7, and conservation of the radiation energy flux is enforced on both sides of the spike. On the downstream edge of the spike, it is assumed that the material and radiation are in equilibrium, such that the radiation energy flux entering the spike from further downstream is zero. Then balance of the radiation energy flux at the downstream edge of the relaxation region imposes

$$\sigma_t f_s^4 T_f^4 \left(1 - \tau_{cl}\right) + 1.2\tau_{cl}\sigma_t T_{ds}^4 - \sigma_t T_f^4 = 0\,. \tag{IV.40}$$

Analogously, at the downstream edge of the precursor, the radiation flux from the spike must balance the radiation flux entering the precursor:

$$\sigma_t f_s T_f^4 - 1.2\tau_{cl}\sigma_t T_{ds} - \sigma_t \left(1 - \tau_{cl}\right) T_f^4 - \left(1 - \frac{2\gamma}{\gamma - 1}\eta + \frac{\gamma + 1}{\gamma - 1}\eta^2\right) = 0\,. \tag{IV.41}$$

The variable f_s relates the precursor material temperature at the shock discontinuity to the final temperature: $T_p = f_s T_f$. For supercritical shocks, nonequilibrium diffusion theory assumes $f_s = 1$. Drake chooses, instead, to consistently solve for f_s and τ_{cl} using the two previous equations. "The factor of 1.2 results from the integral of the radiation transfer equation over angle to find the flux from an optically thin layer given the assumed emission profile and isotropic emission." The term $(1 - \tau_{cl})$ represents the assumption that the cooling layer is exponentially thin, and can be expanded to first order. The maximum temperature and the inverse compression ratio in the Zel'dovich spike are taken from [4]:

$$T_s = \left(3 - \gamma\right) T_f\,, \tag{IV.42a}$$

$$\eta_s = \frac{2\left(\gamma - 1\right)}{\left(\gamma + 1\right)}\,. \tag{IV.42b}$$

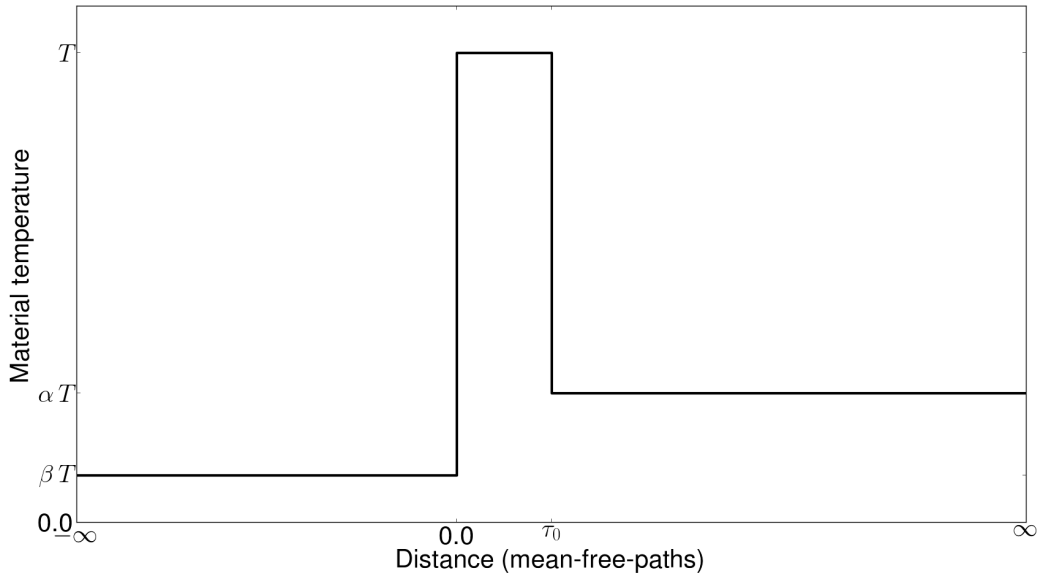

Figure IV.8: An Eulerian shock, between temperatures βT and αT, where $\alpha > \beta$, superposed with a rectangular Zel'dovich spike of optical depth $\tau_0 < 1$ and temperature T. Adapted from [2].

Equations (IV.40) and (IV.41) represent a 2×2 system of equations, with the unknowns f_s and τ_{cl}.

IV.2.2 Anti-diffusive radiative shocks

The work by McClarren and Drake [2] on anti-diffusive radiating shocks supposes an Eulerian type shock for the material temperature, superposed with a rectangular Zel'dovich spike, of a given optical thickness. The maximum temperature is assumed to occur in the Zel'dovich spike, and this value of temperature is normalized to unity, while the upstream temperature is denoted by βT, and the downstream temperature is denoted αT, where $1 > \alpha > \beta$. See Figure IV.8.

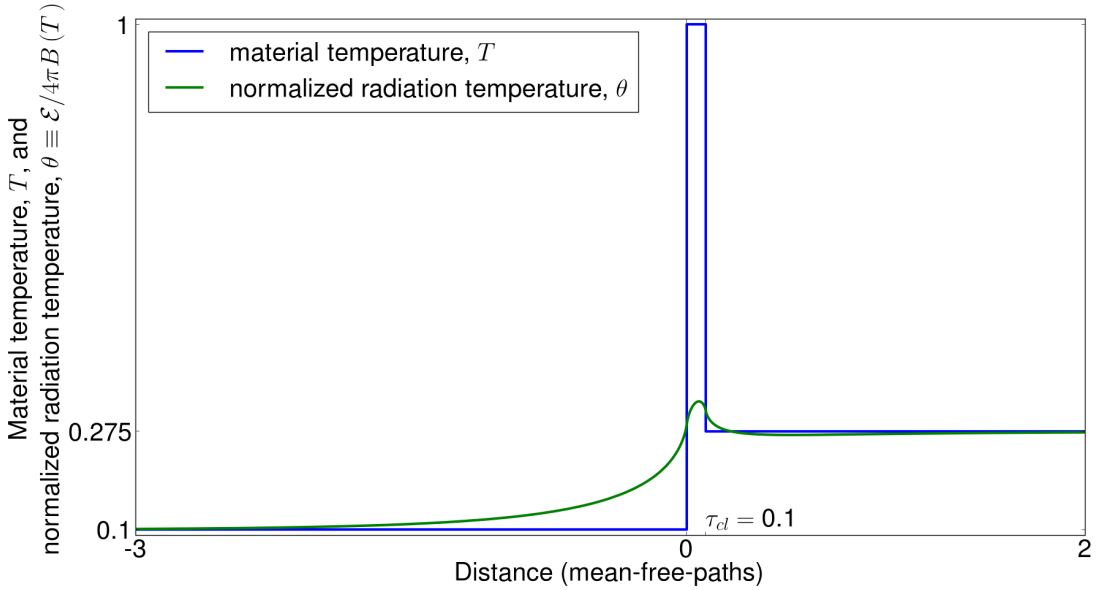

Figure IV.9: The analytic radiation energy density, solved for the simplified Zel'dovich spike shown in Figure IV.8, and normalized with the isotropic Planck function, $4\pi B(T)$. The local maximum in the radiation energy density under the rectangular Zel'dovich spike is obvious, and has been termed "anti-diffusive" radiation by McClarren and Drake. Adapted from [2].

The material is assumed to be a pure-absorber, and the gray steady-state radiation transport equation is:

$$\mu \partial_x I = \frac{\sigma_a c}{4\pi} \left(\alpha_R T^4 - \mathcal{E} \right) . \tag{IV.43}$$

This equation is solved analytically across the spatial-profile of the material temperature for all three distinct regions, and the radiation energy density, radiation energy flux, and radiation pressure, are constructed from the angular moments.

The purpose of the paper is to show that, for the simplified radiative shock model,

it is possible for the radiation temperature to have a local maximum under the Zel'dovich spike. See Figure IV.9. This manifestation of a local maximum in the radiation energy density is termed anti-diffusive radiation, since, for a diffusion theory, the radiation flux is proportional to the negative gradient of the radiation energy density, and if the radiation energy density has a local maximum then the radiation flux would pass through zero and become positive (or change sign from positive to negative, for material flows traveling in the opposite direction). This change of sign for the radiation flux does not make physical sense, and so diffusion theory fails to *qualitatively* capture the correct radiation transport solution. The radiation energy density obtains a local maximum under the Zel'dovich spike because the variable Eddington factor, $f \equiv \mathcal{P}/\mathcal{E}$ obtains a minimum in the same region. See Figure IV.10.

The radiation flux, neglecting material-motion corrections and adopting a variable Eddington factor, can be written as

$$\mathcal{F} = -\frac{1}{\sigma_t}\partial_x \left(f\mathcal{E}\right) = -\frac{1}{\sigma_t}\left(f\partial_x\mathcal{E} + \mathcal{E}\partial_x f\right) . \tag{IV.44}$$

In diffusion theory the VEF is constant, $f = 1/3$, and the scalar product of $\mathcal{F}$ and the gradient of $\mathcal{E}$ is negative:

$$\mathcal{F}\cdot\partial_x\mathcal{E} = -\frac{1}{3\sigma_t}\left(\partial_x\mathcal{E}\right)^2 < 0\,. \tag{IV.45}$$

However, in transport theory the VEF is not constant, and the scalar product of $\mathcal{F}$ and the gradient of $\mathcal{E}$ may not be negative depending on the magnitude, and sign,

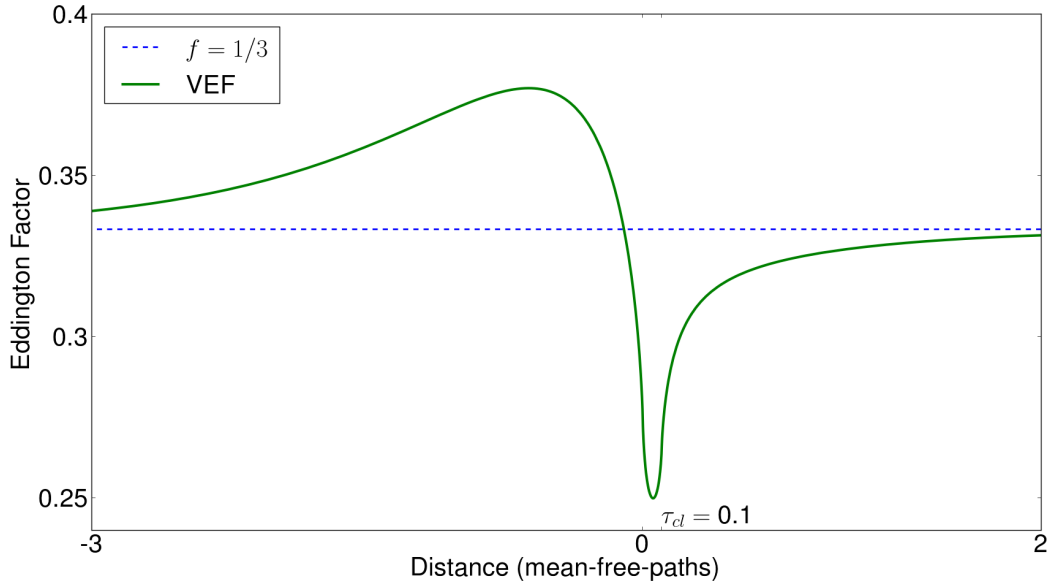

Figure IV.10: The analytic variable Eddington factor (VEF), solved for the simplified Zel'dovich spike shown in Figure IV.8, and the constant Eddington factor, $f = 1/3$, for comparison. The VEF relaxes to the constant value 1/3 near the equilibrium endpoints, but takes on a maximum value late in the precursor region, and obtains a sharp minimum under the rectangular Zel'dovich spike. Adapted from [2].

of $\partial_x f$, and $\partial_x \mathcal{E}$:

$$\mathcal{F} \cdot \partial_x \mathcal{E} = -\frac{1}{\sigma_t} f \left(\partial_x \mathcal{E}\right)^2 - \frac{1}{\sigma_t} \mathcal{E} \left(\partial_x f\right) \left(\partial_x \mathcal{E}\right) . \tag{IV.46}$$

While the first term on the RHS is negative-definite, the second term may be positive if the gradient of either $\mathcal{E}$, or f, is negative, and the whole RHS may be positive if one of these gradients is sufficiently negative. Anti-diffusion is discussed more thoroughly in the next Chapter.

IV.3 Previous semi-analytic solutions and code-verification

IV.3.1 Review of work before 2007

Significant work in the late 1950's, and 1960's, was devoted to semi-analytic solutions of various shock waves, computed from fluid mechanics with a variety of physics. Sen and Guess [18] were the first to recognize that the inclusion of radiation would create an extended precursor region which would be much larger than the smoothing effects of viscosity, or thermal conduction. Heaslet and Baldwin [59] were the first to study the effect of Mach number and radiation strength on the structure of the nonequilibrium diffusion radiating shocks using Euler's equations, i.e., without viscosity and heat-conduction. Jaffrin and Probstein [60] considered fully ionized plasma shock waves by solving the Navier-Stokes equations, i.e., including viscosity and heat-conduction, but without radiation. Traugott [46] verified the claim by Sen and Guess that the radiation precursor extended many photon mean-free-paths, and that the photon mean-free-path was considerably larger than the ion or electron mean-free-path in fluid mechanics calculations.

Reviewing RH code-verification test-suites from the literature, it appears that much of this work was forgotten, or ignored, by the 1990's. Ensman [30] generated her own test-suite of five problems to verify her RH code, VISPHOT, including subcritical and supercritical radiating shocks. Gehmeyr and Mihalas [61] used Ensman's test-suite to verify their adaptive grid RH code, TITAN, as did Hayes and Norman [36] when verifying their parallelized update to the ZEUS code. Ensman's code-verification for radiating shocks continues to be used among the astrophysics community [35, 62–64].

IV.3.2 Semi-analytic solutions by Lowrie and collaborators

More recently, Lowrie and collaborators [1, 7] have reintroduced semi-analytic solution methods for radiating shocks as a code-verification tool. The latter semi-analytic solution method uses nonequilibrium diffusion theory, with the Eddington approximation, $f \equiv \mathcal{P}/\mathcal{E} = 1/3$. This verification tool has been used by many RH codes which solve for the radiation variables via diffusion and the Eddington approximation [39, 55–57], and also by many codes which solve the radiation transport equation with a variable Eddington factor (in 1-D), or a variable Eddington tensor (in 2-D or 3-D) [35, 40–42, 58].

Beyond code-verification, semi-analytic solutions help develop physical intuition, and potentially lead to a deeper understanding of the physics involved, and allow testing specific ideas and established formulae. One particular, and erroneous, formula was introduced in Section IV.1 to determine the maximum material temperature at the shock discontinuity of a supercritical shock, c.f., equation (IV.27),

$$T_s = (3 - \gamma)\, T_f \,, \tag{IV.47}$$

and is shown by Lowrie and Edwards [1] to be qualitatively wrong for Mach numbers spanning two orders of magnitude. In that paper, they derive for the maximum material temperature, the formula:

$$T_{max} = \max\left(T_f, \frac{\left[3\left(\gamma\mathcal{M}_0^2 + 1\right) + \gamma P_0\left(1 - T_f^4\right)\right]^2}{36\gamma\mathcal{M}_0^2}\right) . \tag{IV.48}$$

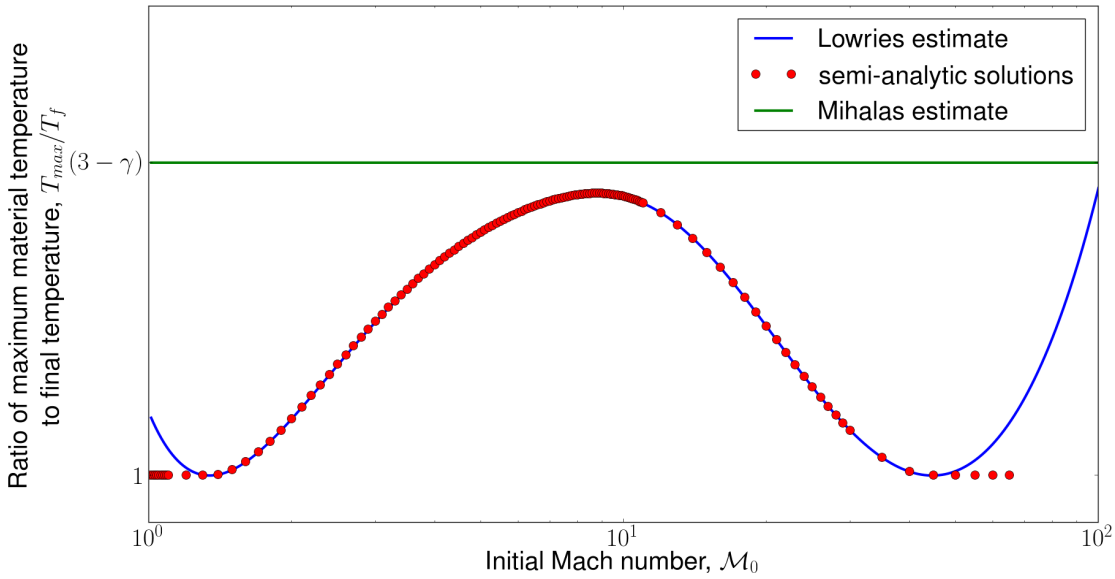

Figure IV.11: Comparison of Mihalas's estimate of the maximum material temperature for a radiative shock, equation (IV.47), with Lowrie's estimate, equation (IV.48), along with semi-analytic solutions computed from Lowrie's nonequilibrium radiation solution method. Mihalas's estimate is qualitatively wrong. Lowrie's estimate is qualitatively wrong for very weak shocks, $\mathcal{M}_0 \lesssim 1.2$, and very strong shocks, $\mathcal{M}_0 \gtrsim 50$, but agrees nicely with the computed results in between. Adapted from [1].

See Figure IV.11.

The semi-analytic solutions of Heaslet and Baldwin [59] showed conclusively that radiating shocks could be smooth across the spatial profile, and not admit an embedded hydrodynamic shock, or, they could admit a Zel'dovich spike associated with the embedded hydrodynamic shock. Lowrie and Edwards [1] closely examined embedded hydrodynamic shocks, and the Zel'dovich spike, and determined that the Zel'dovich spike was not dependent on the existence of the embedded hydrodynamic shock, but instead it depends on the existence, and location, of the isothermal sonic

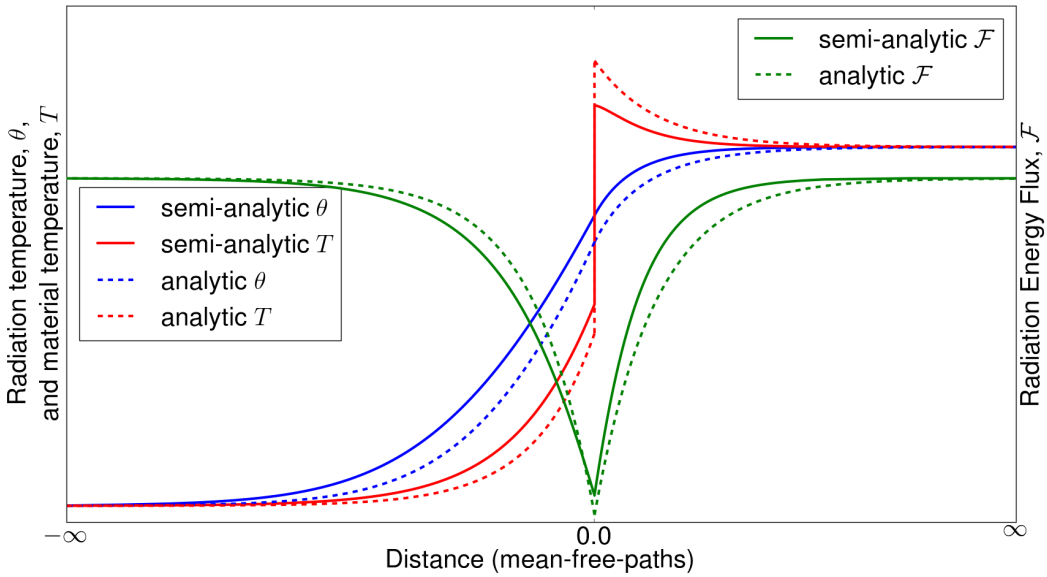

Figure IV.12: Comparison of approximate and semi-analytic solutions for a subcritical shock in a weak radiation field, $P_0 = 1.e-4$. The analytic solutions provide a reasonable estimate of the shock's optical depth, as well as the radiation variables and the material temperature.

point. Thus, even in the absence of an embedded hydrodynamic shock, i.e., for continuous radiating shock solutions, a Zel'dovich spike may exist in the relaxation region. These details aide our intuition and potentially remove false beliefs about radiating shocks, or at least place them in the proper context of the assumptions being made, and the models being used. Figures IV.12 and IV.13 show the difference between the analytic and semi-analytic solutions for a subcritical and supercritical shock.

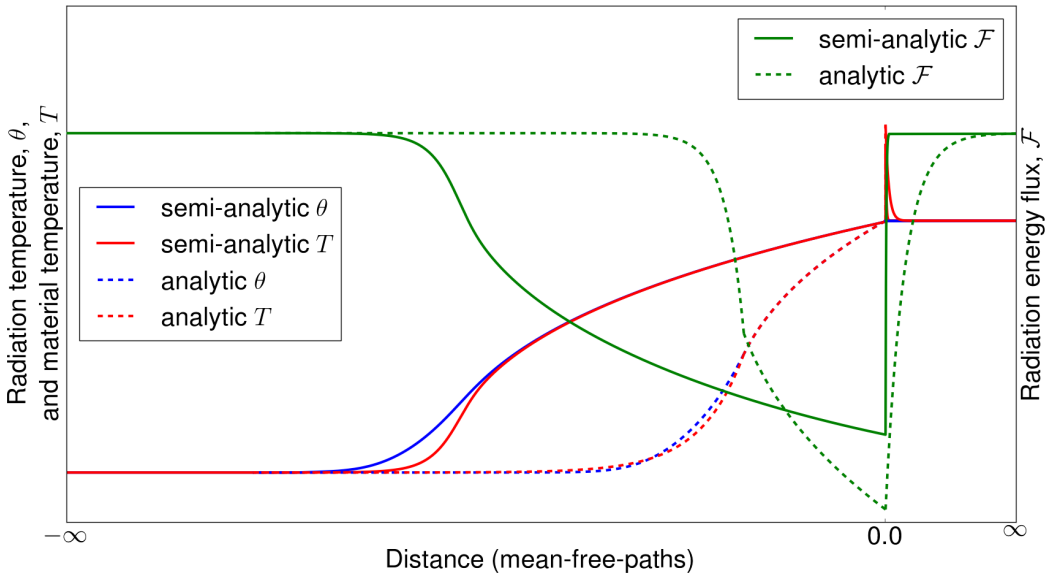

Figure IV.13: Comparison of approximate and semi-analytic solutions for a super-critical shock in a weak radiation field, $P_0 = 1.e-4$. The analytic solutions do not provide a reasonable estimate of the radiating shock.

IV.3.2.1 Lowrie's semi-analytic solution method: General equations

The solution method developed by Lowrie and collaborators is clearly outlined here because it is the foundation for the solution procedure in the next Chapter. Lowrie begins with the RH equations,

$$\partial_x \left(\rho u\right) = 0\,,$$

$$\partial_x \left(\rho u^2 + p\right) = -P_0 S_{rp}\,,$$

$$\partial_x \left[u\left(\frac{1}{2}\rho u^2 + p + \rho e\right)\right] = -P_0 S_{re}\,,$$

$$\mu\partial_x I = -\sigma_t I + \frac{\sigma_s}{4\pi}\mathcal{E} + \frac{\sigma_a}{4\pi}T^4 - 2\frac{\sigma_s}{4\pi}\beta\mathcal{F} + \beta\mu\left(\sigma_t I + \frac{3\sigma_s}{4\pi}\mathcal{E} + \frac{3\sigma_a}{4\pi}T^4\right)\,,$$

and generates the radiation energy and momentum equations by taking the zeroth and first angular-moments of the radiation transport equation,

$$\int_{\mu} \mu \partial_x I d\mu = \partial_x \mathcal{F} = \sigma_a \left(T^4 - \mathcal{E} \right) + \left(\sigma_a - \sigma_s \right) \beta \mathcal{F} \equiv S_{re} \,, \tag{IV.49a}$$

$$\int_{\mu} \mu^2 \partial_x I d\mu = \partial_x \mathcal{P} = -\sigma_t \mathcal{F} + \beta \left(\sigma_t \mathcal{P} + \sigma_s \mathcal{E} + \sigma_a T^4 \right) \equiv S_{rp} \,. \tag{IV.49b}$$

The radiation flux in the material energy equation is nondimensionalized as $a_r u_\infty T_\infty^4$, instead of $a_r c T_\infty^4$. The radiation variables are Lorentz transformed, at first-order in β, from the lab-frame to the comoving-frame,

$$\mathcal{E}_o = \mathcal{E} - 2\beta \mathcal{F} \,, \tag{IV.50a}$$

$$\mathcal{F}_o = \mathcal{F} - \beta \left(\mathcal{E} + \mathcal{P} \right) \,, \tag{IV.50b}$$

and the Eddington approximation is made, $\mathcal{P} = \mathcal{E}/3$, such that the lab-frame radiation energy and momentum equations, in terms of the comoving-frame radiation variables, are:

$$S_{re} = \partial_x \mathcal{F}_o + \frac{4}{3} \partial_x \left(\beta \mathcal{E}_o \right) = \sigma_a \left(T^4 - \mathcal{E}_o \right) - \sigma_t \beta \mathcal{F}_o \,, \tag{IV.51a}$$

$$S_{rp} = \frac{1}{3} \partial_x \mathcal{E}_o + \frac{2}{3} \partial_x \left(\beta \mathcal{F}_o \right) = -\sigma_t \mathcal{F}_o + \sigma_a \beta \left(T^4 - \mathcal{E}_o \right) \,. \tag{IV.51b}$$

The second derivative in the radiation momentum equation, $2\partial_x \left(\beta \mathcal{F}_o \right) /3$, is dropped since it is of second-order in the equilibrium-diffusion limit. The radiation flux can then be solved for in equation (IV.51b),

$$\mathcal{F}_o = -\frac{1}{3\sigma_t} \partial_x \mathcal{E}_o + \beta \left(T^4 - \mathcal{E}_o \right) \,, \tag{IV.52}$$

and used in the radiation energy equation (IV.51a):

$$\partial_x \left(-\frac{1}{3\sigma_t} \partial_x \mathcal{E}_o + \beta \left(T^4 - \mathcal{E}_o \right) + \frac{4}{3} \beta \mathcal{E}_o \right) = \sigma_a \left(T^4 - \mathcal{E}_o \right) - \sigma_t \beta \mathcal{F}_o \,. \tag{IV.53}$$

The term $\beta \left(T^4 - \mathcal{E}_o \right)$ is dropped since, again, it is of second-order in the equilibrium diffusion limit. Thus, the radiation energy equation is

$$-\partial_x \left(\frac{1}{3\sigma_t} \partial_x \mathcal{E}_o \right) + \frac{4}{3} \partial_x \left(\beta \mathcal{E}_o \right) = \sigma_a \left(T^4 - \mathcal{E}_o \right) - \sigma_t \beta \mathcal{F}_o \,. \tag{IV.54}$$

The terms above that were dropped due to being second-order in the EDL are a consequence of Lowrie's original work on radiating shocks [7] for the EDL, and that his primary intentions were to use the semi-analytic solutions as a code-verification tool for a RH code which uses a specific radiation model. Thus, many equations in [7] were transferred to the nonequilibrium diffusion radiating shocks paper [1], with the effect that the only changes to many equations in [1] are to distinguish some valid T^4 terms from terms that should be $\mathcal{E}_o \equiv \theta^4$, where θ is the radiation temperature.

In the case of equilibrium diffusion radiating shocks, there now exist three equations, the three conservation equations, for three unknowns, ρ, u and T, where an ideal-gas EOS is assumed. For nonequilibrium diffusion solutions, the material temperature and radiation temperature are solved separately, and a fourth equation must be introduced. For this purpose Lowrie uses the steady-state material internal energy equation

$$\rho u \partial_x e + p \partial_x u = P_0 \sigma_a \left(\mathcal{E}_o - T^4 \right) \,. \tag{IV.55}$$

The ideal-gas EOS is

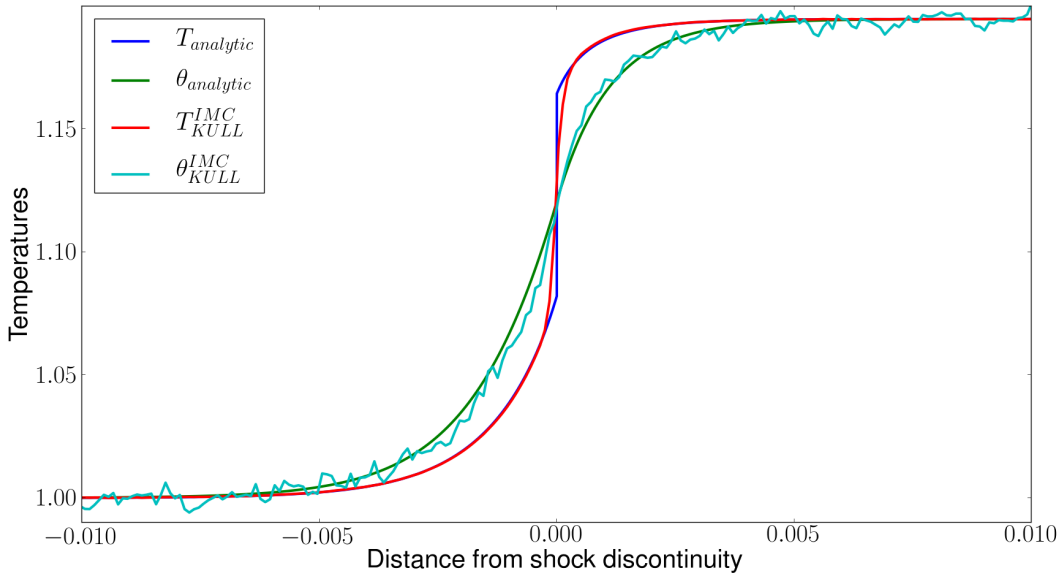

Figure IV.14: Code-verification of the IMC radiation transport package, with relativistic material-motion corrections [65], in KULL using Lowrie's semi-analytic ("analytic") solution for $\mathcal{M}_0 = 1.2$ and $P_0 = 10^{-4}$. The material and radiation temperatures, computed by KULL, reasonably match the analytic solutions.

$$p = \frac{\rho T}{\gamma}\,, \tag{IV.56a}$$

$$e = \frac{T}{\gamma\left(\gamma-1\right)}\,. \tag{IV.56b}$$

The system of equations to be solved, with the ideal-gas EOS implemented, are

$$\partial_x\left(\rho u\right) = 0\,, \tag{IV.57a}$$

$$\partial_x\left(\rho u^2 + \frac{\rho T}{\gamma} + \frac{1}{3}P_0\mathcal{E}_o\right) = 0\,, \tag{IV.57b}$$

$$\partial_x\left[u\left(\frac{1}{2}\rho u^2 + \frac{\rho T}{\gamma-1} + \frac{4}{3}P_0\mathcal{E}_o\right)\right] = P_0\partial_x\left(\kappa\partial_x\mathcal{E}_o\right)\,, \tag{IV.57c}$$

$$\frac{\rho u}{\gamma\left(\gamma-1\right)}\partial_x T + \frac{\rho T}{\gamma}\partial_x u = P_0\sigma_a\left(\mathcal{E}_o - T^4\right)\,, \tag{IV.57d}$$

which represent mass conservation, total momentum conservation, total energy conservation, and the internal energy equation.

IV.3.2.2 Lowrie's semi-analytic solution method: Problem statement

Since the nondimensionalization imposed that the reference dimensional quantities are given at the upstream equilibrium state, the nondimensional variables of the reference dimensional quantities, at the upstream equilibrium state, are set to unity: $\rho_0 = 1$, $T_0 = 1$ and $\mathcal{E}_o = 1$. Given the values of γ, $\mathcal{M}_0$, P_0, and the functions $\sigma_a(\rho, T)$ and $\sigma_t(\rho, T)$, equations (IV.57) allow the functions $\rho(x)$, $u(x)$, $T(x)$ and $\mathcal{E}_o(x)$ to be computed.

IV.3.2.3 Lowrie's semi-analytic solution method: Overall jump conditions

The first three equations of equations (IV.57) can be integrated from the initial upstream equilibrium state-$_0$ to the final downstream equilibrium state-$_f$:

$$\begin{pmatrix} \rho u \\ \rho u^2 + \frac{\rho T}{\gamma} + \frac{1}{3} P_0 T^4 \\ u\left(\frac{1}{2}\rho u^2 + \frac{\rho T}{\gamma - 1} + \frac{4}{3} P_0 T^4\right) \end{pmatrix}_0 = \begin{pmatrix} \rho u \\ \rho u^2 + \frac{\rho T}{\gamma} + \frac{1}{3} P_0 T^4 \\ u\left(\frac{1}{2}\rho u^2 + \frac{\rho T}{\gamma - 1} + \frac{4}{3} P_0 T^4\right) \end{pmatrix}_f , \tag{IV.58}$$

which define the radiation-modified Rankine-Hugoniot jump conditions for the radiating shock at the far-upstream and far-downstream boundaries. These jump conditions must be solved numerically for T_f, and then all of the downstream equilibrium state values may be determined. The first constraint, the first-integral of mass conservation, allows the initial Mach number to be defined:

$$\mathcal{M}_0 = \rho_0 u_0 = u_0. \tag{IV.59}$$

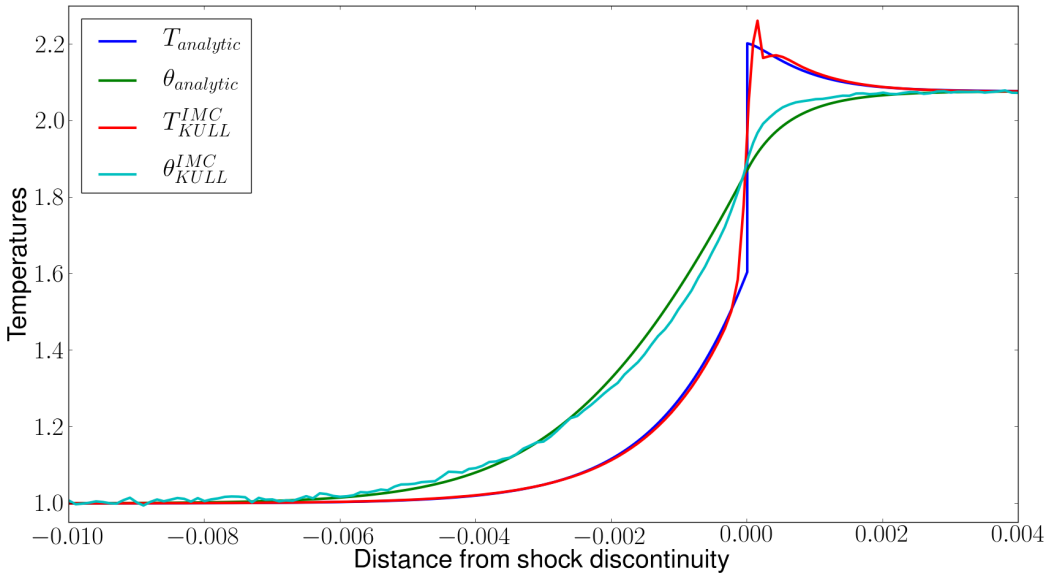

Figure IV.15: Same conditions as Figure IV.14, but with $\mathcal{M}_0 = 2$. The material and radiation temperatures, computed by KULL, begin to show distortions from the analytic temperatures. The radiation temperature shows a "lead-lag-lead" behavior compared to the analytic solution. The material temperature, near the apex of the Zel'dovich spike, appears to have a strongly damped oscillation as it goes into the final downstream equilibrium region.

IV.3.2.4 Lowrie's semi-analytic solution method: Reduced equations

The four equations (IV.57) may be reduced to two ODEs,

$$\frac{d\mathcal{E}_o}{dx} = \frac{\mathcal{M}_0}{P_0\kappa}\left[\frac{T-1}{\gamma-1} + \frac{\mathcal{M}_0^2}{2\rho^2}\left(1-\rho^2\right) + \frac{4}{3}P_0\left(\frac{\mathcal{E}_o}{\rho}-1\right)\right], \tag{IV.60a}$$

$$\frac{dx}{d\mathcal{M}} = -\frac{6\mathcal{M}_0\rho T\left(\mathcal{M}^2-1\right)}{P_0\left(\gamma+1\right)\mathcal{M}\left[\mathcal{M}_0\frac{d\mathcal{E}_o}{dx} + 3\rho\sigma_a\left(\frac{\gamma-1}{\gamma+1}\right)\left(\gamma\mathcal{M}^2+1\right)\left(\mathcal{E}_o - T^4\right)\right]}, \tag{IV.60b}$$

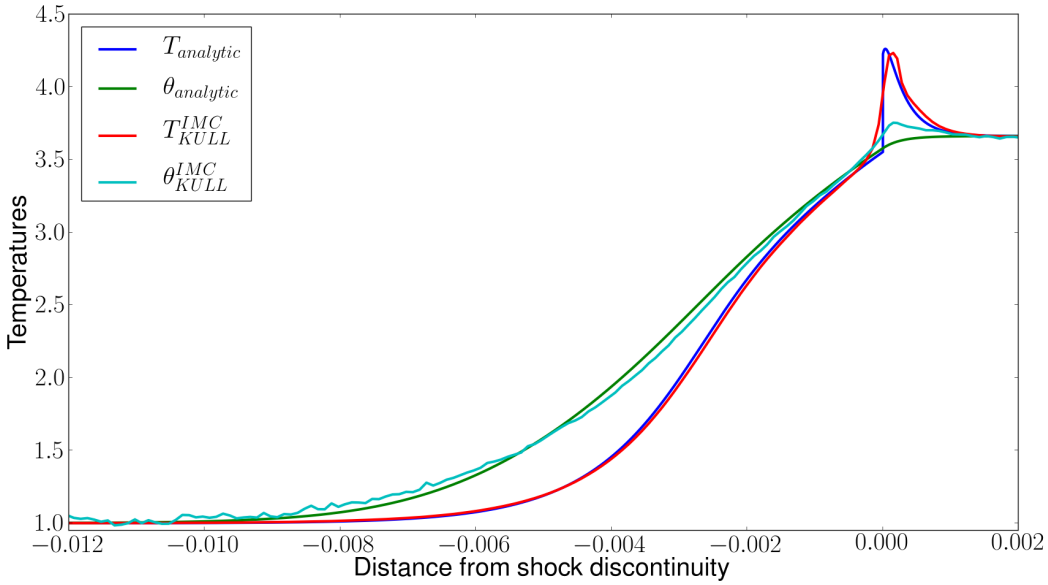

Figure IV.16: Same conditions as Figure IV.14, but with $\mathcal{M}_0 = 3$. The material and radiation temperatures, computed by KULL, show distortions from the analytic temperatures. The radiation temperature and, to a lesser extent the material temperature, shows a "lead-lag-lead" behavior compared to the analytic solution. The radiation temperature, under the Zel'dovich spike, has a local-maximum. The material temperature, around the Zel'dovich spike, shows considerable distortion.

where

$$\rho = \rho\left(\mathcal{M}\right) = \frac{\mathcal{M}_0^2\left(\gamma\mathcal{M}^2+1\right)}{\mathcal{M}^2\left(\gamma\mathcal{M}_0^2+1\right)}\,, \tag{IV.61a}$$

$$T = T\left(\rho\left(\mathcal{M}\right),\mathcal{M}\right) = \frac{\mathcal{M}_0^2}{\rho^2\mathcal{M}^2}\,. \tag{IV.61b}$$

Equations (IV.60) are integrated across the precursor region, $\mathcal{M} \in (\mathcal{M}_0 > 1, 1)$, and the relaxation region, $\mathcal{M} \in (\mathcal{M}_f < 1, 1)$, independently. If the precursor value of $\mathcal{E}_o$, at $\mathcal{M}_p = 1+\epsilon$, is less than the value of $\mathcal{E}_o$ on the relaxation side, at $\mathcal{M}_s = 1-\epsilon$, where $\epsilon \ll 1$, then the shock is continuous across the entire spatial profile. If the shock

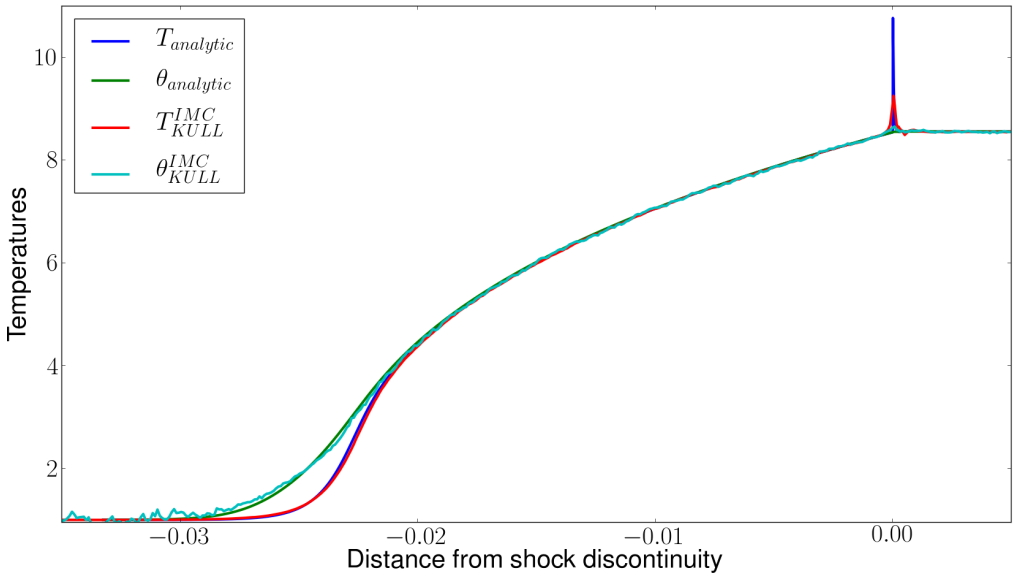

Figure IV.17: Same conditions as Figure IV.14, but with $\mathcal{M}_0 = 5$. The material and radiation temperatures, computed by KULL, show distortions from the analytic solutions in the nonequilibrium region; in the equilibrium region, the KULL results exhibit remarkable agreement with the analytic solutions over an extended distance, up to the Zel'dovich spike. At the Zel'dovich spike, the material temperature is significantly lower than the analytic temperature, and the radiation temperature has a local-maximum.

is not continuous, then there exists an embedded hydrodynamic shock. State-$_p$ and state-$_s$, bounding the embedded hydrodynamic shock, are determined by enforcing continuity of the *lab-frame* radiation energy flux

$$\mathcal{F} = -\kappa \partial_x \mathcal{E}_o + \frac{4}{3} u \mathcal{E}_o \,. \tag{IV.62}$$

The distinction between the analytic results obtained in Section IV.1, and Lowrie's semi-analytic solutions, outlined above, are shown in Figures IV.12 and IV.13.

IV.3.3 Code-verification of KULL's Implicit Monte Carlo radiation transport package using Lowrie's semi-analytic solutions

Lowrie's nonequilibrium diffusion semi-analytic solution method can be used for code-verification of RH codes which generate radiative shocks. For convenience, Lowrie's solution will now be referred to as an analytic solution. In work with Bryan Johnson at LLNL, Lowrie's nonequilibrium radiative shock code was developed for the purpose of testing the Implicit Monte Carlo (IMC) [66] radiation transport package in the multi-physics package, KULL. The variant of IMC tested here solves the radiation transport equation, with modified material-motion corrections, which are not accurate through $\mathcal{O}(\beta)$. Figures IV.14 - IV.17 show the results of these tests for initial Mach numbers, $\mathcal{M}_0 = 1.2$, 2, 3 and 5, respectively, and $P_0 = 10^{-4}$. The KULL input data is initialized with the analytic solution for a given $\mathcal{M}_0$. KULL then propagates the shock wave along a planar-direction, with reflective boundary conditions at the end-planes. The simulation stops after a prescribed time-lapse, which represents a few shock crossing-times. If there are no bugs in the physics packages used by KULL, specific to radiation transport and hydrodynamics, and assuming the physics in the solution is not too dissimilar from the physics packages used by KULL, then KULL should propagate the shock wave without considerable distortion.

Figure IV.14 shows the result from KULL for $\mathcal{M}_0 = 1.2$. The noise in the IMC data, near equilibrium, is an artifact of Monte Carlo processes. Overall, KULL holds the shock wave reasonably well. The material temperature does not hold the shock discontinuity perfectly, but this is expected from a discretized hydrodynamic solver that is not using adaptive mesh refinement. The radiation temperatures appear to be "close enough".

Figure IV.15 was generated with the same conditions as Figure IV.14, but with $\mathcal{M}_0 = 2$. These KULL results show an organized deviation from the analytic solutions, especially in the radiation temperature. The radiation temperature, computed by KULL, is slightly larger than the analytic result near the upstream equilibrium state, then less than it until the shock discontinuity, and then significantly larger than the analytic radiation temperature under the Zel'dovich spike. Due to this "lead-lag" nature, it can not be an artefact of misaligning the KULL result with the analytic solution. The material temperature, computed by KULL, matches the analytic result reasonably well, except near the apex of the Zel'dovich spike where an oscillation appears to be quickly damped going into the relaxation region.

Figure IV.16 shows the results from KULL for $\mathcal{M}_0 = 3$. These results show similar characteristics to those just mentioned. The radiation temperature, computed by KULL, exhibits a "lead-lag" nature, but this time takes on a local-maximum value under the Zel'dovich spike. This last feature under the Zel'dovich spike is a manifestation of anti-diffusion due to a radiation transport solution. The material temperature, computed by KULL, might also be exhibiting the same "lead-lag" nature as the radiation temperature. Approaching the shock discontinuity, the material temperature diverges from the analytic solution.

Figure IV.17 shows the results from KULL for $\mathcal{M}_0 = 5$. These results show the characteristics mentioned previously in the nonequilibrium region, but in the equilibrium region the results from KULL and the analytic solution exhibit remarkable agreement over an extended distance, up to the Zel'dovich spike. At the Zel'dovich spike, the material temperature, computed by KULL, is significantly lower than the

analytic temperature, and the radiation temperature, computed by KULL, still appears to have a local-maximum.

CHAPTER V

RADIATIVE SHOCK SOLUTIONS WITH GREY S_N TRANSPORT

In this chapter, we describe a semi-analytic solution method for planar nonequilibrium radiative shocks using a variable Eddington factor (VEF) computed using angularly-discretized (S_n) radiation transport. This work is an extension of the work by Lowrie and Edwards [1], wherein the radiation is modeled using nonequilibrium-diffusion with a constant Eddington factor, $f(x) \equiv \frac{1}{3}$, and uses ideas, and verifies predictions, made in the work by McClarren and Drake [2]. Specifically, a two-step iteration procedure is described which consistently converges 1) the radiative shock solution and, 2) the VEF. The first step is to compute the spatial structure of the radiative shock, given a VEF, in a manner similar to [1]; this is called "the RH solve". In the first iteration, the VEF for the RH solve is assumed to be one-third everywhere: $f(x) \equiv 1/3$. The second step uses the values of variables computed in step one to solve the S_n radiation transport equation; this is called "the RT solve". The RT solve produces the solutions for n radiation intensities. Quadrature integration of the n radiation intensities produces new values of the radiation variables, and the VEF. Consistently converge means that the measured error of the radiation variables between the RH and RT solves converges, and is controlled by the error tolerance of the numerical integrator. The solutions described here are accurate enough to be used to verify RH codes that solve the radiation transport equation for the radiation intensity, or its angular moments [35, 40, 41]. Because a numerical procedure is required, the solutions are referred to as semi-analytic.

For a given equation of state (EOS), the spatial character of a radiative shock wave is determined by the initial Mach number, $\mathcal{M}_0$, the radiation strength, P_0, and the functional form of the material cross-sections: σ_a and $\sigma_t = \sigma_a + \sigma_s$. Shock waves separate two distinct states of the fluid which are in different equilibrium states. The stronger the shock, the further apart these equilibrium states are. The initial Mach number determines the strength of the shock. The radiation strength measures the relative amount of radiation energy present in the ambient, unshocked,equilibrium system. The cross-sections control the rate at which the radiation-material system interacts.

The VEF is a measure of the dominant direction of the radiation field. We use the direction cosine, $\{\mu \equiv \cos\theta \,|\, 0 \leq \theta \leq 180°; -1 \leq \mu \leq 1\}$, to describe the net macroscopic flow of the radiation field through the fluid. This is because it is $d\mu$, instead of $d\theta$, that produces equal intervals of probability over the reference domain. Given the radiation intensity, as a function of the direction cosine, the VEF is defined as the ratio of the second- and zeroth-angular moments of the radiation intensity

$$f \equiv \frac{\int_{4\pi} \mu^2 I(\mu)\, d\mu}{\int_{4\pi} I(\mu)\, d\mu}\,. \tag{V.1}$$

When $f = 1/3$, radiation is travelling with equal intensity in all directions, resembling isotropic emission and absorption, or diffusion. As will be shown in Subsection V.5.1, when $f > 1/3$, the radiation intensity is strongest for values of $|\mu| \lesssim 1$, resembling forward peaked or transmissive radiation. When $f < 1/3$ the radiation intensity is strongest for values of $|\mu| \gtrsim 0$, resembling oblique radiation. Oblique radiation is strongest under the Zel'dovich spike near the embedded hydrodynamic shock. When the material and radiation temperatures are in equilibrium, then radi-

ation is emitted and absorbed isotropically, and $f \equiv 1/3$. An imperfect measure of the VEF is how far the material and radiation temperatures are out of equilibrium. As a rule-of-thumb, when the radiation temperature is greater than the material temperature then the VEF is greater than 1/3, and conversely, when the radiation temperature is less than the material temperature then the VEF is less than 1/3. Near an embedded hydrodynamic shock, sharp changes in the relationship between the material and radiation temperatures cause the constant Eddington approximation to be invalid.

In order to simplify the analysis, several additional assumptions are made. The material cross-sections are restricted to depend only on the material density and temperature. In particular, the material is assumed to be homogeneous, such that the cross-sections have no explicit spatial dependence. Although the solutions presented here can be useful to help verify RH codes and offer additional physical insight, the assumptions made must be kept in mind. The S_n-transport model assumes that the angular distribution of the radiation intensity is reasonably represented by a finite number of discrete angles. The grey assumption represents each cross-section as a frequency-averaged value. It is particularly invalid when line- or edge-structures of the material cross-sections play a significant role. The ion and electron temperatures are assumed to be equal throughout the material, and heat conduction and viscous effects within the material are ignored. In short, these assumptions may certainly break down.

The rest of this Chapter is devoted to describing the solution method and examining the results. In Section V.1, the general equations of RH are collected, along with the zeroth- and first-angular moments of the radiation transport equation, and

nondimensionalized, as steady-state ODEs. In Section V.2, the problem to be solved is succinctly defined. In Section V.3, the nondimensionalized ODEs are manipulated into a single ODE for the RH solve, and a separate ODE for the RT solve. In Section V.4, the two-step iterated solution procedure is described, and specific attention is given to the initializations of the RH and RT solves. In Section V.5, the semi-analytic results are presented and discussed: they are compared to the nonequilibrium diffusion solutions found in [1]; used for code-verification of the IMC radiation transport package coupled to the KULL multi-physics package developed at LLNL; used to analyze the material and radiation temperature on the precursor side of the Zel'dovich spike and to understand the mechanism of anti-diffusion; and used to re-examine the onset of supercritical ("diffusive") shocks.

V.1 Governing equations and nondimensionalization

We seek consistent shock wave solutions of the RH equations. In this section, the RH equations are written, along with the first two angular moments of the radiation transport equation, and nondimensionalized. The equations are then rewritten in a form that allows them to be solved semi-analytically.

The equations of 1-D grey RH are the Euler equations of fluid-mechanics and the frequency-integrated equation of radiation transport:

$$\partial_t \rho + \partial_x (\rho u) = 0 \,, \tag{V.2a}$$

$$\partial_t (\rho u) + \partial_x \left(\rho u^2 + p\right) = -S_{rp} \,, \tag{V.2b}$$

$$\partial_t \left(\frac{1}{2}\rho u^2 + \rho e\right) + \partial_x \left[u\left(\frac{1}{2}\rho u^2 + \rho e + p\right)\right] = -S_{re} \,, \tag{V.2c}$$

$$\partial_t I + \mu\partial_x I = -\sigma_t I + \frac{\sigma_s}{4\pi}c\mathcal{E} + \frac{\sigma_a}{4\pi}a_r c T^4 + \beta\mu\left(\sigma_t I + 3\frac{\sigma_s}{4\pi}c\mathcal{E} + 3\frac{\sigma_a}{4\pi}a_r c T^4\right) - 2\beta\frac{\sigma_s}{4\pi}\mathcal{F} + \frac{1}{4\pi}\left(C_0 + 3\mu C_1\right) \equiv Q\,, \quad \text{(V.2d)}$$

where S_{re} and S_{rp} are the first two angular moments of the radiation transport equation, and represent the radiation source-rates of energy and momentum

$$S_{re} \equiv \int_{4\pi} Q d\mu = \partial_t\mathcal{E} + \partial_x\mathcal{F} = \sigma_a c\left[a_r T^4 - \left(\mathcal{E} - \frac{2}{c}\beta\mathcal{F}\right)\right] - \sigma_t\beta\mathcal{F} + C_0\,, \quad \text{(V.3a)}$$

$$S_{rp} \equiv \frac{1}{c}\int_{4\pi} Q\mu d\mu = \frac{1}{c^2}\partial_t\mathcal{F} + \partial_x\mathcal{P} = -\frac{\sigma_t}{c}\left[\mathcal{F} - \left(\mathcal{E} + \mathcal{P}\right)u\right] + \sigma_a\beta\left(a_r T^4 - \mathcal{E}\right) + \frac{1}{c}C_1\,. \quad \text{(V.3b)}$$

The purpose of C_0 and C_1 is to ensure that the radiation source-rates go to zero in equilibrium, and to also allow us to define the radiation internal energy source-rate as

$$S_{re} - uS_{rp} = \sigma_a c\left(\alpha_R T^4 - \mathcal{E}_o\right)\,. \quad \text{(V.4)}$$

The values of C_0 and C_1 which accomplish this task are derived in Appendix E:

$$C_0 = \beta^2 c\left(\left(\sigma_s - \sigma_a\right)\left(\mathcal{E} + \mathcal{P}\right) + \sigma_a\left(\alpha_R T^4 - \mathcal{E}\right)\right)\,, \quad \text{(V.5a)}$$

$$C_1 = 0\,. \quad \text{(V.5b)}$$

Thus, the radiation source-rates of energy, momentum, and internal energy, written explicitly in terms of the lab-frame radiation variables, are:

$$S_{re} = \sigma_a c\left[a_r T^4 - \left(\mathcal{E} - \frac{2}{c}\beta\mathcal{F}\right)\right] - \sigma_t\beta\mathcal{F} + \beta^2 c\left(\left(\sigma_s - \sigma_a\right)\left(\mathcal{E} + \mathcal{P}\right) + \sigma_a\left(\alpha_R T^4 - \mathcal{E}\right)\right)\,, \quad \text{(V.6a)}$$

$$S_{rp} = -\frac{\sigma_t}{c}\left[\mathcal{F} - (\mathcal{E}+\mathcal{P})\,u\right] + \sigma_a\beta\left(a_r T^4 - \mathcal{E}\right)\,, \tag{V.6b}$$

$$S_{re} - uS_{rp} = \sigma_a c\left(\alpha_R T^4 - \mathcal{E}\right) + 2\sigma_a\beta\mathcal{F} - 2\sigma_a u\left(\mathcal{E}+\mathcal{P}\right)\,. \tag{V.6c}$$

It is useful to nondimensionalize the RH equations and group the dimensional variables. Each dimensional variable is decomposed into a variable containing the dimension, and a separate variable, with a tilde over it, which contains the value; e.g., a length is nondimensionalized as $\tilde{x} = x\tilde{L}$. The following dimensional quantities are used extensively in the nondimensionalization:

$$\begin{aligned}
&\tilde{L} && \text{(reference length)}\,,\\
&\tilde{\rho}_0 && \text{(reference material mass density)}\,,\\
&\tilde{T}_0 && \text{(reference material temperature)}\,,\\
&\tilde{a}_0 && \text{(reference material sound speed)}\,,\\
&\tilde{c} && \text{(speed of light)}\,,\\
&\tilde{\alpha}_R && \text{(radiation constant)}\,.
\end{aligned}$$

The subscript-"$_0$" indicates that a variable is evaluated at the pre-shock, upstream equilibrium, state. The reference length $\tilde{L}$, is assumed to be $\mathcal{O}(1cm)$. The nondimensional quantities are then defined in terms of their dimensional counterparts as follows:

$$\begin{aligned}
x &= \frac{\tilde{x}}{\tilde{L}} && \text{(spatial coordinate)}\,,\\
t &= \frac{\tilde{t}\tilde{a}_0}{\tilde{L}} && \text{(time coordinate)}\,,\\
\rho &= \frac{\tilde{\rho}}{\tilde{\rho}_0} && \text{(material mass density)}\,,\\
u &= \frac{\tilde{u}}{\tilde{a}_0} && \text{(material velocity)}\,,
\end{aligned}$$

$$
\begin{aligned}
&\mathcal{C} \equiv \frac{\tilde{c}}{\tilde{a}_0}\,, \\
&\beta = \frac{\tilde{u}}{\tilde{c}} = u\frac{\tilde{a}_0}{\tilde{c}} = \frac{u}{\mathcal{C}}\,, \\
&e = \frac{\tilde{e}}{\tilde{a}_0^2} && \text{(material internal energy density)}\,, \\
&p = \frac{\tilde{p}}{\tilde{\rho}\tilde{a}_0^2} && \text{(material pressure)}\,, \\
&T = \frac{\tilde{T}}{\tilde{T}_0} && \text{(material temperature)}\,, \\
&\theta = \frac{\tilde{\theta}}{\tilde{T}_0} && \text{(radiation temperature)}\,, \\
&\sigma_a = \tilde{\sigma}_a\tilde{L} && \text{(absorption cross-section)}\,, \\
&\sigma_s = \tilde{\sigma}_s\tilde{L} && \text{(scattering cross-section)}\,, \\
&\sigma_t = \tilde{\sigma}_t\tilde{L} && \text{(total cross-section)}\,, \\
&\kappa = \frac{1}{\tilde{\sigma}_t\tilde{L}} = \frac{1}{\sigma_t} && \text{(radiation diffusivity)}\,, \\
&I = \frac{\tilde{I}}{\tilde{\alpha}_R\tilde{c}\tilde{T}_0^4} && \text{(radiation intensity)}\,, \\
&\mathcal{E} = \frac{\tilde{\mathcal{E}}}{\tilde{\alpha}_R\tilde{T}_0^4} && \text{(radiation energy density)}\,, \\
&\mathcal{F} = \frac{\tilde{\mathcal{F}}}{\tilde{\alpha}_R c\tilde{T}_0^4} && \text{(radiation flux)}\,, \\
&\mathcal{P} = \frac{\tilde{\mathcal{P}}}{\tilde{\alpha}_R\tilde{T}_0^4} \equiv f\mathcal{E} && \text{(radiation pressure)}\,.
\end{aligned}
$$

The reason for nondimensionalizing the material internal energy density $\tilde{e}$, with the square of the reference sound speed $\tilde{a}_0^2$, is explained in Appendix F. The VEF, f, is introduced in the definition of the radiation pressure $\mathcal{P}$.

We further impose the steady-state condition on the RH equations (V.2) and (V.3),

and write this system in nondimensional form as

$$\partial_x \left(\rho u\right) = 0 \,, \tag{V.7a}$$

$$\partial_x \left(\rho u^2 + p\right) = -P_0 S_{rp} \,, \tag{V.7b}$$

$$\partial_x \left[u\left(\frac{1}{2}\rho u^2 + \rho e + p\right)\right] = -P_0 \mathcal{C} S_{re} \,, \tag{V.7c}$$

$$\begin{aligned}\mu \partial_x I = -\sigma_t I + \frac{\sigma_s}{4\pi}\mathcal{E} + \frac{\sigma_a}{4\pi}T^4 - 2\frac{\sigma_s}{4\pi}\beta\mathcal{F} + \beta\mu\left(\sigma_t I + \frac{3\sigma_s}{4\pi}\mathcal{E} + \frac{3\sigma_a}{4\pi}T^4\right) \\ + \frac{1}{4\pi}\beta^2\left(\left(\sigma_s - \sigma_a\right)\left(\mathcal{E} + \mathcal{P}\right) + \sigma_a\left(T^4 - \mathcal{E}\right)\right) \,,\end{aligned} \tag{V.7d}$$

where the nondimensional radiation source-rates of energy, momentum and internal energy are

$$\begin{aligned}S_{re} = \sigma_a\left[T^4 - \mathcal{E}\right] + \beta\left(\sigma_a - \sigma_s\right)\mathcal{F} \\ + \beta^2\left(\left(\sigma_s - \sigma_a\right)\left(\mathcal{E} + \mathcal{P}\right) + \sigma_a\left(T^4 - \mathcal{E}\right)\right) = \partial_x \mathcal{F} \,,\end{aligned} \tag{V.8a}$$

$$S_{rp} = -\sigma_t\left[\mathcal{F} - \beta\left(\mathcal{E} + \mathcal{P}\right)\right] + \sigma_a\beta\left(T^4 - \mathcal{E}\right) = \partial_x \mathcal{P} \,, \tag{V.8b}$$

$$S_{re} - \beta S_{rp} = \sigma_a\left(T^4 - \mathcal{E}\right) + 2\sigma_a\beta\left(\mathcal{F} - \mathcal{E} - \mathcal{P}\right) \,. \tag{V.8c}$$

The nondimensional constant P_0, defined as $P_0 \equiv \frac{\tilde{\alpha}_R \tilde{T}_0^4}{\tilde{\rho}_0 \tilde{a}_0^2}$, represents the relative contribution of radiation energy to the total energy in the system; P_0 is proportional to the ratio of the radiation pressure to material pressure and alternatively, the radiation energy to the material energy. It is a measure of the influence of radiation on the flow dynamics.

The radiation flux can be derived from the radiation momentum source rate, equation

(V.8b),

$$\mathcal{F} = -\frac{1}{\sigma_t}\partial_x \mathcal{P} + \frac{1}{\sigma_t}\beta\left(\sigma_t \mathcal{P} + \sigma_s \mathcal{E} + \sigma_a T^4\right) . \tag{V.9}$$

Solutions of the RH system, equations (V.7), also satisfy the material internal energy equation

$$\rho u \partial_x e + p \partial_x u = -P_0 \mathcal{C}\left(S_{re} - \beta S_{rp}\right) . \tag{V.10}$$

As stated at the beginning of this section, we seek consistent shock wave solutions of the RH equations (V.7). However, we obtain these solutions by combining equations (V.7a) - (V.7c) with equations (V.8a) and (V.8b), along with equation (V.10) which uses equation (V.8c), and solving the resulting system

$$\partial_x\left(\rho u\right) = 0 , \tag{V.11a}$$

$$\partial_x\left(\rho u^2 + p + P_0 \mathcal{P}\right) = 0 , \tag{V.11b}$$

$$\partial_x\left[u\left(\frac{1}{2}\rho u^2 + \rho e + p\right) + P_0 \mathcal{C}\mathcal{F}\right] = 0 , \tag{V.11c}$$

$$\rho u \partial_x e + p \partial_x u = -P_0 \mathcal{C}\left[\sigma_a\left(T^4 - \mathcal{E}\right) + 2\sigma_a \beta\left(\mathcal{F} - \mathcal{E} - \mathcal{P}\right)\right] , \tag{V.11d}$$

the solutions of which must relate the radiation pressure to the radiation energy density via the VEF, $\mathcal{P} = f\mathcal{E}$, which is constructed by solving the steady-state radiation transport equation

$$\begin{aligned}\mu \partial_x I = -\sigma_t I + \frac{\sigma_s}{4\pi}\mathcal{E} + \frac{\sigma_a}{4\pi}T^4 - 2\frac{\sigma_s}{4\pi}\beta\mathcal{F} + \beta\mu\left(\sigma_t I + \frac{3\sigma_s}{4\pi}\mathcal{E} + \frac{3\sigma_a}{4\pi}T^4\right) \\ + \frac{1}{4\pi}\beta^2\left(\left(\sigma_s - \sigma_a\right)\left(\mathcal{E} + \mathcal{P}\right) + \sigma_a\left(T^4 - \mathcal{E}\right)\right) .\end{aligned} \tag{V.12}$$

These steady-state equations (V.11) and (V.12), represent the conservation statements of mass, total momentum and total energy, the internal energy equation, and the radiation transport equation, respectively. The RH solve determines solutions of equations (V.11); the RT solve determines solutions of equation (V.12). When the separate solutions of equations (V.11) and (V.12) converge via iteration, we say the solutions are consistent and that we have found the steady-state shock wave solutions to the RH equations (V.7), which we sought.

V.2 Problem statement

In this section, the problem to be solved is defined. The material fluid flow is assumed to move in the $+x-$direction. The reference state with subscript-$_0$ refers to the pre-shock, upstream equilibrium conditions, attained as $x \to -\infty$, while the subscript-$_1$ refers to post-shock, downstream equilibrium conditions, attained as $x \to \infty$. Far from the shock the flow is in radiative equilibrium, $\mathcal{E} = T^4$, and isotropic, $f = 1/3$. Note that the nondimensional pre-shock solution state is known since reference dimensional values were taken from this upstream equilibrium region, therefore, $\mathcal{E}_0 = 1$, $T_0 = 1$, $\rho_0 = 1$, and $f_0 = 1/3$. The problem statement then is:

- *Assume:* An ideal-gas γ-law EOS, for a monatomic fluid obeying Eulerian hydrodynamics, and interacting with radiation which is described by grey S_n transport.

- *Given:* The values γ, $\mathcal{M}_0$, P_0, and the functions $\sigma_a(\rho, T)$ and $\sigma_t(\rho, T)$.

- *Calculate:* The functions $p(x)$, $\rho(x)$, $u(x)$, $T(x)$, $\mathcal{M}(x)$, $I(\mu_m, x)$, $\theta^4(x) \equiv \mathcal{E}(x)$, $\mathcal{F}(x)$, $\mathcal{P}(x)$, and $f(x)$.

V.3 Reduced equations

In this Section, the ideal gas γ-law EOS is given, and the reduced set of ODEs that satisfy the steady-state system of RH equations (V.11) and (V.12), for the shock problem given in Section V.2, are derived. In Subsection V.3.1, the steady-state RH moment equations (V.11) are reduced to a single ODE. In Subsection V.3.2, the radiation transport equation (V.12) is angularly discretized, and the angular moments of its solutions are defined, and computed via quadrature integration.

The ideal-gas γ-law EOS is written in nondimensional form as

$$p = \frac{\rho T}{\gamma}\,, \tag{V.13a}$$

$$e = \frac{T}{\gamma\,(\gamma - 1)}\,, \tag{V.13b}$$

where the adiabatic index γ, is assumed constant and equal to $5/3$ for a monatomic gas. This form of the EOS is derived in Appendix F. This EOS is quite restrictive for several radiation-hydrodynamic flow regimes, but greatly simplifies the analysis.

It is also convenient to include here the nondimensional expression for the local Mach number, as derived in Appendix F:

$$\mathcal{M} = \frac{u}{\sqrt{T}}\,. \tag{V.14}$$

The ODEs for the RH solve, which result from the ideal gas γ-law EOS (V.13), are

$$\partial_x\,(\rho u) = 0\,, \tag{V.15a}$$

$$\partial_x \left(\rho u^2 + \frac{\rho T}{\gamma} + P_0 \mathcal{P} \right) = 0 \,, \tag{V.15b}$$

$$\partial_x \left[u \left(\frac{1}{2} \rho u^2 + \frac{\rho T}{\gamma - 1} \right) + P_0 \mathcal{C} \mathcal{F} \right] = 0 \,, \tag{V.15c}$$

$$\frac{\rho u}{\gamma \left(\gamma - 1 \right)} \partial_x T + \frac{\rho T}{\gamma} \partial_x u = -P_0 \mathcal{C} \left[\sigma_a \left(T^4 - \mathcal{E} \right) + 2 \sigma_a \beta \left(\mathcal{F} - \mathcal{E} - \mathcal{P} \right) \right] \,. \tag{V.15d}$$

Again, these equations represent the conservation of mass, conservation of total momentum, conservation of total energy, and the material internal energy equation, respectively. These ODEs are simplified to a single ODE in the next subsection; the ODEs for the RT solve are the angularly discretized radiation transport equations, presented in Subsection V.3.2.

V.3.1 The ordinary differential equations for the radiation hydrodynamic solve

In this subsection, the ODEs that simultaneously describe the precursor and relaxation regions, equations (V.15), are manipulated into a single ODE. This manipulation begins by expressing the equation of mass conservation as an algebraic expression, and the equation of total momentum conservation as a differential expression. Algebraically manipulating the equation of material internal energy produces a gradient expression for the material temperature. Integrating the equation of total energy conservation produces a gradient expression for the radiation pressure, which can be combined with the gradient of the local Mach number, to produce the ODE which is to be integrated. The numerical integration of this ODE, and the method to splice the solutions from the precursor and relaxation regions together is described in Section V.4.

Integrate the equation of mass conservation (V.15a) to give

$$\rho u = \rho_0 u_0 = u_0 = \mathcal{M}_0 \,, \tag{V.16}$$

where it has been recalled, from Section V.2, that $\rho_0 = 1$ $T_0 = 1$, and the equation for the local Mach number (V.14), has been used. The local Mach number (V.14), may now be expressed as a function of density and temperature

$$\mathcal{M} = \frac{u}{\sqrt{T}} = \frac{\mathcal{M}_0}{\rho\sqrt{T}} \,. \tag{V.17}$$

Distribute the derivative in the equation of total momentum conservation (V.15b), and use equations (V.17) and (V.16), to produce:

$$\partial_x \rho = \frac{\rho \partial_x T + \gamma P_0 \partial_x \mathcal{P}}{T\left(\gamma \mathcal{M}^2 - 1\right)} \,. \tag{V.18}$$

Integrate the equation of total energy conservation (V.15c), and use equation (V.16), to produce:

$$\partial_x \mathcal{P} = \frac{\sigma_t \mathcal{M}_0}{\mathcal{C} P_0} \left[\frac{T-1}{\gamma - 1} + \frac{\mathcal{M}_0^2}{2\rho^2}\left(1 - \rho^2\right) + P_0 \left(\frac{\sigma_t \mathcal{P} + \sigma_s \mathcal{E} + \sigma_a T^4}{\rho \sigma_t} - \frac{4}{3} \right) \right] \,. \tag{V.19}$$

The material internal energy equation (V.15d) can be rearranged to solve for the spatial derivative of the material temperature:

$$\begin{aligned} \partial_x T = \frac{P_0\left(\gamma - 1\right)}{\mathcal{M}_0 \rho \left(\mathcal{M}^2 - 1\right)} \big[& \mathcal{M}_0 \partial_x \mathcal{P} \\ & + \left(\gamma \mathcal{M}^2 - 1\right) \rho \sigma_a \mathcal{C} \left[\mathcal{E} - T^4 - 2\beta \mathcal{F} + 2\beta^2 \left(\mathcal{E} + \mathcal{P}\right) \right] \big] \,, \end{aligned} \tag{V.20}$$

where equations (V.16) and (V.18) have been used. The derivative of the local Mach number, equation (V.17),

$$\partial_x \mathcal{M} = -\mathcal{M}\left(\frac{1}{\rho}\partial_x \rho + \frac{1}{2T}\partial_x T\right), \tag{V.21}$$

can be simplified, but this does not provide additional insight. The local Mach number is assumed to be monotonic, and equation (V.21) is inverted,

$$\frac{dx}{d\mathcal{M}} = -\frac{2\rho T}{\mathcal{M}\left(2T\partial_x \rho + \rho \partial_x T\right)}, \tag{V.22}$$

such that the local Mach number may now be used as an integration parameter. No proof of the monotonicity of equation (V.21) is known. Thus, the spatial gradient of the radiation pressure, equation (V.19), may be multiplied by equation (V.22),

$$\frac{d\mathcal{P}}{dx}\frac{dx}{d\mathcal{M}} = \frac{d\mathcal{P}}{d\mathcal{M}}\left(\mathcal{M}, \mathcal{P}\right), \tag{V.23}$$

and integrated along the local Mach number to determine the radiation pressure. Then, integrating equation (V.22) along the local Mach number provides the spatial domain. The radiation pressure and the local Mach number are now the primary variables on which all the other RH variables depend. The only two variables which have not been explicitly written in a functional form are the material density and the material temperature. They can be written as functions of the local Mach number and the radiation pressure by integrating the equation of total momentum conservation, equation (V.15b), and by rearranging equation (V.17):

$$\rho\left(\mathcal{M}, \mathcal{P}\right) = \frac{\mathcal{M}_0^2\left(\gamma\mathcal{M}^2 + 1\right)}{\mathcal{M}^2\left(\gamma\mathcal{M}_0^2 + 1 + \gamma P_0\left(\frac{1}{3} - \mathcal{P}\right)\right)}, \tag{V.24a}$$

$$T\left(\mathcal{M},\mathcal{P}\right)=\frac{\mathcal{M}_0^2}{\rho^2\mathcal{M}^2}\,. \tag{V.24b}$$

Alternatively, the material temperature may be chosen as the dependent variable, instead of the radiation pressure, then the material density and the radiation pressure, as functions of the local Mach number and the material temperature, are:

$$\rho\left(\mathcal{M},T\right)=\frac{\mathcal{M}_0}{\mathcal{M}\sqrt{T}}\,, \tag{V.25a}$$

$$\mathcal{P}\left(\mathcal{M},T\right)=\frac{1}{\gamma P_0}\left[\frac{\gamma\mathcal{M}_0^2}{\rho}\left(\rho-1\right)+1+\frac{1}{3}\gamma P_0-\frac{\mathcal{M}_0^2}{\mathcal{M}^2\rho}\right]\,. \tag{V.25b}$$

V.3.2 The ordinary differential equations for the radiation transport solve

In this subsection, the radiation transport equation (V.7d) is angularly discretized along n angular directions. This is often referred to as the S_n method. Quadrature weights, $0<w_m<1$, and roots, $-1<\mu_m<1$, are used that allow accurate quadrature-integration of an n-th order polynomial, where $m\in\mathbb{Z}\{1,n\}$. The S_n method discretizes the angular-variable, $\mu\rightarrow\mu_m$, and by extension the radiation intensity, $I\left(\mu\right)\rightarrow I_m\equiv I\left(\mu_m\right)$, generating n radiation transport equations

$$\begin{aligned}\mu_m\partial_x I_m+\sigma_t I_m-\beta\mu_m\sigma_t I_m=&\frac{\sigma_s}{4\pi}\mathcal{E}+\frac{\sigma_a}{4\pi}T^4-2\frac{\sigma_s}{4\pi}\beta\frac{\mathcal{F}}{\mathcal{C}}+\beta\mu_m\left(\frac{3\sigma_s}{4\pi}\mathcal{E}+\frac{3\sigma_a}{4\pi}T^4\right)\\&+\frac{1}{4\pi}\beta^2\left(\left(\sigma_s-\sigma_a\right)\left(\mathcal{E}+\mathcal{P}\right)+\sigma_a\left(T^4-\mathcal{E}\right)\right)\,.\end{aligned} \tag{V.26}$$

All terms involving the angularly discretized radiation intensity have been moved to the LHS to emphasize that this is the variable being solved for; all of the terms on the RHS are known from the RH solve described in the previous subsection. After the S_n transport equation has been solved for each radiation intensity, the quadrature

integrated angular moments of the radiation intensities produce new values of the radiation energy density, radiation flux, and radiation pressure, respectively,

$$\mathcal{E} = 2\pi \sum_{m=1}^{n} w_m I_m \,, \tag{V.27a}$$

$$\mathcal{F} = 2\pi \sum_{m=1}^{n} \mu_m w_m I_m \,, \tag{V.27b}$$

$$\mathcal{P} = 2\pi \sum_{m=1}^{n} \mu_m^2 w_m I_m \,, \tag{V.27c}$$

from which the VEF is constructed

$$f = \frac{\mathcal{P}}{\mathcal{E}} \,. \tag{V.27d}$$

V.4 Solution procedure

In Subsection V.4.1, the Rankine-Hugoniot jump conditions, from the upstream equilibrium state to the downstream equilibrium state, are presented. In Subsection V.4.2, the initialization procedure for the integration of the RH solve is described. The ODEs used in the RH solve are identically zero in equilibrium, and an initialization procedure must be used to move the solution away from equilibrium so that equation (V.23) can be integrated. The S_n transport equation (V.26), is not identically zero in equilibrium. This is because we are using the $\mathcal{O}(\beta^2)$ Taylor-expansion of the radiation transport equation, and the $\mathcal{O}(\beta^2)$ truncation destroys the equilibrium condition. Subsequently, in Subsection V.3.2, the correct lab-frame initial values of the S_n radiation intensities are determined.

V.4.1 The Rankine-Hugoniot jump conditions

The Rankine-Hugoniot jump conditions determine the downstream equilibrium state of the shock, where $\mathcal{M}_1 < 1$, given the upstream equilibrium state, where $\mathcal{M}_0 > 1$, by enforcing the conservation statements of mass, total momentum and total energy:

$$\begin{pmatrix} \rho u \\ \rho u^2 + p + \frac{1}{3}P_0T^4 \\ u\left(\frac{1}{2}\rho u^2 + \rho e + p + \frac{4}{3}P_0T^4\right) \end{pmatrix}_{\mathcal{M}_0>1} = \begin{pmatrix} \rho u \\ \rho u^2 + p + \frac{1}{3}P_0T^4 \\ u\left(\frac{1}{2}\rho u^2 + \rho e + p + \frac{4}{3}P_0T^4\right) \end{pmatrix}_{\mathcal{M}_1<1} . \tag{V.28}$$

The upstream equilibrium state is established in the problem statement, see Section V.2, so the terms on the LHS are known. The equation in the first row defines the initial Mach number, $\mathcal{M}_0 = \rho u$, see equation (V.16), which helps simplify the second and third equations. Recalling that the ideal-gas EOS specifies that the material pressure and internal energy density are functions of the material density and temperature, the last two equations are functions only of the material density and temperature. However, the equation produced by solving them is of higher-order than quartic, and must be solved numerically.

V.4.2 The radiation hydrodynamic solve

The first RH solve follows exactly the procedure detailed in [1], and produces a radiative shock profile similar to any of the figures in Section IV.3. Initialization of the ODE integration can be done by linearizing away from the equilibrium state to a state perturbed by ϵ: $(\mathcal{M}, \mathcal{P}, T, ...)_\epsilon$. This is achieved by linearizing the RH variables about their equilibrium values, $Y(x) \mapsto Y(x)_{eq} + \delta Y(x)$, and it is assumed that

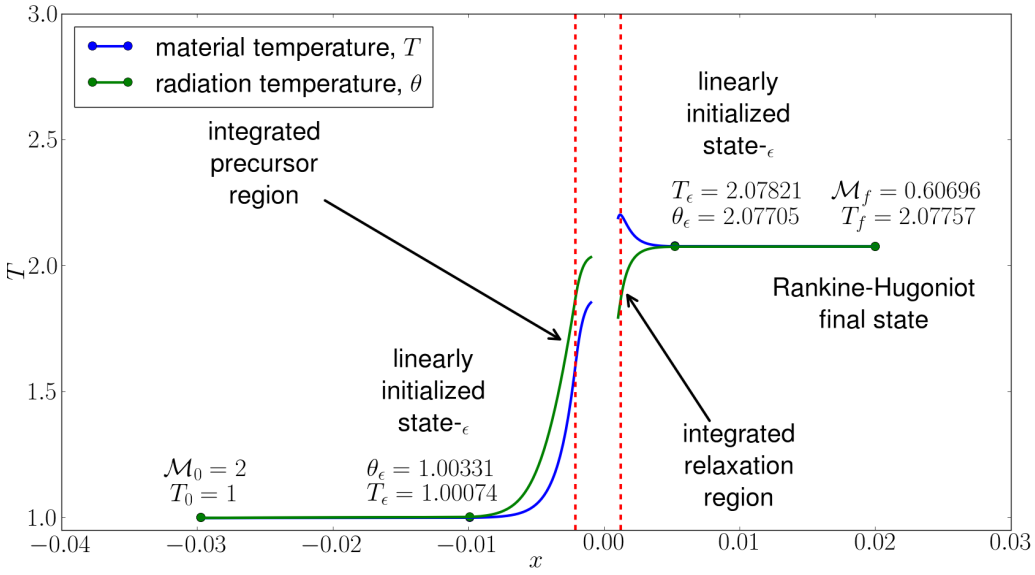

Figure V.1: Solution procedure for the RH solve up to enforcing continuity of the radiation variables. The upstream precursor equilibrium state is given in the problem statement. The radiation modified Rankine-Hugoniot jump conditions allow the downstream relaxation equilibrium state to be determined. The equilibrium states must move to the linearly initialized states-$_\epsilon$ to allow integration of the RH ODEs in the precursor and relaxation regions. If the radiation temperatures from the precursor and relaxation integrations overlap, as shown, then there's an embedded hydrodynamic shock, and continuity of the radiation variables must be enforced; see Figure V.2. The red lines show where to splice the precursor and relaxation regions to construct the complete shock profile. All data between the red lines is discarded.

the linear term can be decomposed into the product of a constant and a spatially dependent exponential term, $\delta Y e^{\alpha x}$, such that $\partial_x \delta Y(x) = \alpha \delta Y e^{\alpha x}$. Then, equations (V.19) - (V.21) are used to obtain a 2×2 system of equations, as derived in Appendix G, which depend only on the equilibrium states, such that the eigenvalue, α, can be determined. Given the local Mach number at state-$_\epsilon$, the radiation pressure at state-$_\epsilon$ can be determined using this linearized initialization. The RH ODEs can

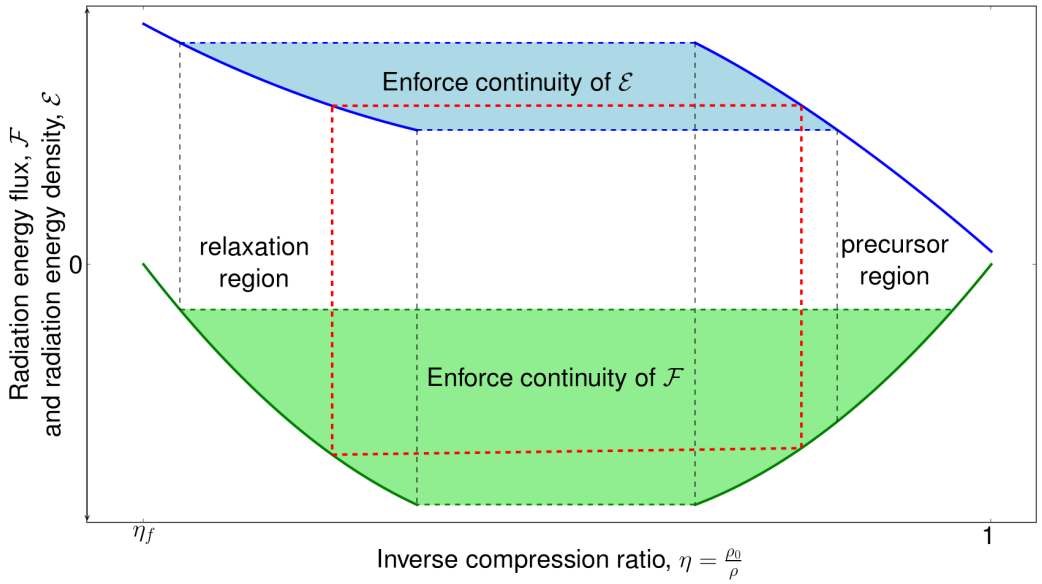

Figure V.2: Radiation energy density and radiation flux plotted versus the inverse compression ratio. Given the values of the integrated radiation variables in the precursor and relaxation regions, continuity of the radiation energy density and radiation pressure is enforced to find the location of the shock. The blue shaded region represents an overlap of the radiation energy density values due to the integrations through the precursor and relaxation regions. The boundary of this overlap is projected onto the values of the radiation flux and defines the boundary of its possible values. The red rectangle represents the correct enforcement of continuity of the radiation variables.

then be integrated in the precursor and relaxation regions; see Figure V.1.

To determine how the solutions in the precursor and relaxation regions are connected requires simultaneously enforcing continuity of the radiation energy density and the radiation flux. See Figure V.2. Enforcing continuity of the radiation flux is equivalent to enforcing conservation of total material energy. Finally, the inverse of the gradient of the local Mach number, equation (V.21), can be integrated to produce the values of the x-coordinate. The RH solves, after the first one, initialize

the radiation pressure by using the value of the radiation pressure determined from the preceding RT solve at the state-$_\epsilon$.

V.4.3 The radiation transport solve

In Appendix F, the radiation energy density in the comoving- and lab-frame is defined such that its equilibrium values are equivalent at $\mathcal{O}(\beta^2)$. The radiation intensity is not invariant between the comoving- and lab-frame, but instead, it transforms invariantly as I/ν^3, where $\frac{\nu_o^3}{\nu^3} = 1 + 3\mu\beta + \mathcal{O}(\beta^2)$. The comoving-frame equilibrium value of the radiation intensity is given as $I_{o,eq} = \frac{\mathcal{E}_{eq}}{4\pi}$, such that the lab-frame equilibrium value is $I_{eq} = \frac{\mathcal{E}_{eq}}{4\pi}\left(1 + 3\mu\beta_{eq}\right) + \mathcal{O}(\beta^2)$. When this expression is discretized along n angular rays it becomes:

$$I_{m,eq} = \frac{\mathcal{E}_{eq}}{4\pi}\left(1 + 3\mu_m\beta_{eq}\right) + \mathcal{O}(\beta^2)\,. \tag{V.29}$$

This provides the initializations for the n lab-frame radiation intensities, so that they can be integrated along the appropriate μ_m. These radiation intensities allow $\mathcal{E}$, $\mathcal{F}$, $\mathcal{P}$, and f to be calculated via equations (V.27), and tested against the solutions from the RH solve for convergence. In this way, $\mathcal{E}$, $\mathcal{F}$ and $\mathcal{P}$ are expected to consistently converge between the RH solve and the RT solve, and f is expected to converge iteratively.

Now, values exist for the local Mach number and the radiation pressure, from the RT solve, which span the spatial domain of the radiative shock wave. Given the value of the local Mach number at the initialization state-$_\epsilon$, the value of the radiation pressure, from the RT solve, at this state can be determined by linear interpolation. This method of determining the initial value of the radiation pressure at state-$_\epsilon$, by

comparing it to the value of the local Mach number at state-$_\epsilon$, is used to initialize subsequent RH solves.

The two-step procedure defines one iteration. At the end of each iteration, L_2 and relative L_∞ errors for the radiation variables between the RH and RT solves are computed, as are L_2 and relative L_∞ errors for the VEF between iterations. The solution procedure is terminated after either 1) the solution tolerance for f is reached, or 2) an iteration occurs wherein no measured error improves. The VEF solution tolerance for the plots shown is 10^{-6}.

V.5 Results and analysis

In this section, the grey S_n radiative shock solutions are discussed. In Subsection V.5.1, differences between the solutions obtained from nonequilibrium diffusion theory [1] and S_n transport are discussed; see Figures V.3 and V.4. In Subsection V.5.2, the S_n radiative shock solutions are used as a code-verification tool for the KULL multi-physics package, as done in Subsection IV.3.3, where Lowrie's nonequilibrium diffusion solutions were used. In Subsection V.5.3, the maximum material and radiation temperatures, and their values on the upstream side of the embedded hydrodynamic shock, in relation to the final equilibrium temperature are discussed; see Figure V.9. Particular emphasis is placed on understanding why the material and radiation temperatures immediately upstream of the embedded hydrodynamic shock may be greater than the final equilibrium temperature, which is in disagreement with nonequilibrium diffusion theory. The anti-diffusive regions found in some shocks, which was first discussed in [2], is a consequence of this behaviour. In Subsection V.5.4, the onset of a diffusive region in strong shocks is briefly discussed. Drake

[5, 6] argues that "subcritical" and "supercritical" shocks are not well separated by the condition of whether $T_p < T_f$, as claimed by nonequilibrium diffusion theory, which is validated.

All of the radiative shock solutions presented in this section use $\gamma = 5/3$, $P_0 = 10^{-4}$, $\sigma_t = 577.35 = \sigma_a$ and $S_n = 16$; S_{16} provides considerably better resolution than S_8, and is computationally cheaper than S_{32} which provides no noticeable improvement.

V.5.1 Comparison of nonequilibrium diffusion and S_n radiative shock solutions

Figure V.3 shows the radiative shock solution for $\mathcal{M}_0 = 2$, comparing the material and radiation temperatures computed from nonequilibrium diffusion, T_{diff} and θ_{diff}, and S_n transport, T and θ, along with the converged profile for $f(x)$, and $f = 1/3$ for reference. The shock profiles do not differ dramatically, despite the distinct difference of the VEF from 1/3. Figure V.4, however, shows a qualitative distinction between the nonequilibrium diffusion solution and the S_n transport solution where $\theta > T_f$ under the Zel'dovich spike. This artifact is discussed in the next subsection. Thus, these solutions are a good test of the hydrodynamic properties via the shock profile, and of the radiation transport properties via the VEF profile and the radiation intensities.

The radiative shock solutions computed from nonequilibrium diffusion theory, and grey S_n transport, are similar because equations (V.19) and (V.20) are not strongly dependent on the radiation model. This can be seen by considering the difference

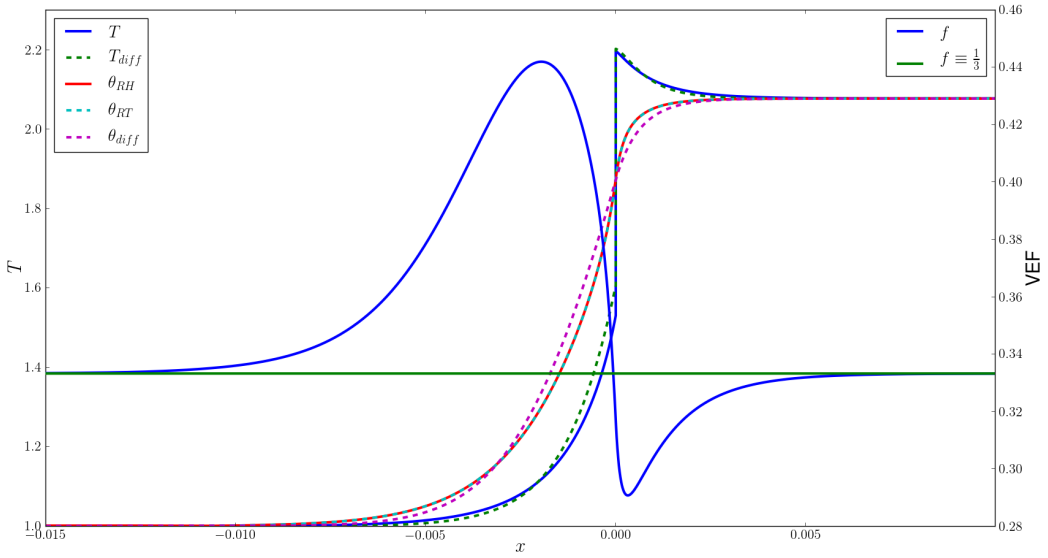

Figure V.3: The converged radiative shock solution for $\mathcal{M}_0 = 2$, $P_0 = 10^{-4}$, and $\sigma_t = 577.35 = \sigma_a$, with temperature scale on the left axis, and VEF scale on the right axis. The nonequilibrium diffusion solution is plotted with dashed lines for comparison. The temperature solutions between the two models are obviously different, and exhibit a "lead-lag-lead" characteristic that was mentioned in Subsection IV.3.3. The converged radiative temperature solutions, θ_{RH} and θ_{RT}, are plotted individually, and are indistinguishable. The VEF is considerably different from 1/3, with values greater than 1/3 in the precursor region leading to the embedded hydrodynamic shock, and dropping below 1/3 in the relaxation region. The constant Eddington factor value of 1/3 is plotted for comparison.

between their gradients for the radiation pressure, and material temperature,

$$\left(\partial_x \mathcal{P}\right)_{S_n} - \left(\frac{1}{3}\partial_x \mathcal{E}\right)_{diff} \propto \frac{T_{S_n} - T_{diff}}{\gamma - 1} + P_0 \left(\frac{\left(f\mathcal{E}_{S_n} - \frac{1}{3}\mathcal{E}_{diff}\right)}{\rho}\right), \tag{V.30a}$$

$$\begin{aligned}\left(\partial_x T\right)_{S_n} - \left(\partial_x T\right)_{diff} \propto \mathcal{M}_0 &\left[\left(\partial_x \mathcal{P}\right)_{S_n} - \left(\frac{1}{3}\partial_x \mathcal{E}\right)_{diff}\right] \\ &+ \left(\gamma \mathcal{M}^2 - 1\right) \rho \sigma_a \mathcal{C} \left[\left(\mathcal{E} - T^4\right)_{S_n} - \left(\mathcal{E} - T^4\right)_{diff}\right], \end{aligned} \tag{V.30b}$$

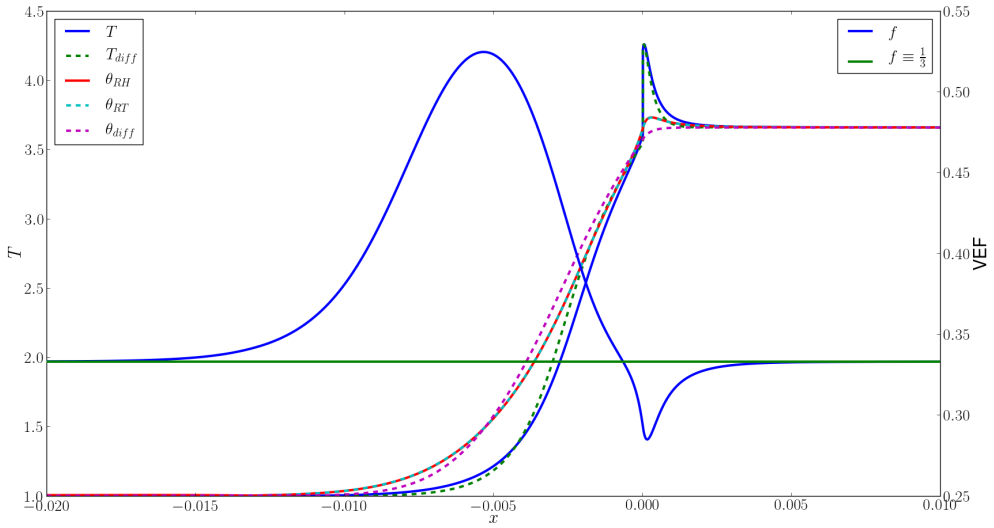

Figure V.4: Same conditions as in Figure V.3 but with $\mathcal{M}_0 = 3$. The nonequilibrium diffusion solutions and the constant Eddington factor of 1/3 are plotted for comparison. The "lead-lag-lead" characteristic is distinctly apparent. The converged radiation temperature solutions, θ_{RH} and θ_{RT}, are plotted individually and are indistinguishable. The anti-diffusive structure of θ, i.e., the local maximum, is apparent under the Zel'dovich spike. The values of the VEF diverge farther from the constant Eddington factor for this solution than for the $\mathcal{M}_0 = 2$ solution in Figure V.3.

where the subscript-$_{diff}$ means nonequilibrium diffusion, and we neglect the difference in material density between the two radiation models. Early in the precursor, while $f(x) \gtrsim 1/3$, the material temperatures, T_{S_n} and T_{diff} are effectively equal, as are the radiation energy densities, $\mathcal{E}_{S_n}$ and $\mathcal{E}_{diff}$, such that the S_n gradient of pressure is slightly larger than the diffusion gradient because $f(x) \gtrsim 1/3$, allowing both of the S_n temperature solutions to exit equilibrium earlier than the nonequilibrium diffusion solutions. To compare the gradients of the radiation energy densities far from equilibrium, we must expand the derivative of the S_n pressure gradient, and

rearrange terms

$$\left(\partial_x \mathcal{E}\right)_{S_n} = \left(\frac{\partial_x \mathcal{P} - \mathcal{E}\partial_x f}{f}\right)_{S_n} \approx \frac{1}{f}\left(\frac{1}{3}\partial_x \mathcal{E}\right)_{diff} - \frac{\mathcal{E}}{f}\partial_x f\,. \tag{V.31}$$

The scales of f and T are not proportional, so what appear to be large fluctuations of f, in Figures V.3 and V.4, are relatively modest, although important. As f and $\partial_x f$ increase, the diffusion gradient of $\mathcal{E}$, $\left(\partial_x \mathcal{E}\right)_{diff}$, grows more quickly than the S_n gradient of $\mathcal{E}$, $\left(\partial_x \mathcal{E}\right)$, such that $\theta_{diff} > \theta$ after a few optical depths, $\tau = \sigma_t \left|x\right|$. However, as f passes through its apex $\partial_x f$ changes sign, and the relationship between the gradients of $\mathcal{E}$ change as well with $\left(\partial_x \mathcal{E}\right)_{S_n} > \left(\partial_x \mathcal{E}\right)_{diff}$. As f descends toward 1/3, the gradients are almost equal, and the values of θ and θ_{diff} approach equality after a few optical depths. If the shock is strong enough, f relaxes to the value 1/3 for a few optical depths, which marks equality between the radiation and material temperatures, regardless of the radiation model. As f proceeds below 1/3, the gradients of $\mathcal{E}$ act to make $\theta > \theta_{diff}$, which holds through the dip in f, which is associated with the relaxation region downstream of the embedded hydrodynamic shock, until both radiation models reach the final equilibrium state where $\theta = T_f = \theta_{diff}$. If the shock is strong enough, upon reaching the embedded hydrodynamic shock f makes a steeper progression towards its minimum, causing $\left(\partial_x \mathcal{E}\right)_{S_n}$ to increase sufficiently such that $\theta > T_f$, resulting in an anti-diffusive region; see Figure V.4. This phenomena is discussed in Subsection V.5.3.

V.5.2 Code-verification of KULL's Implicit Monte Carlo radiation transport package using grey S_n transport

In this subsection, the ability to use the grey S_n transport solutions as a code-verification tool is demonstrated. The multi-physics package, KULL, and partic-

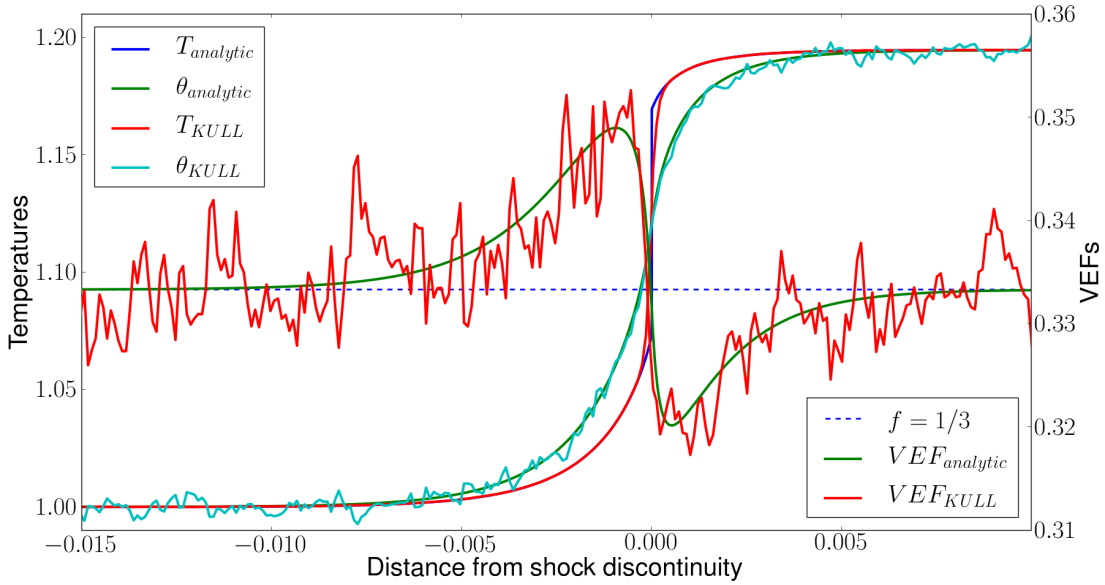

Figure V.5: Code-verification of the IMC radiation transport package in KULL using grey S_n transport with $\mathcal{M}_0 = 1.2$. The material temperature and the analytic solution are indistinguishable except near the embedded hydrodynamic shock. The radiation temperature follows the analytic solution reasonably well, especially near the embedded hydrodynamic shock. The VEF is noisy but the general features follow the analytic solution especially near the apex, through the embedded hydrodynamic shock, and down into the local minimum.

ularly its IMC radiation transport package, are tested for initial Mach numbers, $\mathcal{M}_0 = 1.2$, 2, 3, and 5, and the results are presented in Figures V.5 - V.8. The IMC package solves the radiation transport equation with full material-motion corrections correct through $\mathcal{O}(\beta)$. IMC is then coupled to KULL using operator-splitting. The KULL input data is initialized with the analytic solution, then KULL propagates the shock wave along a planar-direction, with reflective boundary conditions at the end-planes. The simulation stops after a prescribed time-lapse, which represents a few shock crossing-times. If there are no bugs in the physics packages utilized by KULL, specific to radiation transport and hydrodynamics, and assuming the physics

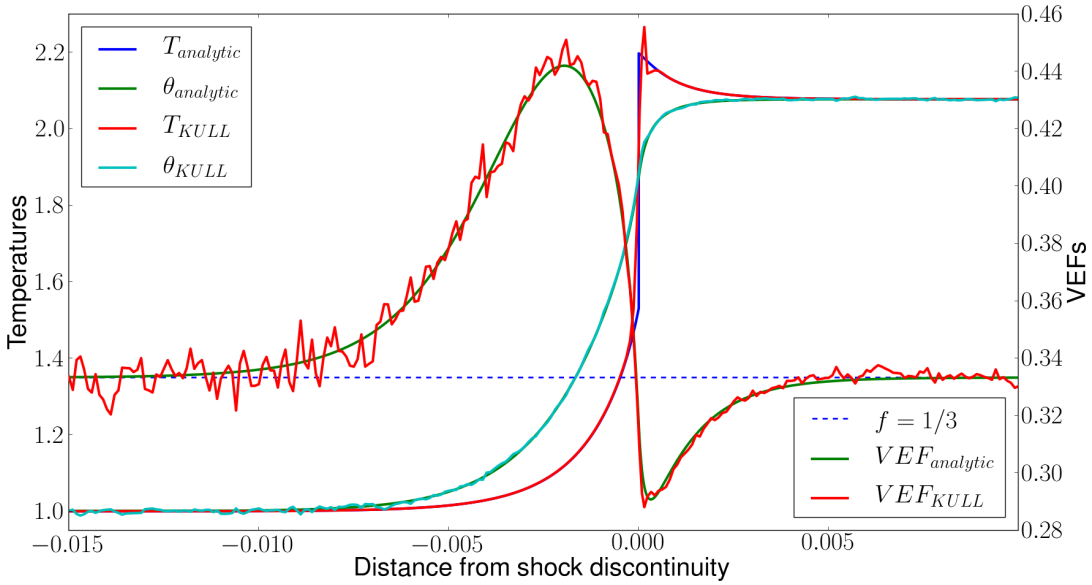

Figure V.6: Code-verification of IMC and KULL using grey S_n transport with $\mathcal{M}_0 = 2$. The material temperature is indistinguishable from the analytic solution except near the embedded hydrodynamic shock. The radiation temperature is almost indistinguishable from the analytic solution. The VEF follows the analytic solution closely in the precursor region, especially after the apex and going into the embedded hydrodynamic shock, and through the local-minimum into equilibrium.

in the solution is not too dissimilar from the physics packages utilized by KULL, then KULL should propagate the shock wave without distortion.

Figure V.5 shows the results from KULL for $\mathcal{M}_0 = 1.2$. The material temperature and the analytic solution are indistinguishable except near the embedded hydrodynamic shock. This is due to the hydrodynamic package in KULL retaining corrections due to viscosity and heat conduction. The radiation temperature follows the analytic solution reasonably well, especially near the embedded hydrodynamic shock. The noise in the IMC data appears to be centered around the analytic solution. The

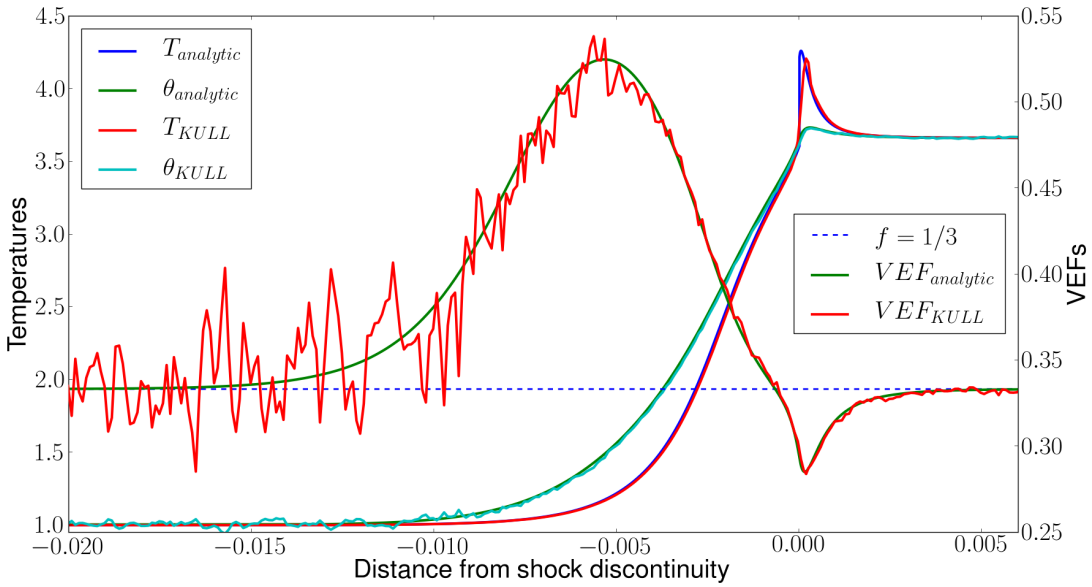

Figure V.7: Code-verification of IMC and KULL using grey S_n transport with $\mathcal{M}_0 = 3$. The material and radiation temperatures are almost indistinguishable from the analytic solutions, except for the material temperature at the Zel'dovich spike. The radiation temperature contains a local-maximum under the Zel'dovich spike which is discussed in Subsection V.5.3. The VEF is noisy in the upstream equilibrium state, but follows the analytic solution reasonably well in the precursor region especially after the apex and going toward the Zel'dovich spike, through the local-minimum, and even into the downstream equilibrium state.

VEF, computed by KULL, is significantly noisier than the radiation temperature, but this is because it is the ratio of two variables which are proportional to the fourth power of the radiation temperature, so the noise is significantly "louder". The VEF does hold the correct general shape, however, especially around the embedded hydrodynamic shock.

Figure V.6 shows the results from KULL for $\mathcal{M}_0 = 2$. Again, the material temperature is indistinguishable from the analytic solution except near the embedded

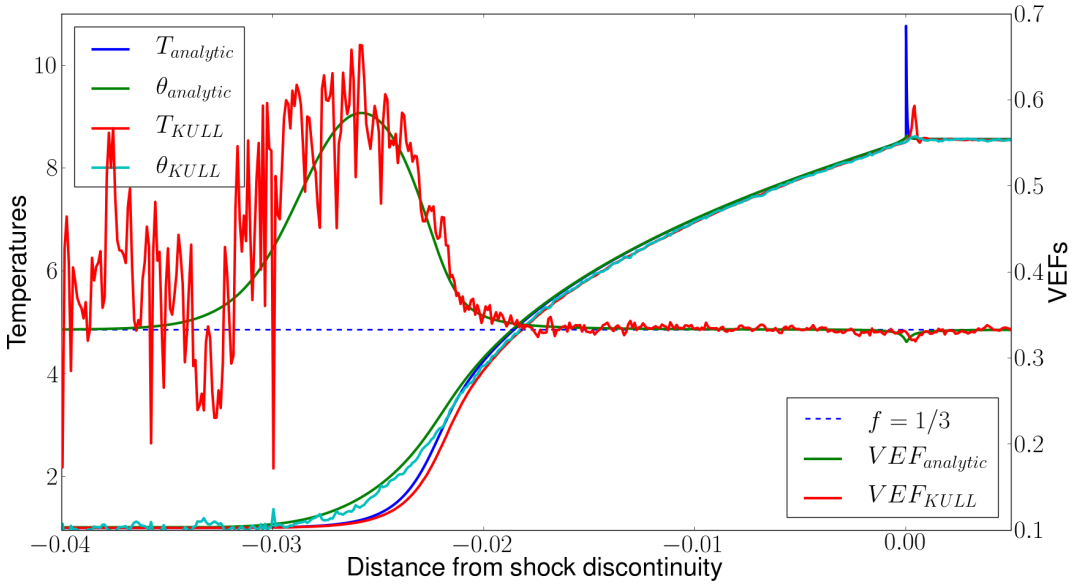

Figure V.8: Code-verification of IMC and KULL using grey S_n transport with $\mathcal{M}_0 = 5$. The material and radiation temperatures appear to lag behind the analytic solution by a constant distance. This is particularly noticeable in the nonequilibrium/transmissive region and under the Zel'dovich spike. The temperature at the Zel'dovich spike is considerably smaller than the temperature spike in the analytic solution, and the optical depth of the spike is wider. The VEF is considerably noisier in the upstream equilibrium state, but follows the analytic solution reasonably well in especially after the apex and going toward the Zel'dovich spike, and through the local-minimum into the downstream equilibrium state. The local minimum in the VEF appears to be lagged by a distance similar to that seen in the temperature profiles.

hydrodynamic shock. The excessive temperature spike was seen in the nonequilibrium diffusion code-verification; it appears to be damped more quickly here. The radiation temperature is almost indistinguishable from the analytic solution, except for some slight noise which uncovers the analytic solution. The VEF follows the analytic solution much better than in Figure V.5, with most of the deviation coming in the equilibrium regions, especially the upstream equilibrium region. The general

structure of the VEF agrees with the analytic result, especially after the apex in the precursor region.

Figure V.7 shows the results from KULL for $\mathcal{M}_0 = 3$. The temperatures, again, are in agreement with the analytic results, including the local-maximum in the radiation temperature under the Zel'dovich spike. This local-maximum was seen in the KULL results from the nonequilibrium diffusion theory code-verification tests, and its origins are discussed in Subsection V.5.3. The material temperature at the Zel'dovich spike is again slightly distorted, but not as badly as in Figure IV.16. The VEF follows the analytic solution, and does an especially good job after the apex in the precursor region.

Figure V.8 shows the results from KULL for $\mathcal{M}_0 = 5$. The KULL data appear to lag the analytic solution by a constant distance. This is particularly noticeable in the nonequilibrium/transmissive region and at the Zel'dovich spike. The temperature at the Zel'dovich spike is considerably smaller than the temperature provided by the analytic solution, and the optical depth of the spike is wider. The VEF is considerably noisier in the upstream equilibrium region, but, again, after the apex settles onto the analytic result. The local minimum in the VEF is also lagged by distance similar to that seen in the temperatures.

As a code-verification test, the grey S_n transport solutions provide richer details of the radiative shock solutions, and for RH codes that are solving the radiation transport equation, these solutions are a closer match to the physics being modelled. The importance of matching this modelling is made apparent when comparing the Figures IV.14 - IV.17 from the code-verification of KULL using nonequilibrium dif-

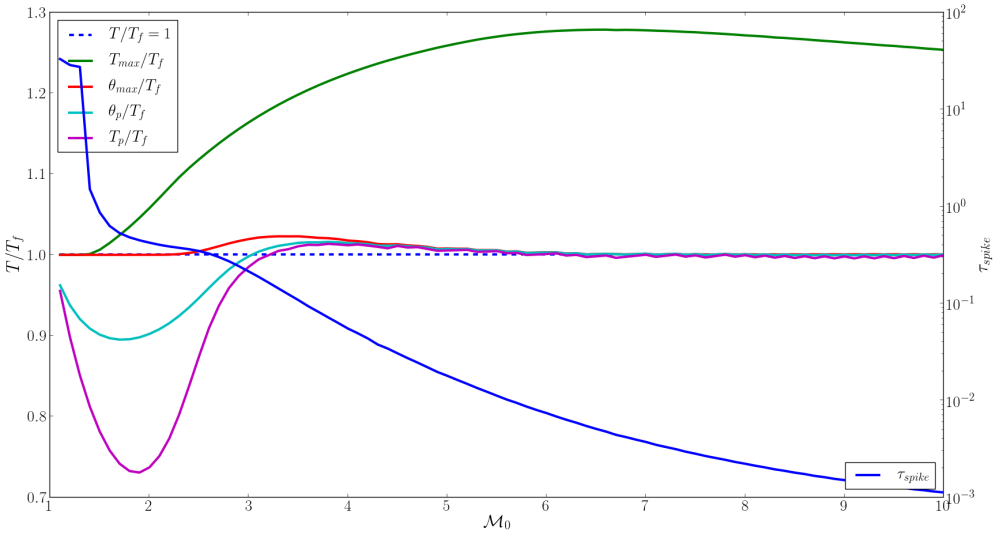

Figure V.9: Ratios of T_{max}, θ_{max}, θ_p and T_p to T_f, taking values on the left axis, along with τ_{spike}, taking logarithmic values on the right axis, plotted against $\mathcal{M}_0$. Nonequilibrium diffusion theory forces T_f to act as an upper-bound on θ and T_p to be T_f; this bound is relaxed in transport theory. When a Zel'dovich spike exists, its full-width-half-maximum optical thickness is represented by τ_{spike}. The capacity for θ_{max} to increase with T_{max} is restricted by the optical depth of the Zel'dovich spike, which is seen to fall off exponentially with increasing $\mathcal{M}_0$.

fusion, and Figures V.5 - V.8 which used grey S_n transport. In addition, the grey S_n solutions produce considerably more data to use for code-verification. As shown above, the VEF can be constructed and is a useful measure of the radiation transport model's ability to correctly simulate the geometric character of the radiation. In addition, the n radiation intensities from an analytic S_n solution could be used to test the solutions of S_n transport codes.

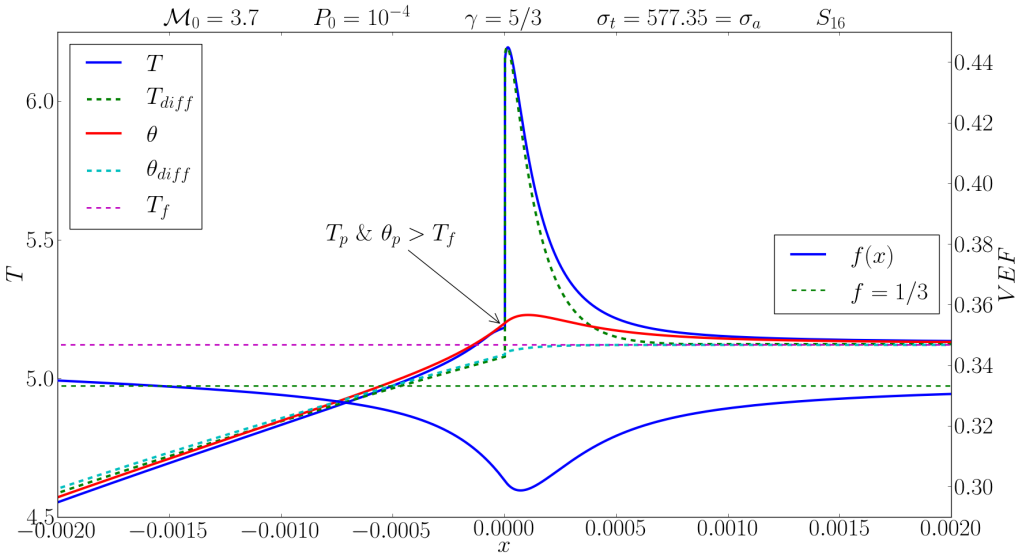

Figure V.10: Same conditions as Figure V.4 but with $\mathcal{M}_0 = 3.7$, and zoomed in on the Zel'dovich spike showing that T_p and θ_p are both greater than T_f. Drake calls this an adaptation zone [5, 6], which is seen to correspond to a local drop in the VEF. See Figure V.11.

V.5.3 Comparison of the material and radiative temperatures near the embedded hydrodynamic shock to the final temperature and anti-diffusive radiation

In standard nonequilibrium diffusion treatments [3, 4], the radiation temperature is monotonic, and strictly bounded by the final temperature. A thermodynamic argument ([3] see sections 7.14 and 7.17, and [4] see sections 104(c)), *based on this premise*, similarly bounds the material temperature in the precursor region, up to the embedded hydrodynamic shock. Recall that on the precursor side of the embedded hydrodynamic shock the material and radiation temperatures are labelled T_p and θ_p, respectively. However, McClarren and Drake [2] showed that a transport treatment of the radiation, for a simple model of a material temperature spike, allowed the

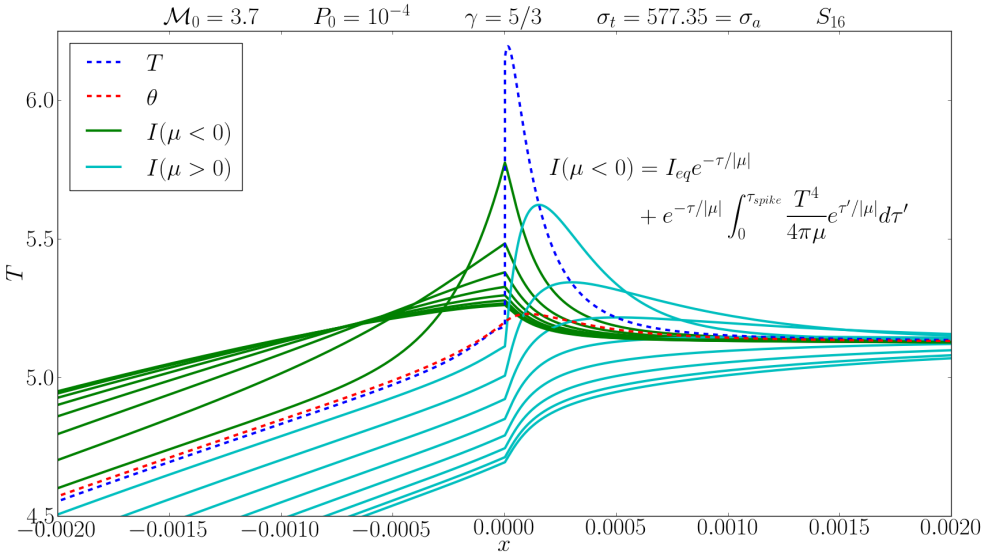

Figure V.11: Same conditions as Figure V.10. Zoomed in on the Zel'dovich spike and showing the 16 radiation intensities, which are normalized to units of temperature, $(4\pi I)^{1/4}$. The right-going intensities, $I(\mu > 0)$, increase proportional to $\sigma_a T^4/\mu$, so intensities along smaller values of μ are larger approaching the shock discontinuity, and are more strongly affected by the Zel'dovich spike. The left-going intensities, $I(\mu)$, exponentially increase under the Zel'dovich spike proportional to $\sigma_a T^4/\mu$, and are similarly attenuated in the precursor region, so large values at the shock discontinuity decay more rapidly. Radiation intensities along values of $|\mu| \lesssim 1$ are more densely packed than radiation intensities along values of $|\mu| \gtrsim 0$ which show more spreading. See Figure V.12.

radiation temperature to exceed this bound.

Figure V.9 shows the maximum values of the material and radiation temperatures, and their upstream values at the embedded hydrodynamic shock, unit-normalized to the final temperature, and plotted against the initial Mach number, taking values on the left axis. In the same Figure, but taking values on the right axis, the natural-log values of the full-width-half-maximum (FWHM) optical thickness of the Zel'dovich spike, τ_{spike}, is plotted. To compute the FWHM, the half-max temperature

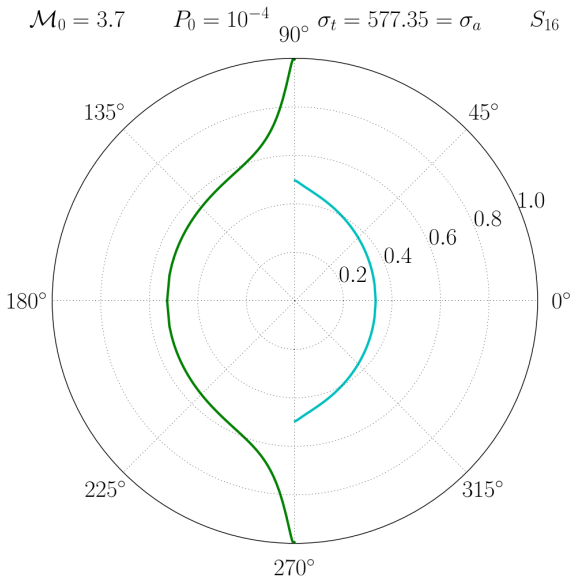

Figure V.12: Polar plot of the values of the radiation intensities at the embedded hydrodynamic shock shown in Figure V.11. The radiation intensity values are largest as $|\mu| \to 0$, but are not monotonically increasing, signifying the dominance of oblique radiation. The radiation is dominantly moving in the $\mu < 0$ direction. If the radiation was diffusive, or isotropic, then the values of intensity would appear more circular and equal for $\mu < 0$ and $\mu > 0$.

is taken between the material temperature's maximum value and the final temperature $\frac{T_{max}+T_f}{2}$, and the full-width is defined as the optical depth of the Zel'dovich spike at this temperature. Figure V.9 shows that θ_p and T_p exceed T_f for certain $\mathcal{M}_0$. The four temperatures, T_{max}, θ_{max}, θ_p, and T_p, being unit normalized against T_f, ascend above one, reach their maximum values, and then θ_{max}, θ_p and T_p asymptote together to one, while T_{max} takes a longer approach to unity. Anti-diffusive regions are defined by $\theta_{max} > T_f$. That T_p may be greater than T_f has been noticed recently [5, 6, 49, 67], and the rest of this Subsection attempts to explain this within the context of grey radiation transport. Figure V.10 explicitly shows T_p and θ_p greater than T_f for a zoomed-in region near the embedded hydrodynamic shock, for $\mathcal{M}_0 = 3.7$.

For radiative shocks with a Zel'dovich spike, T_{max} is effectively the value of the material temperature on the downstream edge of the embedded hydrodynamic shock, T_s, from which the material temperature exponentially decays to T_f. In [1], Lowrie and Edwards estimated T_{max}, which is shown in Figure IV.11. The grey S_n transport equation (V.26), can be approximately solved [68] in the relaxation region by neglecting terms with β, which downstream of the embedded hydrodynamic shock is reasonable:

$$I(\mu < 0, x) = I_{eq} e^{-\tau/|\mu|} + e^{-\tau/|\mu|} \int^{\tau} \frac{T^4}{4\pi\,|\mu|} e^{\tau'/|\mu|} d\tau' \,, \tag{V.32}$$

where τ measures the optical depth, $\sigma_t\,|x - x_{eq}|$, from the downstream equilibrium state toward the embedded hydrodynamic shock, and $I_{eq} = T_f^4/4\pi$. Thus, the leftward radiation intensities $I(\mu < 0, x)$, grow exponentially under the Zel'dovich spike as they approach the embedded hydrodynamic shock, as shown in Figure V.11. For a fixed location, as $\mu = \cos(\theta) \to 0^-$, $I(\mu < 0, x)$ increases, as shown in Figure V.12. So $I(\mu < 0, x)$ grows exponentially with optical depth under the Zel'dovich, and approaches T_{max}^4 at the embedded hydrodynamic shock, as $\mu \to 0^-$. Since the radiation temperature follows the spatial structure of the radiation intensities,

$$\theta \equiv \mathcal{E}^{1/4} = \left(\sum_{m=0}^{n} I_m w_m \right)^{1/4} \,,$$

and the radiation intensity is growing as T^4, especially for $|\mu| \to 0$, where the weights w_m, are larger, it would seem then that θ_{max} should grow with T_{max}, and with it θ_p and T_p. However, Figure V.9 shows that T_{max}/T_f reaches a maximum value of 1.3 when $\mathcal{M}_0 \sim 6$, but θ_{max} has already begun hovering near 1 after peaking around

$\mathcal{M}_0 = 3.2$. This is because the optical depth of the shock τ_{spike}, decays exponentially (linear decay on a log-scale) with $\mathcal{M}_0$, as shown in Figure V.9. In equation (V.32), the integration variable is similar to the shock thickness, $\tau' \sim \tau_{spike}$, such that $I(\mu < 0, x)$ does not have enough optical depth to be significantly affected by Zel'dovich spike, which limits θ_{max}, θ_p and T_p. The material temperature on the upstream side of the embedded hydrodynamic shock is bounded by the radiation temperature there because it is the local absorption of radiation that affects the local material temperature, whereas the local radiation field is the emission of the local material and the transport of radiation energy from nearby neighbors.

Since the radiation temperature may be greater than the final temperature under the Zel'dovich spike, there exists a spatial range where $\partial_x \theta < 0$ as the radiation temperature decays to the final temperature; see Figure V.4. McClarren and Drake [2] refer to this as anti-diffusive radiation.

V.5.4 Onset of supercritical shocks

In much of the literature, subcritical shocks are defined as $T_p < T_f$, and supercritical shocks are defined as $T_p = T_f$, with the claim that they take on different shock structures. The assumption is that above some critical Mach number, for which $T_p = T_f$, an equilibrium region adjacent to the embedded hydrodynamic shock extends into the precursor region, after which a nonequilibrium region allows the radiation to exponentially decay as it is more strongly absorbed by the material trying to attain equilibrium with the radiation. Thus, the supercritical shock is expected to signal the onset of an extended equilibrium (diffusive) region. Figure V.9 shows that $T_p = T_f$ at $\mathcal{M}_0 = 3.1$, but Figure V.13 shows that a diffusive region adjacent to the embedded

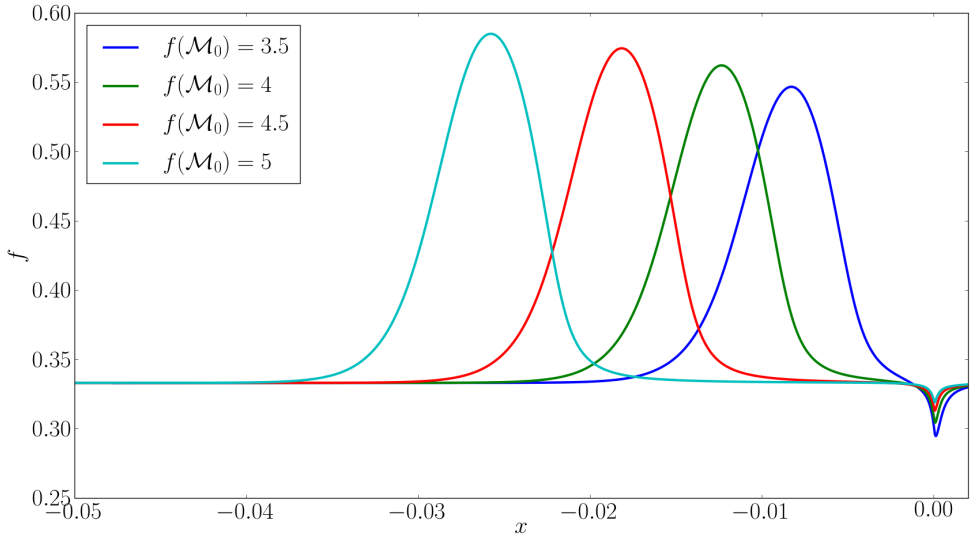

Figure V.13: Plots of the VEFs for four different values of $\mathcal{M}_0$. A diffusive region is defined where $f \approx 1/3$, which nonequilibrium diffusion theory says should begin occurring when $T_p = T_f$, which occurs for $\mathcal{M}_0 = 3.3$ for the parameters in this chapter. The diffusive regime has not begun by $\mathcal{M}_0 = 3.5$, and is not well established until $\mathcal{M}_0 = 4.5$.

hydrodynamic shock does not exist until $\mathcal{M}_0 \gtrsim 4.5$. So if $T_p = T_f$ does not signal the onset of the diffusive region, then what does? Drake [5, 6] suggests considering where $\mathcal{E}$ and $\mathcal{F}$ overlap (in his normalized units). Considering how closely the fluid dynamics between the nonequilibrium diffusion and S_n transport model coincide, and that a diffusive region is ultimately a description of the radiation, it seems most appropriate to look for a radiation answer. This is currently an open problem.

CHAPTER VI

SUMMARY

It is the purpose of this dissertation to contribute to our understanding of RH. Two problems were solved which, hopefully, aide this understanding: 1) we showed that the equilibrium diffusion approximation (EDA) of RH is correct through first-order in the asymptotic equilibrium diffusion limit (EDL), in agreement with other transport models; and, 2) we produced semi-analytic radiative shock solutions using grey S_n transport. These two problems span a broad range of ideas in RH.

The first problem addresses RH systems which are *nearly* in equilibrium, but wherein the radiation intensity is, at most, weakly anisotropic, as opposed to an equilibrium system which has an isotropic radiation field. Such systems are found in stellar interiors, as in the sun, and some high-energy-density laboratory experiments. Computationally, we expect RH codes to reasonably simulate stellar interiors. The asymptotic analysis used to solve the first problem is the first-step to ensuring that RH codes do simulate stellar interiors reasonably. Specifically, the first problem showed that the asymptotic solutions of the RH equations, in the EDL, satisfy the EDA through $\mathcal{O}(\epsilon)$, i.e., through "first-order".

Then, two model approximations of the radiation transport equation, P_1 and grey-diffusion, in the EDL, were treated in the comoving- and lab-frames. The comoving- and lab-frame variants of the P_1 model, in the EDL, were compared and it is found that the two P_1 models are equivalent. The difference between the comoving- and lab-

frame P_1 approximations, after transformation to the lab-frame, is a dyadic tensor which is $\mathcal{O}(\epsilon^2)$. Similarly, the asymptotic solutions of the comoving- and lab-frame variants of the grey-diffusion model, in the EDL, were compared, after transformation to the lab-frame, and it is found that their solutions are equivalent. This work shows that the P_1 and grey-diffusion models can be made in either the comoving- or lab-frame, and in the EDL, the same results will be obtained.

The second problem addresses steady-state shock wave solutions in RH systems. Due to the steady-state character of the equations, semi-analytic solutions can be obtained, i.e., the analytic ODEs are numerically integrated with arbitrary control of the integration tolerance. The work in this dissertation builds on the recent work of Lowrie and collaborators [1, 7], wherein the radiation transport is modelled with nonequilibrium diffusion. We model the radiation with grey S_n radiation transport, with material motion corrections through $\mathcal{O}(\beta)$, and we choose the $\mathcal{O}(\beta^2)$ corrections to ensure conservation of radiation energy and momentum, and to allow a reasonable form of the internal energy equation. These steady-state shock wave solution are accurate enough to be used for code-verification, which we do.

The results from our steady-state shock wave solutions are compared to those from nonequilibrium diffusion. While the differences in the radiation precursor region are not pronounced, though they are noticeable, the differences in the relaxation region are *qualitatively* distinct. For certain radiative shocks, there exists in the relaxation region, under the Zel'dovich spike, a local maximum in the radiation temperature that was predicted by McClarren and Drake [2], which the nonequilibrium diffusion model of radiation fails to simulate. This local maximum in the radiation temperature is called "anti-diffusive" radiation. The anti-diffusive radiation comes from a

precipitous decrease in the VEF near the embedded hydrodynamic shock. Next, our steady-state shock wave solutions were used as a code-verification tool for the IMC radiation model coupled to KULL. The IMC radiation model we tested solves the Lorentz-invariant radiation transport equation, which is correct through all orders in velocity; the KULL hydrodynamic package is only correct through $\mathcal{O}(\beta)$. The IMC radiation model accurately maintained our analytic steady-state radiative shock wave solution, including the anti-diffusive radiation. We had previously used the nonequilibrium diffusion model of Lowrie and Edwards [1] for code-verification of the IMC radiation model, and for certain radiative shock wave solutions, the IMC radiation model (correctly!) generated anti-diffusive radiation, which was not provided by the nonequilibrium diffusion model. Finally, we explored the transition from subcritical to supercritical shocks.

While the solutions to these two problems contribute to a better understanding of RH, they also leave some questions unanswered, and make certain problems more amenable to solution which are not yet solved. With regards to asymptotics: what other models preserve the EDL?; which discretizations, or computational methods, preserve the EDL?; is there an analytic problem that can test whether RH codes preserve the EDL? The solution to the question about which models preserve the EDL should be straight-forward, if tedious. It will be interesting to see if the answers resolving questions about discretizations, and computational methods, is as easy. Perhaps the most important question listed is whether there is an analytic problem to test whether RH codes preserve the EDL. If an analytic solution to an equilibrium diffusion problem is found then it will be possible to determine how satisfactorily RH codes implement the EDA.

Similarly, our method of solving for the steady-state radiative shock wave solutions lays the ground-work for different solution implementations, which will, hopefully, answer deeper questions, and it also leaves untested many different code-verification scenarios. Some possible extensions of the solution implementation would be to include either multi-group, in frequency, radiation diffusion or radiation transport; to use a different initialization than nonequilibrium diffusion before the first radiation transport solve, e.g., any flux-limited-diffusion scheme, this could potentially also serve as a test of flux-limited-diffusion schemes; to model the radiation with the full Lorentz-invariant radiation transport equation, which would serve as a useful code-verification tool for RH codes which seek solutions of relativistic problems. There are many RH codes, especially those using a Monte Carlo solver, which are used to solve problems where frequency-dependence is important, but this can be expensive, and short-cuts are often necessary. Similarly, because radiation transport solutions are often deemed "too expensive", flux-limited-diffusion is often used.

In conclusion, this dissertation only addresses two problems in RH, and exposes many more problems to solve. Hopefully this dissertation will make their solutions easier, and their solutions more insightful, for those who follow.

REFERENCES

[1] R. B. Lowrie and J. D. Edwards, *Radiative shock solutions with grey nonequilibrium diffusion*, Shock Waves **18** (2008), 129–143.

[2] R. G. McClarren and R. P. Drake, *Anti-diffusive radiation flow in the cooling layer of a radiating shock*, Journal of Quantitative Spectroscopy and Radiative Transfer **111** (2010), no. 14, 2095 –2105.

[3] Y. B. Zel'dovich and Y. P. Raizer, *Physics of Shock Waves and High-Temperature Hydrodynamic Phenomena*, Dover Books on Physics Series, Dover Publications, Mineola, N.Y., 2002.

[4] D. Mihalas and B. W. Mihalas, *Foundations of Radiation Hydrodynamics*, Dover Books on Physics Series, Dover, Mineola, N.Y., 1999.

[5] R. P. Drake, *Energy balance and structural regimes of radiative shocks in optically thick media*, Plasma Science, IEEE Transactions **35** (2007), no. 2, 171–180.

[6] R. P. Drake, *Theory of radiative shocks in optically thick media*, Physics of Plasmas **14** (2007), no. 4, 043301.

[7] R. B. Lowrie and R. M. Rauenzahn, *Radiative shock solutions in the equilibrium diffusion limit*, Shock Waves **16** (2007), 445–453.

[8] D. Mihalas and K.-H. A. Winkler, eds., *Radiation Hydrodynamics in Stars and Compact Objects*, vol. 255, Lecture Notes in Physics, Berlin Springer Verlag, Berlin, Germany, 1986.

[9] S. L. Shapiro and S. A. Teukolsky, *Black Holes, White Dwarfs, and Neutron Stars*, Wiley-Interscience, New York, N.Y., 1983.

[10] J. I. Castor, *Radiative transfer in spherically symmetric flows*, The Astrophysical Journal **178** (Dec. 1972), 779–792.

[11] R. B. Lowrie, J. E. Morel, and J. A. Hittinger, *The coupling of radiation and hydrodynamics*, The Astrophysical Journal **521** (1999), no. 1, 432.

[12] E. W. Larsen, J. E. Morel, and W. F. Miller Jr., *Asymptotic solutions of numerical transport problems in optically thick, diffusive regimes I*, Journal of Computational Physics **69** (1987), no. 2, 283 –324.

[13] E. W. Larsen and J. E. Morel, *Asymptotic solutions of numerical transport problems in optically thick, diffusive regimes II*, Journal of Computational Physics **83** (1989), no. 1, 212 –236.

[14] J. E. Morel, *Diffusion-limit asymptotics of the transport equation, the $P_{1/3}$ equations, and two flux-limited diffusion theories*, Journal of Quantitative Spectroscopy and Radiative Transfer **65** (2000), no. 5, 769 –778.

[15] G. L. Olson, L. H. Auer, and M. L. Hall, *Diffusion, P_1, and other approximate forms of radiation transport*, Journal of Quantitative Spectroscopy and Radiative Transfer **64** (2000), no. 6, 619 –634.

[16] R. Gendler, *Simeis 147: Supernova Remnant*, `http://www.phys.ncku.edu.tw/~astrolab/mirrors/apod_e/ap050324.html`, NASA, 24 Mar. 2005. Web. 22 Nov. 2013.

[17] L. Ensman and A. Burrows, *Shock breakout in SN 1987A*, The Astrophysical Journal **393** (July 1992), 742–755.

[18] H. K. Sen and A. W. Guess, *Radiation effects in shock-wave structure*, Physical Review **108** (Nov. 1957), 560–564.

[19] ESA and NASA, *The Mysterious Rings of Supernova 1987A*, `http://apod.nasa.gov/apod/ap120226.html`, NASA, 26 Feb. 2012. Web. 22 Nov. 2013.

[20] R. P. Drake, *Radiative shocks in astrophysics and the laboratory*, Astrophysics and Space Science **298** (2005), no. 1-2, 49–59.

[21] B. A. Remington, R. P. Drake, and D. D. Ryutov, *Experimental astrophysics with high power lasers and Z pinches*, Reviews of Modern Physics **78** (Aug. 2006), 755–807.

[22] B. A. Remington, *High energy density laboratory astrophysics*, Plasma Physics and Controlled Fusion **47** (2005), no. 5A, A191.

[23] R. P. Drake, *Perspectives on high-energy-density physics*, Physics of Plasmas **16** (2009), no. 5, 055501.

[24] R. P. Drake et al., *Radiative effects in radiative shocks in shock tubes*, High Energy Density Physics **7** (2011), no. 3, 130 –140.

[25] P. A. Keiter et al., *Observation of a hydrodynamically driven radiative-precursor shock*, Physical Review Letters **89** (2002), 165003.

[26] S. Bouquet et al., *Observation of laser driven supercritical radiative shock precursors*, Physical Review Letters **92** (2004), 225001.

[27] J. F. Hansen et al., *Laboratory simulations of supernova shockwave propagation*, Astrophysics and Space Science **298** (July 2005), 61–67.

[28] A. B. Reighard et al., *Observation of collapsing radiative shocks in laboratory experiments*, Physics of Plasmas **13** (2006), no. 8, 082901.

[29] J. M. Stone, D. Mihalas, and M. L. Norman, *ZEUS-2D: A radiation magnetohydrodynamics code for astrophysical flows in two space dimensions. III - The radiation hydrodynamic algorithms and tests*, The Astrophysical Journal **80** (1992), 819–845.

[30] L. Ensman, *Test problems for radiation and radiation-hydrodynamics codes*, The Astrophysical Journal **424** (Mar. 1994), 275–291.

[31] M. W. Sincell, M. Gehmeyr, and D. Mihalas, *The quasi-stationary structure of radiating shock waves. I: The one-temperature fluid*, Shock Waves **9** (1999), 391–402.

[32] M. W. Sincell, M. Gehmeyr, and D. Mihalas, *The quasi-stationary structure of radiating shock waves. II: The two-temperature fluid*, Shock Waves **9** (1999), 403–411.

[33] R. B. Lowrie and J. E. Morel, *Issues with high-resolution Godunov methods for radiation hydrodynamics*, Journal of Quantitative Spectroscopy and Radiative Transfer **69** (2001), no. 4, 475 –489.

[34] R. B. Lowrie and J. E. Morel, *Methods for hyperbolic systems with stiff relaxation*, International Journal for Numerical Methods in Fluids **40** (2002), no. 3-4, 413–423.

[35] M. D. Sekora and J. M. Stone, *A hybrid Godunov method for radiation hydrodynamics*, Journal of Computational Physics **229** (2010), no. 19, 6819 –6852.

[36] J. C. Hayes and M. L. Norman, *Beyond flux-limited diffusion: parallel algorithms for multidimensional radiation hydrodynamics*, The Astrophysical Journal **147** (2003), 197–220.

[37] M. R. Krumholz, R. I. Klein, C. F. McKee, and J. Bolstad, *Equations and algorithms for mixed-frame flux-limited diffusion radiation hydrodynamics*, The Astrophysical Journal **667** (2007), no. 1, 626.

[38] R. Klein and J. Stone, "Numerical methods for radiation magnetohydrodynamics in astrophysics", *Structure Formation in Astrophysics*, ed. by G. Chabrier, Cambridge University Press, New York, N.Y., 2009.

[39] D. R. Reynolds, J. C. Hayes, P. Paschos, and M. L. Norman, *Self-consistent solution of cosmological radiation-hydrodynamics and chemical ionization*, Journal of Computational Physics **228** (2009), no. 18, 6833 –6854.

[40] W. Zhang, L. Howell, A. Almgren, A. Burrows, and J. Bell, *CASTRO: A new compressible astrophysical solver. II - Gray radiation hydrodynamics*, The Astrophysical Journal **196** (Oct. 2011).

[41] Y.-F. Jiang, J. M. Stone, and S. W. Davis, *A Godunov method for multidimensional radiation magnetohydrodynamics based on a variable Eddington tensor*, The Astrophysical Journal **199** (Mar. 2012).

[42] W. Zhang et al., *CASTRO: A new compressible astrophysical solver. III - Multigroup radiation hydrodynamics*, The Astrophysical Journal **204** (Jan. 2013).

[43] Unknown, *Wikipedia: Planck's Law*, `http://en.wikipedia.org/wiki/File:EffectiveTemperature_300dpi_e.png`, Wikipedia, 05 May 2006. Web. 22 Nov. 2013.

[44] J. Goodman, *Topics in High-Energy Astrophysics*, `http://www.astro.princeton.edu/~jeremy/heap.pdf`, 08 Apr. 2013. Web. 11 Dec. 2013.

[45] G. B. Rybicki and A. P. Lightman, *Radiative Processes in Astrophysics*, A Wiley-Interscience publication, Berlin, Germany, 1979.

[46] S. C. Traugott, *Shock structure in a radiating, heat conducting, and viscous gas*, Physics of Fluids **8** (1965), no. 5, 834–849.

[47] B. Su and G. L. Olson, *An analytical benchmark for non-equilibrium radiative transfer in an isotropically scattering medium*, Annals of Nuclear Energy **24** (1997), no. 13, 1035 –1055.

[48] S. Chandrasekhar, *An Introduction to the Study of Stellar Structure*, Dover Books on Astronomy Series, Dover, Mineola, N.Y., 1958.

[49] J. I. Castor, *Radiation Hydrodynamics*, Cambridge University Press, New York, N.Y., 2007.

[50] R. Becker, *Stosswelle und detonation*, Zeitschrift fur Physik **8** (1922), 321 –362.

[51] W. F. Noh, *Errors for calculations of strong shocks using an artificial viscosity and an artificial heat flux*, Journal of Computational Physics **72** (Sept. 1987), 78–120.

[52] S. V. Coggeshall, *Analytic solutions of hydrodynamics equations*, Physics of Fluids A **3** (1991), no. 5, 757–769.

[53] B. M. Johnson, *Analytical shock solutions at large and small Prandtl number*, Journal of Fluid Mechanics **726** (2013), no. R4.

[54] J. A. Rathkopf et al., *KULL: LLNL's ASCI inertial confinement fusion simulation code*, (2000), Technical Report UCRL-JC-137053, Lawrence Livermore National Laboratory, Livermore CA.

[55] S. Y. Kadioglu, D. A. Knoll, R. B. Lowrie, and R. M. Rauenzahn, *A second order self-consistent IMEX method for radiation hydrodynamics*, Journal of Computational Physics **229** (2010), no. 22, 8313 –8332.

[56] B. van der Holst et al., *CRASH: A block-adaptive-mesh code for radiative shock hydrodynamics - Implementation and verification*, The Astrophysical Journal **194** (June 2011).

[57] D. Chauveheid, J. M. Ghidaglia, and M. Peybernes, "A Finite Volume Solver for Radiation Hydrodynamics in the Non Equilibrium Diffusion Limit", *Finite Volumes for Complex Applications VI: Problems & Perspectives*, ed. by J. Fort, J. Furst, J. Halama, R. Herbin, and F. Hubert, vol. 4, Springer Proceedings in Mathematics, Springer Berlin Heidelberg, Heidelberg, Germany, 2011, pp. 245–252, ISBN: 978-3-642-20670-2.

[58] S. W. Davis, J. M. Stone, and Y. F. Jiang, *A radiation transfer solver for Athena using short characteristics*, The Astrophysical Journal **199** (Mar. 2012).

[59] M. A. Heaslet and B. S. Baldwin, *Predictions of the structure of radiation-resisted shock waves*, Physics of Fluids **6** (1963), no. 6, 781–791.

[60] M. Y. Jaffrin and R. F. Probstein, *Structure of a plasma shock wave*, Physics of Fluids **7** (1964), no. 10, 1658–1674.

[61] M. Gehmeyr and D. Mihalas, *Adaptive grid radiation hydrodynamics with TITAN*, Physica D: Nonlinear Phenomena **77** (1994), 320 –341.

[62] M. González, E. Audit, and P. Huynh, *HERACLES - a three-dimensional radiation hydrodynamics code*, Astronomy and Astrophysics **464** (Mar. 2007), 429–435.

[63] R. Kuiper, H. Klahr, C. Dullemond, W. Kley, and T. Henning, *Fast and accurate frequency-dependent radiation transport for hydrodynamics simulations in massive star formation*, Astronomy and Astrophysics **511** (Feb. 2010).

[64] U. M. Noebauer, S. A. Sim, M. Kromer, F. K. Röpke, and W. Hillebrandt, *Monte Carlo radiation hydrodynamics*, Monthly Notices of the Royal Astronomical Society **425** (Sept. 2012), 1430–1444.

[65] N. Gentile, Personal communication, Sept. 3, 2013.

[66] N. A. Gentile, N. Keen, and J. Rathkopf, *The KULL IMC package*, (1998), Technical Report UCRL-JC-132743, Lawrence Livermore National Laboratory, Livermore CA.

[67] N. Vaytet, M. González, E. Audit, and G. Chabrier, *The influence of frequency-dependent radiative transfer on the structures of radiative shocks*, Journal of Quantitative Spectroscopy and Radiative Transfer **125** (2013), 105–122.

[68] S. Chandrasekhar, *Radiative Transfer*, Dover Books on Intermediate and Advanced Mathematics, Dover Publications, Mineola, N.Y., 1960.

APPENDIX A

DERIVATION OF THE FOUR LORENTZ INVARIANTS

Quantum statistics is interested in counting the number of quantum states, $d\mathcal{N} = g\, d^3x\, d^3p/h^3$, where g represents the degrees of photon polarization, and generally represents the degeneracy of the state. These countable states represent an invariant, and Planck's constant is an invariant, such that the phase-space measure, $d^3x\, d^3p$, must be an invariant. There are n particles in each state, and this represents another invariant. All of these n particles have the same energy, E_n, so if the total energy of the quantum state is known then the number of particles in the state can be determined. The preceding discussion is an outline of the counting procedure below.

The photon momentum and the momentum-space volume are

$$p_i = \frac{h\nu}{c}\Omega_i\,, \tag{A.1a}$$

$$d^3p = p^2\, dp\, d\Omega = \frac{h^3\nu^2}{c^3}\, d\nu d\Omega\,, \tag{A.1b}$$

and the three-space volume for a cylinder of height $c\, dt$ and base area dA is

$$d^3x = c\, dt dA\,. \tag{A.2}$$

The number of quantum mechanical photon-states with a given frequency, $d\mathcal{N}_\nu$, in a phase-space volume is

$$d\mathcal{N}_\nu = \frac{2\, d^3x\, d^3p}{h^3}\,, \tag{A.3}$$

where the factor of 2 accounts for the photon polarization. Using equations (A.1) and (A.2) above for the phase-space volume, this can be written as

$$d\mathcal{N}_\nu = 2\frac{\nu^2}{c^2} d\nu d\Omega\, dt dA\,. \tag{A.4}$$

The radiation intensity is, by definition, the total radiation energy travelling in the frequency range $(\nu, \nu + d\nu)$, within the solid-angle $d\Omega$, crossing a normalized area dA, within a time interval dt:

$$dE = I_\nu d\nu d\Omega\, dt dA\,. \tag{A.5}$$

Thus, the total energy in each photon-state is $I_\nu c^2/2\nu^2$. Since each photon in the state has energy $h\nu$, then the number of photons in each state n_ν, is

$$n_\nu = \frac{I_\nu c^2}{2h\nu^3}\,. \tag{A.6}$$

As mentioned previously, the number of photons in a quantum state is an invariant, so an invariant radiation intensity transforms as:

$$\mathfrak{I} = \frac{I_\nu}{\nu^3}\,. \tag{A.7}$$

The transformation of the absorption cross-section may be determined by considering a beam of photons crossing a homogeneous pure-absorber, i.e., $\sigma_s = 0$, of infinite width in the $x-$direction, and thickness l in the $y-$direction. Since the initial and final number of photons are invariants, then so is the fraction that survive $e^{-\tau}$, where $\tau = \sigma_a x$ is the optical depth of the material; "obviously", τ is also an invariant. When the material is at rest, and the beam crosses at an angle θ, with respect to the $x-$axis,

the optical depth is

$$\tau = \frac{\sigma_a l}{\sin(\theta)}\,, \tag{A.8}$$

and the photon momentum may be decomposed into its $x-$ and $y-$components

$$p_x = \frac{h\nu}{c}\cos(\theta)\,, \tag{A.9a}$$

$$p_y = \frac{h\nu}{c}\sin(\theta)\,. \tag{A.9b}$$

Since the $y-$component of momentum (A.9b), is invariant under a boost along the $x-$direction then so is $\nu\sin(\theta)$, and similarly for l as the $y-$component of travelled distance. Then the optical depth may be rewritten as

$$\tau = \frac{l}{\nu\sin(\theta)}\nu\sigma_a\,, \tag{A.10}$$

and since the optical depth, and the fraction $l/\nu\sin(\theta)$, are invariant, the invariant absorption is written

$$\mathfrak{a} = \nu\sigma_a\,. \tag{A.11}$$

The transformation of the emission term, $\sigma_a B_\nu(T)$, is now straight-forward. The Planck function must obey the same transformation as the radiation intensity, and combined with the result for the invariant absorption (A.11), produces the invariant emission

$$\mathfrak{e} = \frac{\sigma_a B_\nu(T)}{\nu^2}\,. \tag{A.12}$$

The Lorentz transformation between two coordinate frames of reference, $\boldsymbol{x}$ going to $\boldsymbol{x}'$, can be written in the form

$$\boldsymbol{x}' = \begin{pmatrix} \gamma_u & -\gamma_u \boldsymbol{\beta}^\intercal \\ -\gamma_u \boldsymbol{\beta} & \mathbf{I} + (\gamma_u - 1)\,\beta^{-2} \boldsymbol{\beta}\boldsymbol{\beta}^\intercal \end{pmatrix} \boldsymbol{x}\,, \tag{A.13}$$

where $\gamma_u = (1 - \beta^2)^{-1}$ is the Lorentz factor, $\boldsymbol{\beta} = \mathbf{u}/c$ is a column-vector and $\boldsymbol{\beta}^\intercal$ is its transpose, $\mathbf{I}$ is the 3×3 unit-matrix, and $\boldsymbol{x} = (ct, \mathbf{x})^\intercal$ represents the space-time four-vector. Similarly, the photon's four-momentum may be Lorentz transformed between the two frames of reference as

$$\boldsymbol{p}' = \begin{pmatrix} \gamma_u & -\gamma_u \boldsymbol{\beta}^\intercal \\ -\gamma_u \boldsymbol{\beta} & \mathbf{I} + (\gamma_u - 1)\,\beta^{-2} \boldsymbol{\beta}\boldsymbol{\beta}^\intercal \end{pmatrix} \boldsymbol{p}\,, \tag{A.14}$$

where $\boldsymbol{p} = (p_0, \mathbf{p}) = (h\nu/c)(1, \boldsymbol{\Omega})^\intercal$ is the photon four-momentum, and $\boldsymbol{\Omega}$ represents the photon's unit-normalized direction of travel. Since the photon is "light-like", its squared four-momentum is identically zero

$$\boldsymbol{p}^2 = -p_0^2 + \mathbf{p}^2 = 0 \quad \Rightarrow \quad \mathbf{p}^2 = p_i p_i = p_0^2\,, \tag{A.15}$$

and this constraint reduces the number of unknowns in the photon four-momentum to three; the typical reduction to the two gauge degrees-of-freedom is due to the transversality of the photon four-momentum, but this is not important in this dissertation because we are not concerned with electromagnetic interactions. It is important to emphasize the three-vector components of the photon four-momentum:

$\mathbf{p} = (h\nu/c)\mathbf{\Omega}$. The transformation of the photon frequency, p_0/h, is

$$\nu' = \nu\gamma_u \left(1 - \boldsymbol{\beta}\cdot\mathbf{\Omega}\right) . \tag{A.16}$$

The transformation of the momentum-space volume, $d^3p \mapsto d^3p'$, for a boost along the $x-$direction is found by focusing on the three-vector transformation of the Lorentz matrix, and constructing its Jacobian J:

$$\begin{vmatrix} \partial p_1'/\partial p_1 & \partial p_1'/\partial p_2 & \partial p_1'/\partial p_3 \\ \partial p_2'/\partial p_1 & \partial p_2'/\partial p_2 & \partial p_2'/\partial p_3 \\ \partial p_3'/\partial p_1 & \partial p_3'/\partial p_2 & \partial p_3'/\partial p_3 \end{vmatrix} = \begin{vmatrix} \gamma_u\left(1 - \beta\partial p_0/\partial p_1\right) & -\gamma_u\beta\partial p_0/\partial p_2 & -\gamma_u\beta\partial p_0\partial p_3 \\ 0 & 1 & 0 \\ 0 & 0 & 1 \end{vmatrix}$$
$$= \gamma_u\left(1 - \beta\partial p_0/\partial p_1\right) \equiv J\,. \tag{A.17}$$

The derivative term can be evaluated by recalling the constraint on the photon momentum in equation (A.15):

$$p_0 = \sqrt{p_i p_i}\,, \tag{A.18a}$$
$$\frac{\partial p_0}{\partial p_1} = \frac{1}{2}\frac{2p_1}{\sqrt{p_i p_i}} = \frac{p_1}{p_0}\,. \tag{A.18b}$$

Then, the Jacobian is $J = \gamma_u(1 - \beta p_1/p_0) = \gamma_u(p_0 - \beta p_1)/p_0$, which can be simplified via equation (A.16), $J = \frac{p_0'}{p_0}$, and the transformation of the photon momentum-space volume, and its invariant, are

$$d^3p' = \frac{p_0'}{p_0}d^3p\,, \tag{A.19a}$$
$$\frac{d^3p}{p_0} = \frac{p_i^2 dp d\Omega}{p_0} = p_0\, dp d\Omega = \left(\frac{h}{c}\right)^2 \nu\, d\nu d\Omega\,. \tag{A.19b}$$

APPENDIX B

DERIVATION OF THE TRANSFORMED IN-SCATTER SOURCE

The derivation of the correctly transformed in-scatter source in Chapter II, the second term in equation (II.1), begins

$$\begin{aligned}
\frac{\sigma_s}{4\pi}\phi_\nu \mapsto & \left(\frac{\nu}{\nu_0}\right)^2 \frac{\sigma_s}{4\pi}\int_{4\pi} I_{0,\nu}(\nu_0,\Omega_0')\,d\Omega_0' \\
&= \left(\frac{\nu}{\nu_0}\right)^2 \frac{\sigma_s}{4\pi}\int_0^\infty\int_{4\pi} I_{0,\nu}(\nu_0',\Omega_0')\delta\left(\nu_0'-\nu_0\right)\left(\frac{\nu_0'}{\nu_0'}\right)\,d\nu_0' d\Omega_0' \\
&= \left(\frac{\nu}{\nu_0}\right)^2 \frac{\sigma_s}{4\pi}\int_0^\infty\int_{4\pi} \left(\frac{\nu_0'}{\nu'}\right)^3 I_\nu(\nu',\Omega')\delta\left(\nu_0'-\nu_0\right)\left(\frac{\nu'}{\nu_0'}\right)\,d\nu' d\Omega' \\
&= \left(\frac{\nu}{\nu_0}\right)^2 \frac{\sigma_s}{4\pi}\int_0^\infty\int_{4\pi} \left(\frac{\nu_0'}{\nu'}\right)^2 I_\nu(\nu',\Omega')\delta\left(\nu_0'-\nu_0\right)\,d\nu' d\Omega'\,. \qquad \text{(B.1)}
\end{aligned}$$

The first line represents the mapping from the lab-frame to the comoving-frame. The second line introduces a Dirac-delta function, and multiplies the integrand by unity to introduce an invariant momentum-space volume; see equation (A.19b). The third line transforms the radiation intensity, and the invariant momentum-space volume, to the lab-frame. The fourth line simplifies the result. Focusing on the frequency-integral, it is useful to recall a property of the Dirac-delta function:

$$\begin{aligned}
\int f(x)\delta\left(y(x)-y(x_0)\right)dx &= \left[\left.\frac{dy(x)}{dx}\right|_{x=x_0}\right]^{-1} f(x_0) \\
&= \left[\left(\frac{dy(x)}{dx}\right)^{-1} f(x)\right]_{y(x)=y(x_0)}\,. \qquad \text{(B.2)}
\end{aligned}$$

Mapping the terms in equation (B.1) to the property just given yields:

$$x = \nu' \,, \tag{B.3a}$$

$$f(x) = \left(\frac{\nu_0'}{\nu'}\right)^2 I_\nu(\nu', \Omega') \,, \tag{B.3b}$$

$$y(x) = \nu_0' = \nu' \gamma_u \left(1 - \boldsymbol{\beta} \cdot \mathbf{n}\right) \,, \tag{B.3c}$$

$$y(x_0) = \nu_0 \,, \tag{B.3d}$$

$$\begin{aligned} \frac{dy(x)}{dx} &= \left. \frac{d}{d\nu'} \left[\nu' \gamma_u \left(1 - \boldsymbol{\beta} \cdot \mathbf{n}\right)\right] \right|_{\substack{\nu_0' = \nu' \\ \Omega = \text{constant}}} \\ &= \partial_{\nu'} \left[\nu' \gamma_u \left(1 - \boldsymbol{\beta} \cdot \mathbf{n}\right)\right] \\ &= \gamma_u \left(1 - \boldsymbol{\beta} \cdot \mathbf{n}\right) \\ &= \frac{\nu_0'}{\nu'} \,, \end{aligned} \tag{B.3e}$$

and the frequency-integral becomes:

$$\begin{aligned} \int_0^\infty \left(\frac{\nu_0'}{\nu'}\right)^2 I(\nu', \Omega') \delta\left(\nu_0' - \nu'\right) \, d\nu' &= \left[\frac{\nu'}{\nu_0'} \left(\frac{\nu_0'}{\nu'}\right)^2 I_\nu(\nu', \Omega')\right]_{\nu_0' = \nu_0} \\ &= \left(\frac{\nu_0}{\nu'}\right) I_\nu(\nu', \Omega') \,. \end{aligned} \tag{B.4}$$

Thus, the second term in equation (II.1), with the correct transformations, is:

$$\frac{\sigma_s}{4\pi} \phi \mapsto \left(\frac{\nu}{\nu_0}\right)^2 \frac{\sigma_s}{4\pi} \int_{4\pi} \frac{\nu_0}{\nu'} I_\nu(\nu', \Omega') \, d\Omega' \,. \tag{B.5}$$

APPENDIX C

DERIVATION OF THE LAB-FRAME RADIATION TRANSPORT EQUATION THROUGH $\mathcal{O}(\beta^2)$

The lab-frame radiation transport equation, correct through all orders in velocity, is:

$$\frac{1}{c}\partial_t I_\nu + \Omega_i \partial_i I_\nu \\ = -\frac{\nu_0}{\nu}\sigma_t I_\nu + \left(\frac{\nu}{\nu_0}\right)^2 \frac{\sigma_s}{4\pi}\int_{4\pi} \frac{\nu_0}{\nu'} I_\nu(\nu', \Omega')\, d\Omega' + \left(\frac{\nu}{\nu_0}\right)^2 \sigma_a B(T)\,. \quad \text{(C.1)}$$

The ratio of the comoving-frame frequency to the lab-frame frequency is given in equation (A.16):

$$\frac{\nu_0}{\nu} = \gamma_u \left(1 - \beta_i \Omega_i\right)\,. \quad \text{(C.2)}$$

The frequency ratio in the integrand can be written

$$\frac{\nu_0}{\nu'} = \gamma_u \left(1 - \beta_i \Omega'_i\right)\,, \quad \text{(C.3)}$$

and it is helpful to recored here the ratio of the primed and unprimed frequencies:

$$\frac{\nu'}{\nu} = \frac{1 - \beta_i \Omega_i}{1 - \beta_i \Omega'_i}\,. \quad \text{(C.4)}$$

The objective of this appendix is to Taylor expand the frequency ratios, the comoving-frame cross-sections, and the Planck function, in order to make their lab-frame values manifest. This includes Taylor-expanding the radiation intensity in the integrand

since it is a function of ν', and according to equation (C.4), ν' is a function of ν, an appropriate lab-frame value, and Ω', the integration variable. To ignore this dependence would produce the wrong results.

The expanded Lorentz factor, through $\mathcal{O}(\beta^2)$, is well-known in physics as it represents the sum of the rest mass and the kinetic energy from classical physics,

$$\gamma_u = 1 + \frac{1}{2}\beta^2 \,, \tag{C.5}$$

so the frequency ratios expanded through $\mathcal{O}(\beta^2)$ are

$$\frac{\nu_0}{\nu} = \gamma_u \left(1 - \beta_i \Omega_i\right) = \left(1 + \frac{1}{2}\beta^2\right)\left(1 - \beta_i \Omega_i\right) = 1 - \beta_i \Omega_i + \frac{1}{2}\beta^2 \,, \tag{C.6a}$$

$$\frac{\nu_0}{\nu'} = \gamma_u \left(1 - \beta_i \Omega_i'\right) = 1 - \beta_i \Omega_i' + \frac{1}{2}\beta^2 \,, \tag{C.6b}$$

$$\begin{aligned}\left(\frac{\nu}{\nu_0}\right)^2 &= \left(\frac{1}{\gamma_u \left(1 - \beta_i \Omega_i\right)}\right)^2 \\ &= \frac{1 - \beta^2}{\left(1 - \beta_i \Omega_i\right)^2} \\ &= 1 + 2\beta_i \Omega_i + \beta_i \beta_j \left(3\Omega_i \Omega_j - \delta_{ij}\right) \,.\end{aligned} \tag{C.6c}$$

It is convenient to record here other results that will be useful for Taylor-expanding the cross-section and Planck function:

$$\nu_0 - \nu = \nu \left(-\beta_i \Omega_i + \frac{1}{2}\beta^2\right) \,, \tag{C.7a}$$

$$\left(\nu_0 - \nu\right)^2 = \nu^2 \beta_i \beta_j \Omega_i \Omega_j \,, \tag{C.7b}$$

$$\nu = \frac{\nu_0}{\gamma_u \left(1 - \beta_i \Omega_i\right)} = \nu_0 \left(1 + \beta_i \Omega_i + \beta_i \beta_j \left(\Omega_i \Omega_j + \frac{1}{2}\delta_{ij}\right)\right) \,, \tag{C.7c}$$

$$\partial_{\nu_0}\nu = 1 + \beta_i\Omega_i + \beta_i\beta_j\left(\Omega_i\Omega_j + \frac{1}{2}\delta_{ij}\right) = \frac{\nu}{\nu_0}\,, \tag{C.7d}$$

$$(\nu_0 - \nu)\,\frac{\nu}{\nu_0} = \nu\left[-\beta_i\Omega_i + \beta_i\beta_j\left(\frac{1}{2}\delta_{ij} - \Omega_i\Omega_j\right)\right]\,, \tag{C.7e}$$

$$(\nu_0 - \nu)^2\, f(\nu_0) = (\nu_0 - \nu)^2\, f(\nu)\,. \tag{C.7f}$$

Since the comoving-frame cross-section, and Planck function, are Taylor-expanded with respect to the lab-frame frequency, the first two expressions are obviously necessary. The second expression implies that since the radiation transport equation is only to be expanded through $\mathcal{O}(\beta^2)$, then it is only necessary to Taylor-expand the cross-section and Planck function through $\mathcal{O}\left((\nu_0 - \nu)^2\right)$. The last expression is simply stating that since the squared difference in frequencies is already $\mathcal{O}(\beta^2)$, then any function of frequency that multiplies it transforms at leading-order. The Taylor-expansion of a general function of the comoving-frame frequency, with respect to the lab-frame frequency, through $\mathcal{O}((\nu_0 - \nu)^2) \sim \mathcal{O}(\beta^2)$, is

$$\begin{aligned}
f(\nu_0) &= f + (\nu_0 - \nu)\,\partial_{\nu_0} f + \frac{1}{2}(\nu_0 - \nu)^2\,\partial_{\nu_0}^2 f \\
&= f + (\nu_0 - \nu)\,(\partial_{\nu_0}\nu)\,\partial_\nu f + \frac{1}{2}(\nu_0 - \nu)^2\,(\partial_{\nu_0}\nu)\,\partial_\nu\big((\partial_{\nu_0}\nu)\,\partial_\nu f\big) \\
&= f + (\nu_0 - \nu)\left(\frac{\nu}{\nu_0}\right)\partial_\nu f + \frac{1}{2}(\nu_0 - \nu)^2\left(\frac{\nu}{\nu_0}\right)\left(\frac{1}{\nu_0}\partial_\nu f + \frac{\nu}{\nu_0}\partial_\nu^2 f\right) \\
&= f + (\nu_0 - \nu)\left(\frac{\nu}{\nu_0}\right)\partial_\nu f + \frac{1}{2}(\nu_0 - \nu)^2\left(\frac{1}{\nu}\partial_\nu f + \partial_\nu^2 f\right) \\
&= f + \nu\left[-\beta_i\Omega_i + \beta_i\beta_j\left(\frac{1}{2}\delta_{ij} - \Omega_i\Omega_j\right)\right]\partial_\nu f + \frac{1}{2}\nu^2\beta_i\beta_j\Omega_i\Omega_j\left(\frac{1}{\nu}\partial_\nu f + \partial_\nu^2 f\right) \\
&= f - \beta_i\Omega_i\nu\partial_\nu f + \frac{1}{2}\beta_i\beta_j\left(\left(\delta_{ij} - 2\Omega_i\Omega_j\right)\nu\partial_\nu f + \Omega_i\Omega_j\nu^2\partial_\nu^2 f\right)\,.
\end{aligned} \tag{C.8}$$

Thus, the Taylor-expansions of the total cross-section, and the Planck function, with respect to the lab-frame frequency, are

$$\sigma_t(\nu_0) = \sigma_t - \beta_i\Omega_i\nu\partial_\nu\sigma_t + \frac{1}{2}\beta_i\beta_j\left(\left(\delta_{ij} - 2\Omega_i\Omega_j\right)\nu\partial_\nu\sigma_t + \Omega_i\Omega_j\nu^2\partial_\nu^2\sigma_t\right)\,, \tag{C.9a}$$

$$B_{\nu_0} = B_\nu - \beta_i\Omega_i\nu\partial_\nu B_\nu + \frac{1}{2}\beta_i\beta_j\left(\left(\delta_{ij} - 2\Omega_i\Omega_j\right)\nu\partial_\nu B_\nu + \Omega_i\Omega_j\nu^2\partial_\nu^2 B_\nu\right)\,, \tag{C.9b}$$

$$\sigma_a(\nu_0)B_{\nu_0} = \sigma_a B_\nu - \beta_i\Omega_i\nu\partial_\nu\left(\sigma_a B_\nu\right) + \frac{1}{2}\beta_i\beta_j\left(\left(\delta_{ij} - 2\Omega_i\Omega_j\right)\nu\partial_\nu\left(\sigma_a B_\nu\right) + \Omega_i\Omega_j\nu^2\partial_\nu^2\left(\sigma_a B_\nu\right)\right)\,. \tag{C.9c}$$

The Taylor-expansion of the radiation intensity in the integrand proceeds along the same lines as shown for the general function in equation (C.8), except the comoving-frame frequency carries a prime-$'$ here, and the required relations take the form:

$$\nu = \nu'\frac{1-\beta_i\Omega_i}{1-\beta_i\Omega_i'} = \nu'\left(1+\beta_i\left(\Omega_i'-\Omega_i\right)\right) + \mathcal{O}(\beta^3)\,, \tag{C.10a}$$

$$\left(\nu'-\nu\right) = \nu\beta_i\left(\Omega_i'-\Omega_i\right) + \mathcal{O}(\beta^3)\,, \tag{C.10b}$$

$$\left(\nu'-\nu\right)^2 = \nu^2\beta_i\beta_j\left(\Omega_i'-\Omega_i\right)\left(\Omega_j'-\Omega_j\right) = \mathcal{O}(\beta^3)\,, \tag{C.10c}$$

$$\partial_{\nu'}\nu = 1 + \beta_i\left(\Omega_i'-\Omega_i\right) + \mathcal{O}(\beta^3) = \frac{\nu}{\nu'}\,, \tag{C.10d}$$

$$\left(\nu'-\nu\right)\frac{\nu}{\nu'} = \nu\beta_i\left(\Omega_i'-\Omega_i\right) + \mathcal{O}(\beta^3)\,. \tag{C.10e}$$

In the relations above containing the term $\mathcal{O}(\beta^3)$, it has been used that terms like $\beta_i\beta_j\Omega_i(\Omega_j - \Omega_j')$ are zero at $\mathcal{O}(\beta^2)$ since the angular variables are the same at $\mathcal{O}(\beta^0)$. The first two expressions come from equation (C.4), and the rest are analogous to those given in equations (C.7). Beginning from the fourth line of equation (C.8), and

recognizing that ν_0 is now ν', the Taylor-expansion of the general function, using the relations in (C.10), is

$$\begin{aligned} f(\nu') &= f + (\nu' - \nu)\left(\frac{\nu}{\nu'}\right)\partial_\nu f + \frac{1}{2}(\nu' - \nu)^2\left(\frac{1}{\nu}\partial_\nu f + \partial_\nu^2 f\right) \\ &= f + \beta_i(\Omega_i' - \Omega_i)\,\nu\partial_\nu f + \mathcal{O}(\beta^3)\,, \end{aligned} \tag{C.11}$$

such that the Taylor-expanded radiation intensity is

$$I_\nu(\Omega') = I_\nu + \beta_i(\Omega_i' - \Omega_i)\,\nu\partial_\nu I_\nu\,. \tag{C.12}$$

Now that all of the Taylor-expansions have been performed it is necessary to combine them appropriately according to the three terms on the RHS of equation (C.1), retaining terms of $\mathcal{O}(\beta^2)$. The first term is straight-forward:

$$\begin{aligned} -\frac{\nu_0}{\nu}\sigma_t I_\nu &= -I_\nu\left(1 - \beta_i\Omega_i + \frac{1}{2}\beta^2\right) \\ &\quad\times\left(\sigma_t - \beta_i\Omega_i\nu\partial_\nu\sigma_t + \frac{1}{2}\beta_i\beta_j\left(\left(\delta_{ij} - 2\Omega_i\Omega_j\right)\nu\partial_\nu\sigma_t + \Omega_i\Omega_j\nu^2\partial_\nu^2\sigma_t\right)\right) \\ &= I_\nu\left(-\sigma_t + \beta_i\Omega_i\nu\partial_\nu\sigma_t - \frac{1}{2}\beta_i\beta_j\left(\left(\delta_{ij} - 2\Omega_i\Omega_j\right)\nu\partial_\nu\sigma_t + \Omega_i\Omega_j\nu^2\partial_\nu^2\sigma_t\right)\right) \\ &\quad+ \beta_i\Omega_i I_\nu\left(\sigma_t - \beta_i\Omega_i\nu\partial_\nu\sigma_t\right) - \frac{1}{2}\beta^2\sigma_t I_\nu \\ &= -\sigma_t I_\nu + \beta_i\Omega_i\left(\sigma_t I_\nu + I_\nu\nu\partial_\nu\sigma_t\right) \\ &\quad- \frac{1}{2}\beta_i\beta_j\left(\sigma_t\delta_{ij}I_\nu + \delta_{ij}I_\nu\nu\partial_\nu\sigma_t + \Omega_i\Omega_j I_\nu\nu^2\partial_\nu^2\sigma_t\right)\,. \end{aligned} \tag{C.13}$$

The second term,

$$\left(\frac{\nu}{\nu_0}\right)^2\frac{\sigma_s}{4\pi}\int_{4\pi}\frac{\nu_0}{\nu'}I_{\nu'}(\Omega')\,d\Omega'\,, \tag{C.14}$$

is, again, involved, and is best broken into parts. The integrand is

$$\begin{aligned}\frac{\nu_0}{\nu'}I_{\nu'}(\Omega') &= \left(I_\nu + \beta_i\left(\Omega_i' - \Omega_i\right)\nu\partial_\nu I_\nu\right)\left(1 - \beta_j\Omega_j' + \frac{1}{2}\beta^2\right) \\ &= I_\nu + \beta_i\left(-\Omega_i' I_\nu + \left(\Omega_i' - \Omega_i\right)\nu\partial_\nu I_\nu\right) + \frac{1}{2}\beta^2 I_\nu\,, \end{aligned} \tag{C.15}$$

where the dependence of the radiation intensity on the angular variable, $I_\nu = I_\nu(\Omega')$, has been suppressed for notational convenience. The integral then is

$$\int_{4\pi}\frac{\nu_0}{\nu'}I_{\nu'}(\Omega')\,d\Omega' = \phi_\nu + \beta_i\left(-\Omega_i\nu\partial_\nu\phi_\nu - F_{i,\nu} + \nu\partial_\nu F_{i,\nu}\right) + \frac{1}{2}\beta^2\phi_\nu\,. \tag{C.16}$$

The ratio $\left(\frac{\nu}{\nu_0}\right)^2$ multiplying the integral is given in equation (C.6c), and the second term is

$$\begin{aligned}\left(\frac{\nu}{\nu_0}\right)^2\frac{\sigma_s}{4\pi}\int_{4\pi}\frac{\nu_0}{\nu'}I_{\nu'}(\Omega')\,d\Omega' &= \frac{\sigma_s}{4\pi}\left(1 + 2\beta_i\Omega_i + \beta_i\beta_j\left(3\Omega_i\Omega_j - \delta_{ij}\right)\right) \\ &\quad\times\left(\phi_\nu + \beta_k\left(-\Omega_k\nu\partial_\nu\phi_\nu - F_{k,\nu} + \nu\partial_\nu F_{k,\nu}\right) + \frac{1}{2}\beta^2\phi_\nu\right) \\ &= \frac{\sigma_s}{4\pi}\Bigg[\phi_\nu + \beta_i\left(2\Omega_i\phi_\nu - \Omega_i\nu\partial_\nu\phi_\nu - F_{i,\nu} + \nu\partial_\nu F_{i,\nu}\right) \\ &\quad + \beta_i\beta_j\left(\left(3\Omega_i\Omega_j - \frac{1}{2}\delta_{ij}\right)\phi_\nu - 2\Omega_i\Omega_j\nu\partial_\nu\phi_\nu\right) \\ &\quad + \beta_i\beta_j\left(-2\Omega_i F_{j,\nu} + 2\Omega_i\nu\partial_\nu F_{j,\nu}\right)\Bigg]\,. \end{aligned} \tag{C.17}$$

The third term is relatively straight-forward to compute, if tedious:

$$\begin{aligned}&\left(\frac{\nu}{\nu_0}\right)^2\sigma_a B(T) = \left(1 + 2\beta_i\Omega_i + \beta_i\beta_j\left(3\Omega_i\Omega_j - \delta_{ij}\right)\right) \\ &\times\left(\sigma_a B_\nu - \beta_i\Omega_i\nu\partial_\nu\left(\sigma_a B_\nu\right) + \frac{1}{2}\beta_i\beta_j\left(\left(\delta_{ij} - 2\Omega_i\Omega_j\right)\nu\partial_\nu\left(\sigma_a B_\nu\right) + \Omega_i\Omega_j\nu^2\partial_\nu^2\left(\sigma_a B_\nu\right)\right)\right) \\ &= \sigma_a B_\nu - \beta_i\Omega_i\nu\partial_\nu\left(\sigma_a B_\nu\right) + \frac{1}{2}\beta_i\beta_j\left(\left(\delta_{ij} - 2\Omega_i\Omega_j\right)\nu\partial_\nu\left(\sigma_a B_\nu\right) + \Omega_i\Omega_j\nu^2\partial_\nu^2\left(\sigma_a B_\nu\right)\right)\end{aligned}$$

$$
\begin{aligned}
&+ 2\beta_i\Omega_i\left(\sigma_a B_\nu - \beta_i\Omega_i\nu\partial_\nu\left(\sigma_a B_\nu\right)\right) + \beta_i\beta_j\left(3\Omega_i\Omega_j - \delta_{ij}\right)\sigma_a B_\nu \\
&= \sigma_a B_\nu + \beta_i\Omega_i\left(2\sigma_a B_\nu - \nu\partial_\nu\left(\sigma_a B_\nu\right)\right) \\
&+ \beta_i\beta_j\left(\left(3\Omega_i\Omega_j - \delta_{ij}\right)\sigma_a B_\nu + \left(\frac{1}{2}\delta_{ij} - 3\Omega_i\Omega_j\right)\nu\partial_\nu\left(\sigma_a B_\nu\right) + \frac{1}{2}\Omega_i\Omega_j\nu^2\partial_\nu^2\left(\sigma_a B_\nu\right)\right).
\end{aligned}
\tag{C.18}
$$

The lab-frame radiation transport equation expanded through $\mathcal{O}(\beta^2)$, which is the primary goal of this appendix, is:

$$
\begin{aligned}
&\frac{1}{c}\partial_t I_\nu + \Omega_i\partial_i I_\nu = \frac{\sigma_s}{4\pi}\phi_\nu + \sigma_a B_\nu - \sigma_t I_\nu \\
&+ \beta_i\Omega_i\left(\sigma_t I_\nu + I_\nu\nu\partial_\nu\sigma_t + 2\frac{\sigma_s}{4\pi}\phi_\nu + 2\sigma_a B_\nu - \frac{\sigma_s}{4\pi}\nu\partial_\nu\phi_\nu - \nu\partial_\nu\left(\sigma_a B_\nu\right)\right) \\
&- \frac{\sigma_s}{4\pi}\beta_i\left(F_{i,\nu} - \nu\partial_\nu F_{i,\nu}\right) - \frac{1}{2}\beta_i\beta_j\left(\sigma_t\delta_{ij}I_\nu + \delta_{ij}I_\nu\nu\partial_\nu\sigma_t + \Omega_i\Omega_j I_\nu\nu^2\partial_\nu^2\sigma_t\right) \\
&+ \frac{\sigma_s}{4\pi}\beta_i\beta_j\left(\left(3\Omega_i\Omega_j - \frac{1}{2}\delta_{ij}\right)\phi_\nu - 2\Omega_i\Omega_j\nu\partial_\nu\phi_\nu - 2\Omega_i F_{j,\nu} + 2\Omega_i\nu\partial_\nu F_{j,\nu}\right) \\
&+ \beta_i\beta_j\left(\left(3\Omega_i\Omega_j - \delta_{ij}\right)\sigma_a B_\nu + \left(\frac{1}{2}\delta_{ij} - 3\Omega_i\Omega_j\right)\nu\partial_\nu\left(\sigma_a B_\nu\right) + \frac{1}{2}\Omega_i\Omega_j\nu^2\partial_\nu^2\left(\sigma_a B_\nu\right)\right).
\end{aligned}
\tag{C.19}
$$

For the purposes of the asymptotic analysis in Chapter III, it is necessary to split the absorption cross-section into the difference between the total and scattering cross-sections: $\sigma_a = \sigma_t - \sigma_s$. As a reminder, the scattering cross-section is frequency independent. The result is

$$
\begin{aligned}
&\frac{1}{c}\partial_t I_\nu + \Omega_i\partial_i I_\nu = \frac{\sigma_s}{4\pi}\phi_\nu + \sigma_t B_\nu - \sigma_s B_\nu - \sigma_t I_\nu - \frac{\sigma_s}{4\pi}\beta_i\left(F_{i,\nu} - \nu\partial_\nu F_{i,\nu}\right) \\
&+ \beta_i\Omega_i\left(\sigma_t I_\nu + I_\nu\nu\partial_\nu\sigma_t + \frac{\sigma_s}{4\pi}\left(2\phi_\nu - \nu\partial_\nu\phi_\nu\right) + 2\sigma_t B_\nu - \nu\partial_\nu\left(\sigma_t B_\nu\right) + \sigma_s\left(\nu\partial_\nu B_\nu - 2B_\nu\right)\right) \\
&- \frac{1}{2}\beta_i\beta_j\left(\sigma_t\delta_{ij}I_\nu + \delta_{ij}I_\nu\nu\partial_\nu\sigma_t + \Omega_i\Omega_j I_\nu\nu^2\partial_\nu^2\sigma_t\right) \\
&+ \frac{\sigma_s}{4\pi}\beta_i\beta_j\left(\left(3\Omega_i\Omega_j - \frac{1}{2}\delta_{ij}\right)\phi_\nu - 2\Omega_i\Omega_j\nu\partial_\nu\phi_\nu - 2\Omega_i F_{j,\nu} + 2\Omega_i\nu\partial_\nu F_{j,\nu}\right)
\end{aligned}
$$

$$+\beta_i\beta_j\left(\left(3\Omega_i\Omega_j-\delta_{ij}\right)\sigma_t B_\nu+\left(\frac{1}{2}\delta_{ij}-3\Omega_i\Omega_j\right)\nu\partial_\nu\left(\sigma_t B_\nu\right)+\frac{1}{2}\Omega_i\Omega_j\nu^2\partial_\nu^2\left(\sigma_t B_\nu\right)\right)$$
$$-\sigma_s\beta_i\beta_j\left(\left(3\Omega_i\Omega_j-\delta_{ij}\right)B_\nu-\left(\frac{1}{2}\delta_{ij}-3\Omega_i\Omega_j\right)\nu\partial_\nu B_\nu+\frac{1}{2}\Omega_i\Omega_j\nu^2\partial_\nu^2 B_\nu\right). \qquad \text{(C.20)}$$

For the purposes of the radiative shock solutions, in Chapters IV and V, it is helpful to present the 1-D time-independent grey radiation transport equation, truncated at $\mathcal{O}(\beta)$

$$\mu\partial_x I=\frac{\sigma_s}{4\pi}c\mathcal{E}+\frac{\sigma_a}{4\pi}a_r cT^4-\sigma_t I-2\frac{\sigma_s}{4\pi}\beta\mathcal{F}$$
$$+\beta\mu\left(\sigma_t I+3\frac{\sigma_s}{4\pi}c\mathcal{E}+3\frac{\sigma_a}{4\pi}a_r cT^4\right). \qquad \text{(C.21)}$$

APPENDIX D

ASYMPTOTIC DERIVATION OF THE RADIATION VARIABLES THROUGH $\mathcal{O}(\epsilon^2)$

The asymptotic analysis of the radiation transport equation (III.23d) requires implementing the scaled ratios (III.25), and retaining terms through $\mathcal{O}(\epsilon^2)$, such that the scaled redimensionalized radiation transport equation is

$$\begin{aligned}
&\epsilon^2\frac{1}{c}\partial_t I_\nu + \epsilon\Omega_i\partial_i I_\nu = \sigma_t\left(B_\nu - I_\nu\right)\\
&+\epsilon\left(\beta_i\Omega_i\left(\sigma_t I_\nu + I_\nu\nu\partial_\nu\sigma_t + 2\sigma_t B_\nu - \nu\partial_\nu\left(\sigma_t B_\nu\right)\right) + \frac{\sigma_s}{4\pi}\left(\phi_\nu - 4\pi B_\nu\right)\right)\\
&+\epsilon^2\beta_i\beta_j\left(\left(3\Omega_i\Omega_j - \delta_{ij}\right)\sigma_t B_\nu + \left(\frac{1}{2}\delta_{ij} - 3\Omega_i\Omega_j\right)\nu\partial_\nu\left(\sigma_t B_\nu\right) + \frac{1}{2}\Omega_i\Omega_j\nu^2\partial_\nu^2\left(\sigma_t B_\nu\right)\right)\\
&-\epsilon^2\frac{1}{2}\beta_i\beta_j\left(\sigma_t\delta_{ij}I_\nu + \delta_{ij}I_\nu\nu\partial_\nu\sigma_t + \Omega_i\Omega_j I_\nu\nu^2\partial_\nu^2\sigma_t\right)\ . \qquad \text{(D.1)}
\end{aligned}$$

It is worth noticing a few things about equation (D.1), and choosing the order of angle- and frequency-integration to be made. First, the Planck function B_ν, and the angle-integrated radiation variables ϕ_ν and $F_{i,\nu}$, are angle-independent, such that odd angular moments of these variables are identically zero; i.e., the radiation flux will not include contain contributions from these terms. Second, there exist a few terms where the frequency derivative is pre-multiplied by frequency, and integration-by-parts in the frequency variable will help in the analysis of these terms. The only frequency derivative where this fails is the second term on the second line which is also pre-multiplied by the frequency-dependent radiation intensity I_ν. As for the integration-by-parts in the frequency variable, it is assumed that all radiation variables have finite bounded support over the frequency domain, $\nu \in [0, \infty)$, such

that the radiation variables are zero at the frequency boundaries:

$$I_{\nu=0} = 0 = I_{\nu=\infty}\,, \tag{D.2a}$$

$$B_{\nu=0} = 0 = B_{\nu=\infty}\,, \tag{D.2b}$$

$$\phi_{\nu=0} = 0 = \phi_{\nu=\infty}\,, \tag{D.2c}$$

$$F_{i,\nu=0} = 0 = F_{i,\nu=\infty}\,. \tag{D.2d}$$

Based on the comments above, it is preferable to angle-integrate, and then frequency-integrate, the radiation intensity when constructing its angle- and frequency-integrated angular moments. The leading-, first- and second-order expansion in ϵ, and the associated angle-integrations, and angle- and frequency integrations, are given below.

$\underline{\epsilon^{(0)}}$

The leading-order radiation transport equation, from equation (D.1), is

$$0 = \left[\sigma_t \left(B\nu - I_\nu\right)\right]^{(0)}\,, \tag{D.3}$$

such that the $\mathcal{O}(\epsilon^{(0)})$ radiation intensity, and its angle-integrated, and angle- and frequency-integrated radiation variables, are

$$I_\nu^{(0)} = B_\nu^{(0)}\,, \tag{D.4a}$$

$$\phi_\nu^{(0)} = \int_{4\pi} I_\nu^{(0)}\, d\Omega = 4\pi B_\nu^{(0)}\,, \tag{D.4b}$$

$$F_{i,\nu}^{(0)} = \int_{4\pi} \Omega_i I_\nu^{(0)}\, d\Omega = 0\,, \tag{D.4c}$$

$$P_{ij,\nu}^{(0)} = \int_{4\pi} \Omega_i \Omega_j I_\nu^{(0)}\, d\Omega = \frac{4\pi}{3}\delta_{ij} B_\nu^{(0)} = \frac{1}{3}\delta_{ij}\phi_\nu^{(0)}\,, \tag{D.4d}$$

$$\mathcal{E}^{(0)} = \frac{1}{c}\int_0^\infty \int_{4\pi} I_\nu^{(0)}\, d\Omega d\nu = a_r T^{(0),4}\,, \tag{D.4e}$$

$$\mathcal{F}_i^{(0)} = \int_0^\infty \int_{4\pi} \Omega_i I_\nu^{(0)} \, d\Omega d\nu = 0 \,, \tag{D.4f}$$

$$\mathcal{P}_{ij}^{(0)} = \frac{1}{c} \int_0^\infty \int_{4\pi} \Omega_i \Omega_j I_\nu^{(0)} \, d\Omega d\nu = \frac{1}{3} \delta_{ij} a_r T^{(0),4} = \frac{1}{3} \delta_{ij} \mathcal{E}^{(0)} \,. \tag{D.4g}$$

It is interesting to notice that the P_1 approximation naturally appears in the equations above. This will also be seen in the $\mathcal{O}(\epsilon)$ equations below, and the connection to the comoving-frame P_1 approximation is made in Section III.4.1.

$\underline{\epsilon^{(1)}}$

The first-order radiation transport equation, from equation (D.1), is

$$\begin{aligned}
&\left[\Omega_i \partial_i I_\nu\right]^{(0)} \\
&= \left[\sigma_t \left(B_\nu - I_\nu\right)\right]^{(1)} + \left[\beta_i \Omega_i \left(\sigma_t I_\nu + I_\nu \nu \partial_\nu \sigma_t + 2\sigma_t B_\nu - \nu \partial_\nu \left(\sigma_t B_\nu\right)\right) + \frac{\sigma_s}{4\pi} \left(\phi_\nu - 4\pi B_\nu\right)\right]^{(0)} \\
&= \sigma_t^{(1)} \left[B_\nu - I_\nu\right]^{(0)} + \sigma_t^{(0)} \left[B_\nu - I_\nu\right]^{(1)} \\
&+ \left[\beta_i \Omega_i \left(\sigma_t I_\nu + I_\nu \nu \partial_\nu \sigma_t + 2\sigma_t B_\nu - \nu \partial_\nu \left(\sigma_t B_\nu\right)\right) + \frac{\sigma_s}{4\pi} \left(\phi_\nu - 4\pi B_\nu\right)\right]^{(0)} \,,
\end{aligned} \tag{D.5}$$

and using results from equations (D.4), the first-order radiation transport equation simplifies to:

$$\left[\Omega_i \partial_i B_\nu\right]^{(0)} = \sigma_t^{(0)} \left[B_\nu - I_\nu\right]^{(1)} + \Omega_i \left[\beta_i \left(3\sigma_t B_\nu - \sigma_t \nu \partial_\nu B_\nu\right)\right]^{(0)} \,. \tag{D.6}$$

The $\mathcal{O}(\epsilon^{(1)})$ radiation intensity, and the angle-integrated and angle- and frequency-integrated radiation variables are

$$I_\nu^{(1)} = B_\nu^{(1)} + \Omega_i \left[-\frac{1}{\sigma_t} \partial_i B_\nu + \beta_i \left(3B_\nu - \nu \partial_\nu B_\nu\right)\right]^{(0)} \,, \tag{D.7a}$$

$$\phi_\nu^{(1)} = \int_{4\pi} I_\nu^{(1)} \, d\Omega = 4\pi B_\nu^{(1)} \,, \tag{D.7b}$$

$$F_{i,\nu}^{(1)} = \int_{4\pi} \Omega_i I_\nu^{(1)}\, d\Omega = \frac{4\pi}{3}\left[-\frac{1}{\sigma_t}\partial_i B_\nu + \beta_i\left(3B_\nu - \nu\partial_\nu B_\nu\right)\right]^{(0)}, \tag{D.7c}$$

$$P_{ij,\nu}^{(1)} = \int_{4\pi} \Omega_i\Omega_j I_\nu^{(1)}\, d\Omega = \frac{4\pi}{3}\delta_{ij}B_\nu^{(1)} = \frac{1}{3}\delta_{ij}\phi_\nu^{(1)}, \tag{D.7d}$$

$$\mathcal{E}^{(1)} = \frac{1}{c}\int_0^\infty \int_{4\pi} I_\nu^{(1)}\, d\Omega d\nu = a_r T^{(1),4}, \tag{D.7e}$$

$$\mathcal{F}_i^{(1)} = \int_0^\infty \int_{4\pi} \Omega_i I_\nu^{(1)}\, d\Omega d\nu = \frac{1}{3}\left[-\frac{a_r c}{\sigma_{t,R}}\partial_i T^4 + 4a_r u_i T^4\right]^{(0)}, \tag{D.7f}$$

$$\mathcal{P}_{ij}^{(1)} = \frac{1}{c}\int_0^\infty \int_{4\pi} \Omega_i\Omega_j I_\nu^{(1)}\, d\Omega d\nu = \frac{1}{3}\delta_{ij}a_r T^{(1),4} = \frac{1}{3}\delta_{ij}\mathcal{E}^{(1)}. \tag{D.7g}$$

In passing from equation (D.7c) to (D.7f), the Rosseland mean opacity $\sigma_{t,R}$, has been defined,

$$\int_0^\infty \frac{1}{\sigma_t}\partial_i B_\nu\, d\nu = \partial_i T\int_0^\infty \frac{1}{\sigma_t}\partial_T B_\nu\, d\nu = \partial_i T \underbrace{\frac{\int_0^\infty \frac{1}{\sigma_t}\partial_T B_\nu}{\int_0^\infty \partial_T B_\nu\, d\nu}}_{\equiv\frac{1}{\sigma_{t,R}}}\underbrace{\int_0^\infty \partial_T B_\nu\, d\nu}_{=\partial_T\int_0^\infty B_\nu\, d\nu}$$

$$= \frac{1}{\sigma_{t,R}}\partial_i T\left(\partial_T\frac{a_r c T^4}{4\pi}\right) = \frac{a_r c}{4\pi\sigma_{t,R}}\partial_i T^4,$$

and an integration-by-parts has been performed. Again, the P_1 approximation appears in equations (D.7d) and (D.7g). It is also interesting to notice that the first-order radiation flux depends solely on $\mathcal{O}(\epsilon^{(0)})$ variables.

$\underline{\epsilon^{(2)}}$

The second-order radiation transport equation, from equation (D.1), is

$$\frac{1}{c}\partial_t I_\nu^{(0)} + \Omega_i\partial_i I_\nu^{(1)} = \left[\sigma_t\left(B_\nu - I_\nu\right)\right]^{(2)}$$
$$+\left[\beta_i\Omega_i\left(\sigma_t I_\nu + I_\nu\nu\partial_\nu\sigma_t + 2\sigma_t B_\nu - \nu\partial_\nu\left(\sigma_t B_\nu\right)\right) + \frac{\sigma_s}{4\pi}\left(\phi_\nu - 4\pi B_\nu\right)\right]^{(1)}$$
$$+\left[\frac{\sigma_s}{4\pi}\beta_i\left(\Omega_i\left(2\left(\phi_\nu - 4\pi B_\nu\right) + \nu\partial_\nu\left(4\pi B_\nu - \phi_\nu\right)\right) - F_{i,\nu} + \nu\partial_\nu F_{i,\nu}\right)\right]^{(0)}$$

$$+\left[\beta_i\beta_j\left(\left(3\Omega_i\Omega_j-\delta_{ij}\right)\sigma_t B_\nu+\left(\frac{1}{2}\delta_{ij}-3\Omega_i\Omega_j\right)\nu\partial_\nu\left(\sigma_t B_\nu\right)+\frac{1}{2}\Omega_i\Omega_j\nu^2\partial_\nu^2\left(\sigma_t B_\nu\right)\right)\right]^{(0)}$$
$$-\left[\frac{1}{2}\beta_i\beta_j\left(\sigma_t\delta_{ij}I_\nu+\delta_{ij}I_\nu\nu\partial_\nu\sigma_t+\Omega_i\Omega_j I_\nu\nu^2\partial_\nu^2\sigma_t\right)\right]^{(0)}, \tag{D.8}$$

and using results from equations (D.4) and (D.7), the second-order radiation transport equation simplifies

$$\begin{aligned}
&\frac{1}{c}\partial_t B_\nu^{(0)}+\Omega_i\partial_i I_\nu^{(1)}=\sigma_t^{(0)}\left[B_\nu-I_\nu\right]^{(2)}+\sigma_t^{(1)}\left[B_\nu-I_\nu\right]^{(1)}\\
&+\Omega_i\left[\beta_i\left(\sigma_t I_\nu+I_\nu\nu\partial_\nu\sigma_t+2\sigma_t B_\nu-\nu\partial_\nu\left(\sigma_t B_\nu\right)\right)\right]^{(1)}\\
&-\frac{1}{2}\left[\beta^2\left(3\sigma_t B_\nu-\sigma_t\nu\partial_\nu B_\nu\right)\right]^{(0)}\\
&+\Omega_i\Omega_j\left[\beta_i\beta_j\left(3\sigma_t B_\nu-3\nu\partial_\nu\left(\sigma_t B_\nu\right)+\nu^2\left(\partial_\nu\sigma_t\right)\left(\partial_\nu B_\nu\right)+\frac{1}{2}\sigma_t\nu^2\partial_\nu^2 B_\nu\right)\right]^{(0)}.
\end{aligned} \tag{D.9}$$

The $\mathcal{O}(\epsilon^{(2)})$ radiation intensity is

$$\begin{aligned}
&I_\nu^{(2)}=B_\nu^{(2)}+\frac{1}{\sigma_t^{(0)}}\Omega_i\left[-\partial_i I_\nu+\beta_i\left(\sigma_t I_\nu+I_\nu\nu\partial_\nu\sigma_t+2\sigma_t B_\nu-\nu\partial_\nu\left(\sigma_t B_\nu\right)\right)\right]^{(1)}\\
&+\frac{\sigma_t^{(1)}}{\sigma_t^{(0)}}\left[B_\nu-I_\nu\right]^{(1)}-\left[\frac{1}{c\sigma_t}\partial_t B_\nu+\frac{1}{2}\beta^2\left(3B_\nu-\nu\partial_\nu B_\nu\right)\right]^{(0)}\\
&+\frac{1}{\sigma_t^{(0)}}\Omega_i\Omega_j\left[\beta_i\beta_j\left(3\sigma_t B_\nu-3\nu\partial_\nu\left(\sigma_t B_\nu\right)+\nu^2\left(\partial_\nu\sigma_t\right)\left(\partial_\nu B_\nu\right)+\frac{1}{2}\sigma_t\nu^2\partial_\nu^2 B_\nu\right)\right]^{(0)}.
\end{aligned} \tag{D.10}$$

Before deriving the angle-integrated radiation variables it is worth noticing that there is already one factor of the angular variable coupled to the radiation intensity. Thus, the second angular moment for the radiation pressure will involve an angular integral of the radiation intensity with three angular variables, and the result will be a radiation variable with three-indices. Since this variable has not been defined herein, this derivation is avoided, and is unnecessary. The second-order angle-integrated

radiation intensity is

$$
\begin{aligned}
\phi_\nu^{(2)} &= 4\pi B_\nu^{(2)} + \frac{1}{\sigma_t^{(0)}}\left[-\partial_i F_{i,\nu} + \beta_i\left(\sigma_t F_{i,\nu} + F_{i,\nu}\nu\partial_\nu\sigma_t\right)\right]^{(1)} \\
&+ \frac{4\pi}{3\sigma_t^{(0)}}\left[\beta^2\left(3\sigma_t B_\nu - 3\nu\partial_\nu\left(\sigma_t B_\nu\right) + \nu^2\left(\partial_\nu\sigma_t\right)\left(\partial_\nu B_\nu\right) + \frac{1}{2}\sigma_t\nu^2\partial_\nu^2 B_\nu\right)\right]^{(0)} \\
&- \frac{4\pi}{\sigma_t^{(0)}}\left[\frac{1}{c}\partial_t B_\nu + \frac{1}{2}\beta^2\left(3\sigma_t B_\nu - \sigma_t\nu\partial_\nu B_\nu\right)\right]^{(0)} \\
&= 4\pi B_\nu^{(2)} + \frac{1}{\sigma_t^{(0)}}\left(-\partial_i F_{i,\nu}^{(1)} + \beta_i^{(0)} F_{i,\nu}^{(1)}\left(\sigma_t^{(0)} + \nu\partial_\nu\sigma_t^{(0)}\right)\right) \\
&+ \frac{4\pi}{3\sigma_t^{(0)}}\left[\beta^2\left(3\sigma_t B_\nu - 3\nu\partial_\nu\left(\sigma_t B_\nu\right) + \nu^2\left(\partial_\nu\sigma_t\right)\left(\partial_\nu B_\nu\right) + \frac{1}{2}\sigma_t\nu^2\partial_\nu^2 B_\nu\right)\right]^{(0)} \\
&- 4\pi\left[\frac{1}{c\sigma_t}\partial_t B_\nu + \frac{1}{2}\beta^2\left(3B_\nu - \nu\partial_\nu B_\nu\right)\right]^{(0)} \\
&= 4\pi B_\nu^{(2)} - \frac{4\pi}{3\sigma_t^{(0)}}\partial_i\left[-\frac{1}{\sigma_t}\partial_i B_\nu + \beta_i\left(3B_\nu - \nu\partial_\nu B_\nu\right)\right]^{(0)} \\
&+ \frac{4\pi}{3}\beta_i^{(0)}\left[-\frac{1}{\sigma_t^2}\partial_i B_\nu + \frac{1}{\sigma_t}\beta_i\left(3B_\nu - \nu\partial_\nu B_\nu\right)\right]^{(0)}\left[1 + \frac{1}{\sigma_t}\nu\partial_\nu\sigma_t\right]^{(0)} \\
&+ \frac{4\pi}{3\sigma_t^{(0)}}\left[\beta^2\left(3\sigma_t B_\nu - 3\nu\partial_\nu\left(\sigma_t B_\nu\right) + \nu^2\left(\partial_\nu\sigma_t\right)\left(\partial_\nu B_\nu\right) + \frac{1}{2}\sigma_t\nu^2\partial_\nu^2 B_\nu\right)\right]^{(0)} \\
&- 4\pi\left[\frac{1}{c\sigma_t}\partial_t B_\nu + \frac{1}{2}\beta^2\left(3B_\nu - \nu\partial_\nu B_\nu\right)\right]^{(0)} . \qquad \text{(D.11a)}
\end{aligned}
$$

In passing from the second equality to the third, equation (D.7c) has been used for $F_{i,\nu}$. The second-order angle-integrated radiation flux is comparatively straightforward

$$
\begin{aligned}
&F_{i,\nu}^{(2)} \\
&= -\frac{\sigma_t^{(1)}}{\sigma_t^{(0)}}F_{i,\nu}^{(1)} + \frac{1}{\sigma_t^{(0)}}\left[-\partial_j P_{ij,\nu} + \beta_j\left(\sigma_t P_{ij,\nu} + P_{ij,\nu}\nu\partial_\nu\sigma_t + \frac{4\pi}{3}\left(2\sigma_t B_\nu - \nu\partial_\nu\left(\sigma_t B_\nu\right)\right)\right)\right]^{(1)} \\
&= \frac{4\pi\sigma_t^{(1)}}{3}\left[\frac{1}{\sigma_t^2}\partial_i B_\nu - \frac{1}{\sigma_t}\beta_i\left(3B_\nu - \nu\partial_\nu B_\nu\right)\right]^{(0)} + \frac{4\pi}{3\sigma_t^{(0)}}\left[-\partial_i B_\nu + \beta_i\left(3\sigma_t B_\nu - \sigma_t\nu\partial_\nu B_\nu\right)\right]^{(1)}
\end{aligned}
$$

$$= -\frac{4\pi}{3}\left(\frac{1}{\sigma_t^{(0)}}\partial_i B_\nu^{(1)} - \sigma_t^{(1)}\left[\frac{1}{\sigma_t^2}\partial_i B_\nu\right]^{(0)}\right)$$
$$+ \frac{4\pi}{3}\left(-\sigma_t^{(1)}\left[\frac{1}{\sigma_t}\beta_i\left(3B_\nu - \nu\partial_\nu B_\nu\right)\right]^{(0)} + \frac{1}{\sigma_t^{(0)}}\left[\beta_i\left(3\sigma_t B_\nu - \sigma_t\nu\partial_\nu B_\nu\right)\right]^{(1)}\right)$$
$$= \frac{4\pi}{3}\left[-\frac{1}{\sigma_t}\partial_i B_\nu + \beta_i\left(3B_\nu - \nu\partial_\nu B_\nu\right)\right]^{(1)} . \tag{D.11b}$$

In passing to the last line, it must be recognized that the first term is a ratio of two terms, which obey the property:

$$\left[\frac{A}{B}\right]^{(1)} = A^{(1)}\left[\frac{1}{B}\right]^{(0)} + A^{(0)}\left[\frac{1}{B}\right]^{(1)} = \frac{1}{B^{(0)}}A^{(1)} - \left[\frac{A}{B^2}\right]^{(0)} B^{(1)} .$$

The radiation flux can be frequency-integrated immediately:

$$\mathcal{F}_i^{(2)} = \int_0^\infty F_{i,\nu}^{(2)}\, d\nu = \left[-\frac{a_r c}{3\sigma_{t,R}}\partial_i T^4 + \frac{4}{3}a_r u_i T^4\right]^{(1)} . \tag{D.11c}$$

Since the second-order angle-integrated radiation intensity is so different from its leading- and first-order counterparts, and since the second-order radiation intensity is considerably more involved than its first-order counterpart, it is fairly surprising that the first- and second-order angle-integrated radiation fluxes have the same form.

The second-order angle-integrated radiation intensity was presented only to impress that the second-order radiation energy density, and radiation pressure, will not take the same form as their leading- and first-order counterparts. Thus, the RH equations, in the EDL, cannot satisfy the EDA beyond $\mathcal{O}(\epsilon)$.

APPENDIX E

DERIVATION OF THE $\mathcal{O}(\beta^2)$ CORRECTIONS TO THE RADIATION TRANSPORT EQUATION

The 1-D grey RH equations are the Euler equations of fluid-mechanics, and the frequency-integrated equation of radiation transport:

$$\partial_t \rho + \partial_x (\rho u) = 0 \,, \tag{E.1a}$$

$$\partial_t (\rho u) + \partial_x \left(\rho u^2 + p\right) = -S_{rp} \,, \tag{E.1b}$$

$$\partial_t \left(\frac{1}{2}\rho u^2 + \rho e\right) + \partial_x \left[u\left(\frac{1}{2}\rho u^2 + \rho e + p\right)\right] = -S_{re} \,, \tag{E.1c}$$

$$\begin{aligned}\partial_t I + \mu \partial_x I = -\sigma_t I + \frac{\sigma_s}{4\pi} c\mathcal{E} + \frac{\sigma_a}{4\pi} a_r c T^4 + \beta\mu\left(\sigma_t I + 3\frac{\sigma_s}{4\pi}\mathcal{E} + 3\frac{\sigma_a}{4\pi} a_r T^4\right) \\ - 2\beta\frac{\sigma_s}{4\pi}\mathcal{F} + \frac{1}{4\pi}\left(C_0 + 3\mu C_1\right) \equiv Q \,,\end{aligned} \tag{E.1d}$$

where S_{re} and S_{rp} are the radiation source-rates of energy and momentum, which are defined according to equations (II.25e),

$$S_{re} = \int_{4\pi} Q d\mu = \partial_t \mathcal{E} + \partial_x \mathcal{F} = \sigma_a c\left[a_r T^4 - \left(\mathcal{E} - \frac{2}{c}\beta\mathcal{F}\right)\right] - \sigma_t \beta \mathcal{F} + C_0 \,, \tag{E.2a}$$

$$\begin{aligned} S_{rp} = \frac{1}{c}\int_{4\pi} Q\mu d\mu = \frac{1}{c^2}\partial_t \mathcal{F} + \partial_x \mathcal{P} \\ = -\frac{\sigma_t}{c}\left[\mathcal{F} - \left(\mathcal{E} + \mathcal{P}\right) u\right] + \sigma_a \beta\left(a_r T^4 - \mathcal{E}\right) + \frac{1}{c} C_1 \,. \end{aligned} \tag{E.2b}$$

The purpose of C_0 and C_1 is to ensure that the radiation energy and momentum source-rates go to zero in equilibrium, and to allow us to define the radiation internal

energy source-rate as

$$S_{re} - uS_{rp} = \sigma_a c \left(\alpha_R T^4 - \mathcal{E}_o\right) . \tag{E.3}$$

Thus, to define C_0 and C_1 correctly, it is necessary to define the equilibrium state. As mentioned previously, the RH equations (E.1), including the radiation source-rates equations (E.2) and (E.3), are correct through $\mathcal{O}(\beta)$. In equilibrium, we know on physical grounds that the following identities hold in the comoving-frame

$$\left(\mathcal{E}_o\right)_{eq} = \alpha_R T_{eq}^4 , \tag{E.4a}$$

$$\left(\mathcal{F}_o\right)_{eq} = 0 , \tag{E.4b}$$

$$\left(\mathcal{P}_o\right)_{eq} = \frac{1}{3}\left(\mathcal{E}_o\right)_{eq} , \tag{E.4c}$$

and that these identities may be approximately transformed to the lab-frame, via Lorentz transformations with $\mathcal{O}(\beta^2)$ truncations

$$\mathcal{E}_o = \mathcal{E} - \frac{2}{c}\beta\mathcal{F} + \mathcal{O}(\beta^2) , \tag{E.5a}$$

$$\mathcal{F}_o = \mathcal{F} - (\mathcal{E} + \mathcal{P})\, u + \mathcal{O}(\beta^2) , \tag{E.5b}$$

$$\mathcal{P}_o = \mathcal{P} - \frac{2}{c}\beta\mathcal{F} + \mathcal{O}(\beta^2) . \tag{E.5c}$$

The reason we want to transform the comoving-frame equilibrium identities to the lab-frame is because the source-rate equations (E.2) are written using lab-frame variables, which are also used to solve equations (E.1). We modify the Lorentz transformations for the radiation energy density, and radiation pressure, at $\mathcal{O}(\beta^2)$,

by writing them as

$$\mathcal{E}_o = \mathcal{E} - \frac{2}{c}\beta\mathcal{F}_o + \mathcal{O}(\beta^2)\,, \tag{E.6a}$$

$$\mathcal{F}_o = \mathcal{F} - (\mathcal{E}+\mathcal{P})\,u + \mathcal{O}(\beta^2)\,, \tag{E.6b}$$

$$\mathcal{P}_o = \mathcal{P} - \frac{2}{c}\beta\mathcal{F}_o + \mathcal{O}(\beta^2)\,, \tag{E.6c}$$

where we have rewritten the radiation flux for completeness, although it has not been changed. It is worth emphasizing that this change to the Lorentz transformations is at $\mathcal{O}(\beta^2)$, which is at the same order of the truncation of the Lorentz transformations, such that no extra error has been introduced. These are the Lorentz transformations that we choose to use. Now, in equilibrium, the lab-frame radiation variables, to $\mathcal{O}(\beta^2)$, are

$$\mathcal{E}_{eq} = \mathcal{E}_o = \alpha_R T_{eq}^4\,, \tag{E.7a}$$

$$\mathcal{F}_{eq} = (\mathcal{E}+\mathcal{P})_{eq}\,u_{eq} = \frac{4}{3}\,(\mathcal{E}u)_{eq}\ , \tag{E.7b}$$

$$\mathcal{P}_{eq} = (\mathcal{P}_o)_{eq} = \frac{1}{3}\,(\mathcal{E}_o)_{eq} = \frac{1}{3}\mathcal{E}_{eq}\,. \tag{E.7c}$$

From now on, when we talk about equilibrium we mean equations (E.7). Having defined the equilibrium state, we now consider C_0 and C_1. The radiation momentum source-rate equation (E.2b), in equilibrium, is zero without any modifications

$$(S_{rp})_{eq} = -\frac{\sigma_t}{c}\left[\mathcal{F} - (\mathcal{E}+\mathcal{P})\,u\right]_{eq} + \sigma_a\beta_{eq}\left(a_r T^4 - \mathcal{E}\right)_{eq} + \frac{1}{c}\,(C_1)_{eq} = 0\,, \tag{E.8}$$

therefore, we set $C_1 = 0$. Next, consider the radiation internal source-rate as found from the radiation energy and momentum source-rates given in equations (E.2),

$$\begin{aligned} S_{re} - uS_{rp} &= \sigma_a c \left[a_r T^4 - \left(\mathcal{E} - \frac{2}{c}\beta\mathcal{F} \right) \right] - \sigma_t \beta \mathcal{F} + C_0 \\ &\quad - u \left(-\frac{\sigma_t}{c} \left[\mathcal{F} - (\mathcal{E} + \mathcal{P})\, u \right] + \sigma_a \beta \left(a_r T^4 - \mathcal{E} \right) \right) \\ &= \sigma_a c \left[a_r T^4 - \left(\mathcal{E} - \frac{2}{c}\beta\mathcal{F} \right) \right] - \beta^2 c \left(\sigma_t \mathcal{P} + \sigma_s \mathcal{E} + \sigma_a \alpha_R T^4 \right) + C_0. \end{aligned} \tag{E.9}$$

The first term on the RHS almost matches the radiation internal source-rate equation (E.3), but the radiation flux term must be Lorentz transformed via equation (E.6b) so that the Lorentz transformed radiation energy density agrees with equation (E.6a):

$$\begin{aligned} S_{re} - uS_{rp} &= \sigma_a c \left[a_r T^4 - \left(\mathcal{E} - \frac{2}{c}\beta\mathcal{F}_o \right) \right] + 2\sigma_a \beta \left(\mathcal{F} - \mathcal{F}_o \right) \\ &\quad - \beta^2 c \left(\sigma_t \mathcal{P} + \sigma_s \mathcal{E} + \sigma_a \alpha_R T^4 \right) + C_0 \\ &= \sigma_a c \left[a_r T^4 - \mathcal{E}_o \right] + \beta^2 c \left(\left(\sigma_a - \sigma_s \right) (\mathcal{E} + \mathcal{P}) + \sigma_a \left(\mathcal{E} - \alpha_R T^4 \right) \right) + C_0 \,, \\ \Rightarrow C_0 &= \beta^2 c \left(\left(\sigma_s - \sigma_a \right) (\mathcal{E} + \mathcal{P}) + \sigma_a \left(\alpha_R T^4 - \mathcal{E} \right) \right) \,. \end{aligned} \tag{E.10a}$$

It is worth testing C_0 in the radiation energy source-rate equation (E.2a) to ensure that the equation does go to zero in equilibrium as expected

$$\begin{aligned} \left(S_{re} \right)_{eq} &= \sigma_a c \left[a_r T^4 - \left(\mathcal{E} - \frac{2}{c}\beta\mathcal{F} \right) \right]_{eq} - \sigma_t \beta_{eq} \mathcal{F}_{eq} + \left(C_0 \right)_{eq} \\ &= \left(\sigma_a - \sigma_s \right) \beta_{eq} \mathcal{F}_{eq} + \left(C_0 \right)_{eq} \\ &= \beta_{eq}^2 c \left(\sigma_a - \sigma_s \right) \left(\mathcal{E} + \mathcal{P} \right)_{eq} + \beta_{eq}^2 c \left(\sigma_s - \sigma_a \right) \left(\mathcal{E} + \mathcal{P} \right)_{eq} \\ &= 0 \,. \end{aligned} \tag{E.11}$$

APPENDIX F

DERIVATION OF THE WAVE EQUATION AND NONDIMENSIONALIZATION OF THE IDEAL GAS EQUATION OF STATE

We assume an ideal-gas $\gamma-$law equation-of-state (EOS) to describe the thermodynamics of the material system. Since we are ultimately interested in shock waves in the ideal-gas, it is necessary to go beyond standard thermodynamic treatments and obtain information about the speed of sound for the ideal-gas. The standard equation of an ideal-gas is

$$p = nk_BT = nm\frac{k_B}{m}T = \rho R_{\text{specific}}T\,, \tag{F.1}$$

where p is the material pressure with units $[energy/volume]$, n is the number density of atoms or molecules in the system with units $[number/volume]$, m is the mass of an individual atom or molecule, ρ is the mass density with units $[mass/volume]$, k_B is Boltzmann's constant with units $[energy/Kelvin]$, R_{specific} is the specific gas constant which is equivalent to the gas constant R divided by the molar mass of interest, and T is the material temperature with units of $[Kelvin]$. For an ideal-gas, R_{specific} is the difference between the specific heat at constant pressure and constant volume, $R_{\text{specific}} = c_p - c_V$, and the ratio of the specific heat at constant pressure to the specific heat at constant volume is the adiabatic index, γ,

$$\frac{c_p}{c_V} = \gamma\,, \tag{F.2}$$

such that

$$\frac{R_{\text{specific}}}{c_V} = \frac{c_p}{c_V} - 1 = \gamma - 1\,. \tag{F.3}$$

For a monatomic gas, $\gamma = 5/3$. The ideal-gas equation (F.1) can now be written as

$$p = \rho \frac{R_{\text{specific}}}{c_V} c_V T = \rho\,(\gamma - 1)\,e\,, \tag{F.4}$$

where the material's specific internal energy, $e = c_V T$, has been introduced. Since the material motion is described by the Euler equations, sound waves are isentropic propagation waves of a *small* disturbance about the material's equilibrium state:

$$\rho = \rho_0 + \rho' \tag{F.5a}$$

$$p = p_0 + p' \tag{F.5b}$$

$$u = u'. \tag{F.5c}$$

The last expression, for the velocity, implies that the material is at rest prior to the disturbance, and also shows that the velocity is inherently a first-order valued quantity. Linearizing the Euler equations with respect to the disturbance, and neglecting the radiation sources, produces

$$\partial_t \rho' + \rho_0 \partial_x u' = 0\,, \tag{F.6a}$$

$$\rho_0 \partial_t u' + \partial_x p' = 0\,, \tag{F.6b}$$

$$\frac{1}{\gamma - 1}\partial_t p' + \frac{\gamma p_0}{\gamma - 1}\partial_x u' = 0\,. \tag{F.6c}$$

The difference between the time-derivative of the momentum conservation equation, and the spatial-derivative of the energy conservation equation, produces the wave equation for the velocity field

$$\rho_0 \partial_t^2 u' - \gamma p_0 \partial_x^2 u' = 0 \quad \Rightarrow \partial_t^2 u' = \frac{\gamma p_0}{\rho_0} \partial_x^2 u' \,, \tag{F.7}$$

such that the propagation speed a_0 of a small disturbance is:

$$a_0 = \sqrt{\frac{\gamma p_0}{\rho_0}}. \tag{F.8}$$

Similarly, the pressure may be written as a function of the two thermodynamic quantities, entropy and density: $p = p\,(s, \rho)$. The isentropic Taylor expansion of the pressure is

$$p\,(s, \rho) = p\,(s, \rho_0) + \rho' \left(\frac{\partial p}{\partial \rho} \right)_{s=\text{const}} + \ldots \tag{F.9}$$

and the squared speed of sound a^2 is canonically defined as

$$a^2 \equiv \left(\frac{\partial p}{\partial \rho} \right)_{s=\text{const}} . \tag{F.10}$$

The derivative is computed by considering the thermodynamic first-law for an isentropic process,

$$T ds = de + p d \left(\frac{1}{\rho} \right) = 0 \,, \tag{F.11}$$

and noting that the ideal-gas equation (F.4) can be rearranged

$$e = \frac{p}{\rho\left(\gamma - 1\right)}\,. \tag{F.12}$$

Then the thermodynamic first-law for an isentropic process is

$$\begin{aligned} 0 &= d\left(\frac{p}{\rho\left(\gamma-1\right)}\right) + pd\left(\frac{1}{\rho}\right) \\ &= \frac{1}{\rho\left(\gamma-1\right)}dp - \frac{p}{\rho^2\left(\gamma-1\right)}d\rho - \frac{p}{\rho^2}d\rho \\ &= \frac{1}{\rho\left(\gamma-1\right)}dp - \frac{\gamma p}{\rho^2\left(\gamma-1\right)}d\rho\,, \\ &\Rightarrow \left(\frac{dp}{d\rho}\right)_{s=\text{const}} = \frac{\gamma p}{\rho}\,, \end{aligned} \tag{F.13}$$

and the speed of sound, as determined by thermodynamic reasoning, is

$$a = \sqrt{\frac{\gamma p}{\rho}}\,. \tag{F.14}$$

While the two equations for the speed of sound derived above, (F.8) and (F.14), look slightly different, they are the same. The derivation of equation (F.14) uses the canonical definition of the speed of sound, which truncates the Taylor expansion after the first-derivative, and the thermodynamic first law, equation (F.11), which implies the use of the equilibrium state; thermodynamics only strictly applies to physical systems in equilibrium and at rest. Therefore, the values of pressure and density in equation (F.14) are their equilibrium values, which are written as p_0 and ρ_0 in equation (F.8). The squared speed of sound may be written in two equal, but different, ways

$$a^2 = \frac{\gamma p}{\rho}$$

$$= \gamma R_{\text{specific}} T \tag{F.15a}$$

$$= \gamma \left(\gamma - 1\right) e \,, \tag{F.15b}$$

and it is apparent that the material specific internal energy has the dimensions of speed squared.

Having defined the local sound speed, we also define the local Mach number $\mathcal{M}$, as the ratio of the local flow velocity u, to the local sound speed a:

$$\mathcal{M} = \frac{u}{a} \,. \tag{F.16}$$

We now seek to understand how to nondimensionalize the thermodynamic quantities associated with the ideal-gas. Dimensional variables can be decomposed into their nondimensional reference values, and their dimensional quantities, e.g., $\tilde{x} = x\tilde{x}_0$. Items with a tilde over them carry physical dimensions. For nondimensionalization, we choose to use reference variables for the sound speed $\tilde{a}_0$, and the temperature $\tilde{T}_0$, but not the internal energy. Further, for consistency, reference quantities for sound speed, and temperature, should agree,

$$\tilde{a}_0^2 = \gamma \tilde{R}_{\text{specific}} \tilde{T}_0 \,, \tag{F.17}$$

which implies that the nondimensional sound speed, determined from the local sound speed, is

$$\begin{aligned} \tilde{a}^2 = a^2 \tilde{a}_0^2 &= a^2 \gamma \tilde{R}_{\text{specific}} \tilde{T}_0 \\ &= \gamma \tilde{R}_{\text{specific}} \tilde{T} = T \gamma \tilde{R}_{\text{specific}} \tilde{T}_0 \end{aligned}$$

$$\Rightarrow a^2 = T\,. \tag{F.18}$$

The material is described by three forms of energy density, kinetic energy density ρu^2, internal energy density ρe, and pressure p, and it is convenient to nondimensionalize these quantities with the same parameters, $\tilde{\rho}_0 \tilde{a}_0^2$. Nondimensionalization of the material specific internal energy produces the nondimensional form of the specific heat at constant volume, c_V,

$$\begin{aligned} \tilde{e} = e\tilde{a}_0^2 &= c_V T \gamma \tilde{R}_{\text{specific}} \tilde{T}_0 \\ &= \tilde{c}_V \tilde{T} = T \tilde{c}_V \tilde{T}_0 \\ \Rightarrow c_V = \frac{\tilde{c}_V}{\gamma \tilde{R}_{\text{specific}}} &= \frac{1}{\gamma\,(\gamma - 1)}\,, \end{aligned} \tag{F.19}$$

where $\tilde{c}_V$ is the specific heat at constant volume, and we have used equation (F.3) to get $(\gamma - 1)$ in the denominator of equation (F.19). We have assumed that the nondimensional specific internal energy can still be written as the product of the specific heat at constant volume and temperature:

$$e = c_V T = \frac{1}{\gamma\,(\gamma - 1)} T\,. \tag{F.20}$$

The nondimensional equation for the pressure follows from the dimensional ideal-gas equation:

$$\begin{aligned} \tilde{p} &= p \tilde{\rho}_0 \tilde{a}_0^2 \\ &= \tilde{\rho}\tilde{e}\,(\gamma - 1) = \rho e\,(\gamma - 1)\,\tilde{\rho}_0 \tilde{a}_0^2 \\ \Rightarrow p &= \rho e\,(\gamma - 1)\,. \end{aligned} \tag{F.21}$$

The local Mach number may be rewritten by recalling equation (F.16):

$$\mathcal{M} = \frac{\tilde{u}}{\tilde{a}} = \frac{u\tilde{a}_0}{a\tilde{a}_0} = \frac{u}{\sqrt{T}}\,. \tag{F.22}$$

APPENDIX G

DERIVATION OF THE LINEARIZATION PROCEDURE USED FOR THE RADIATION HYDRODYNAMIC SOLVE IN THE FIRST ITERATION

In equilibrium, the RH variables assume constant values, and their respective ODEs are zero, as expected. The purpose of linearizing the RH ODEs is to provide a value of the RH variables away from equilibrium which is consistent with the equations to be solved.

We begin with ODEs for the spatial gradient of the radiation pressure, and the material temperature, equations (V.20) and (V.19), which are rewritten here for convenience, and where $\mathcal{P} = \frac{1}{3}\mathcal{E}$ is used since we are stepping out of equilibrium:

$$\partial_x \mathcal{E} = \frac{3\sigma_t \mathcal{M}_0}{\mathcal{C} P_0} \left[\frac{T-1}{\gamma - 1} + \frac{\mathcal{M}_0^2}{2\rho^2}\left(1-\rho^2\right) + P_0 \left(\frac{\frac{4}{3}\sigma_s \mathcal{E} + \sigma_a \left(\frac{1}{3}\mathcal{E} + T^4\right)}{\rho \sigma_t} - \frac{4}{3} \right) \right] , \quad \text{(G.1a)}$$

$$\partial_x T = \frac{P_0 \left(\gamma - 1\right)}{\mathcal{M}_0 \rho \left(\mathcal{M}^2 - 1\right)} \left[\frac{\mathcal{M}_0}{3} \partial_x \mathcal{E} + \left(\gamma \mathcal{M}^2 - 1\right) \rho \sigma_a \mathcal{C} \left[\mathcal{E} - T^4 - 2\beta \mathcal{F} + \frac{8}{3}\beta^2 \mathcal{E} \right] \right] . \quad \text{(G.1b)}$$

The first step is to expand each variable about an equilibrium state, $Y = Y_{eq} + \delta Y$, and retain only the terms which are linear in an expanded variable δ:

$$\partial_x \delta \mathcal{E} = \frac{3\sigma_t \mathcal{M}_0}{\mathcal{C} P_0} \left[\frac{\delta T}{\gamma - 1} \right.$$

$$- \left(\frac{\mathcal{M}_0^2}{\rho^2} + \frac{4P_0}{3}\frac{\mathcal{E}}{\rho} \right) \frac{\delta\rho}{\rho} + P_0 \frac{\frac{4}{3}\sigma_s \delta\mathcal{E} + \sigma_a \left(\frac{1}{3}\delta\mathcal{E} + 4T^3\delta T \right)}{\rho\sigma_t} \Bigg] , \quad \text{(G.2a)}$$

$$\partial_x \delta T = \frac{P_0 \left(\gamma - 1\right)}{\mathcal{M}_0 \rho \left(\mathcal{M}^2 - 1\right)} \left[\frac{\mathcal{M}_0}{3} \partial_x \delta\mathcal{E} + \left(\gamma\mathcal{M}^2 - 1\right) \rho\sigma_a \mathcal{C} \left[\delta\mathcal{E} - 4T^3\delta T \right] \right] . \quad \text{(G.2b)}$$

The cross-sections have not been expanded above for simplicity. We now assume that $\delta Y(x) = \delta Y e^{\alpha x}$, such that $\partial_x Y(x) = \alpha \delta Y(x)$, and we choose to divide both equations by the equilibrium value of T:

$$\alpha \frac{\delta\mathcal{E}}{T} = \frac{3\sigma_t \mathcal{M}_0}{\mathcal{C} P_0} \Bigg[\frac{1}{\gamma - 1} \frac{\delta T}{T} - \left(\frac{\mathcal{M}_0^2}{\rho^2 T} + \frac{4P_0}{3}\frac{\mathcal{E}}{\rho T} \right) \frac{\delta\rho}{\rho} + P_0 \frac{\frac{4}{3}\sigma_s \delta\mathcal{E} + \sigma_a \left(\frac{1}{3}\delta\mathcal{E} + 4T^3\delta T \right)}{\rho T \sigma_t} \Bigg] , \quad \text{(G.3a)}$$

$$\alpha \frac{\delta T}{T} = \frac{P_0 \left(\gamma - 1\right)}{\mathcal{M}_0 \rho T \left(\mathcal{M}^2 - 1\right)} \left[\frac{\mathcal{M}_0}{3} \partial_x \delta\mathcal{E} + \left(\gamma\mathcal{M}^2 - 1\right) \rho\sigma_a \mathcal{C} \left[\delta\mathcal{E} - 4T^3\delta T \right] \right] . \quad \text{(G.3b)}$$

Some algebraic manipulation is in order. Let $P_0\mathcal{E} = \rho T P$, recall that $\mathcal{M}^2 \equiv \frac{\mathcal{M}_0^2}{\rho^2 T}$, and recognize that in equilibrium $\mathcal{E} = T^4$, then these two equations become:

$$\alpha \frac{\delta\mathcal{E}}{\mathcal{E}} = \frac{3\sigma_t \mathcal{M}_0}{\mathcal{C} P \rho} \Bigg[\frac{1}{\gamma - 1} \frac{\delta T}{T} - \left(\mathcal{M}^2 + \frac{4P}{3} \right) \frac{\delta\rho}{\rho} + P \left(\left(\frac{1}{3} + \frac{\sigma_s}{\sigma_t} \right) \frac{\delta\mathcal{E}}{\mathcal{E}} + 4\frac{\sigma_a}{\sigma_t}\frac{\delta T}{T} \right) \Bigg] , \quad \text{(G.4a)}$$

$$\alpha \frac{\delta T}{T} = \frac{P \left(\gamma - 1\right)}{\mathcal{M}_0 \left(\mathcal{M}^2 - 1\right)} \left[\frac{\alpha}{3} \mathcal{M}_0 \frac{\delta\mathcal{E}}{\mathcal{E}} + \left(\gamma\mathcal{M}^2 - 1\right) \rho\sigma_a \mathcal{C} \left[\frac{\delta\mathcal{E}}{\mathcal{E}} - 4\frac{\delta T}{T} \right] \right] . \quad \text{(G.4b)}$$

Obviously, we must find a relation for $\frac{\delta\rho}{\rho}$ in terms of $\frac{\delta\mathcal{E}}{\mathcal{E}}$ and $\frac{\delta T}{T}$. Consider the first-integral of the total momentum conservation equation

$$\rho u^2 + p + P_0 \mathcal{P} = K_{eq} , \quad \text{(G.5a)}$$

which may also be written as

$$\frac{\mathcal{M}_0^2}{\rho} + \frac{\rho T}{\gamma} + \frac{1}{3} P_0 \mathcal{E} = K_{eq}\,, \tag{G.5b}$$

where K_{eq} represents the equilibrium value of the LHS. Linearizing this equation produces:

$$-\frac{\mathcal{M}_0^2}{\rho}\frac{\delta\rho}{\rho} + \frac{\rho T}{\gamma}\frac{\delta\rho}{\rho} + \frac{\rho T}{\gamma}\frac{\delta T}{T} + \frac{1}{3} P_0 \delta\mathcal{E} = 0\,. \tag{G.6}$$

Rearranging the equation above yields the desired result:

$$\frac{\delta\rho}{\rho} = \frac{1}{(\gamma\mathcal{M}^2 - 1)}\left(\frac{\delta T}{T} + \frac{\gamma P}{3}\frac{\delta\mathcal{E}}{\mathcal{E}}\right)\,. \tag{G.7}$$

Using this result in equation G.4a, and rearranging terms manifests a 2×2 system of equations:

$$\left(\frac{1}{\gamma - 1} - \frac{\left(\mathcal{M}^2 + \frac{4P}{3}\right)}{(\gamma\mathcal{M}^2 - 1)} + 4P\frac{\sigma_a}{\sigma_t}\right)\frac{\delta T}{T} + \left(-\alpha\frac{\mathcal{C}\rho}{3\sigma_t\mathcal{M}_0} + \frac{\left(\mathcal{M}^2 + \frac{4P}{3}\right)}{(\gamma\mathcal{M}^2 - 1)}\frac{\gamma}{3} + \left(\frac{1}{3} + \frac{\sigma_s}{\sigma_t}\right)\right) P\frac{\delta\mathcal{E}}{\mathcal{E}} = 0\,, \tag{G.8a}$$

$$\left(\alpha\frac{\mathcal{M}_0\left(\mathcal{M}^2 - 1\right)}{(\gamma - 1)} + 4P\left(\gamma\mathcal{M}^2 - 1\right)\rho\sigma_a\mathcal{C}\right)\frac{\delta T}{T} - \left(\frac{\alpha}{3}\mathcal{M}_0 - \left(\gamma\mathcal{M}^2 - 1\right)\rho\sigma_a\mathcal{C}\right) P\frac{\delta\mathcal{E}}{\mathcal{E}} = 0\,. \tag{G.8b}$$

Since the RHS is zero, the determinant of this 2×2 system must be zero, which generates a second-order characteristic equation for α:

$$\left(\frac{1}{\gamma - 1} - \frac{\left(\mathcal{M}^2 + \frac{4P}{3}\right)}{(\gamma\mathcal{M}^2 - 1)} + 4P\frac{\sigma_a}{\sigma_t}\right)\left(\frac{\alpha}{3}\mathcal{M}_0 - \left(\gamma\mathcal{M}^2 - 1\right)\rho\sigma_a\mathcal{C}\right)$$

$$+\left(-\alpha\frac{\mathcal{C}\rho}{3\sigma_t\mathcal{M}_0}+\frac{\left(\mathcal{M}^2+\frac{4P}{3}\right)}{\left(\gamma\mathcal{M}^2-1\right)}\frac{\gamma}{3}+\left(\frac{1}{3}+\frac{\sigma_s}{\sigma_t}\right)\right)$$
$$\times\left(\alpha\frac{\mathcal{M}_0\left(\mathcal{M}^2-1\right)}{\left(\gamma-1\right)}+4P\left(\gamma\mathcal{M}^2-1\right)\rho\sigma_a\mathcal{C}\right)=0\,. \quad \text{(G.9)}$$

Of course, this equation can be made to look less intimidating since all of the variables except α are known from their equilibrium values, and can be rewritten as constants:

$$a\left(b\,\alpha+c\right)+\left(d\,\alpha+e\right)\left(f\,\alpha+g\right)=0\,, \quad \text{(G.10a)}$$
$$\Rightarrow d\,f\,\alpha^2+\left(a\,b+d\,g+e\,f\right)\alpha+e\,g+a\,c=0\,, \quad \text{(G.10b)}$$

where

$$a=\frac{1}{\gamma-1}-\frac{\left(\mathcal{M}^2+\frac{4P}{3}\right)}{\left(\gamma\mathcal{M}^2-1\right)}+4P\frac{\sigma_a}{\sigma_t}\,, \quad \text{(G.10c)}$$
$$b=-\frac{\mathcal{M}_0}{3}\,, \quad \text{(G.10d)}$$
$$c=-\left(\gamma\mathcal{M}^2-1\right)\rho\sigma_a\mathcal{C}\,, \quad \text{(G.10e)}$$
$$d=\frac{\mathcal{C}\rho}{3\sigma_t\mathcal{M}_0}\,, \quad \text{(G.10f)}$$
$$e=\frac{\left(\mathcal{M}^2+\frac{4P}{3}\right)}{\left(\gamma\mathcal{M}^2-1\right)}\frac{\gamma}{3}-\frac{1}{3}-\frac{\sigma_s}{\sigma_t}\,, \quad \text{(G.10g)}$$
$$f=\frac{\mathcal{M}_0\left(\mathcal{M}^2-1\right)}{\left(\gamma-1\right)}\,, \quad \text{(G.10h)}$$
$$g=4P\left(\gamma\mathcal{M}^2-1\right)\rho\sigma_a\mathcal{C}\,. \quad \text{(G.10i)}$$

From the current context, the f above is obviously not the VEF. Then α is:

$$\alpha=\frac{-\left(a\,b+d\,g+e\,f\right)\pm\sqrt{\left(a\,b+d\,g+e\,f\right)^2-4\,d\,f\left(e\,g+a\,c\right)}}{2\,d\,f}\,. \quad \text{(G.11)}$$

The positive root of the discriminant appears to consistently give the desired results at upstream and downstream equilibrium. Of course, the ultimate test is that the radiation energy density should be increased at the upstream state and decreased at the downstream state.

The 2×2 system of equations (G.8) can now be solved, but we know neither $\delta\mathcal{E}$, nor δT, explicitly. Instead, since we are integrating along $\mathcal{M}$, this is the variable we control. Recalling $\mathcal{M} = \frac{\mathcal{M}_0}{\rho\sqrt{T}}$, this equation can be linearized,

$$\delta\mathcal{M} = -\mathcal{M}\left(\frac{\delta\rho}{\rho} + \frac{\delta T}{2T}\right), \tag{G.12}$$

and using equation (G.7) for $\frac{\delta\rho}{\rho}$, the solution for α in equation (G.11), and the 2×2 system of equations (G.8), then $\delta\mathcal{E}$ can be written in terms of $\delta\mathcal{M}$, as

$$\delta\mathcal{E} = \frac{6\,a\,(\gamma\mathcal{M}^2 - 1)\,\mathcal{E}}{P\,(3\,(\gamma\mathcal{M}^2 + 1)\,(b\,\alpha + c) - 2\,a\,\gamma)}\frac{\delta\mathcal{M}}{\mathcal{M}}\,. \tag{G.13}$$

It is important to remember that all of the variables above take their equilibrium values. If the upstream equilibrium integration is being performed then it is necessary to use the upstream equilibrium values, and similarly, if the downstream equilibrium integration is being performed then it is necessary to use the downstream equilibrium values.